CONSTRAINT ON STRESS TENSOR FROM SLIP ON A SINGLE FAULT PLANE

Bernard Célérier

Institute for Geophysics Technical Report no. 73.

The University of Texas at Austin
Institute for Geophysics
8701 Mopac Blvd
AUSTIN, TX 78759-8345

September 23rd, 1987.
Revised November 22nd, 1988.

CONTENT

For an abbreviated version of this work: B. Célérier, How much does slip on a single fault plane constrain the stress tensor ?, *Tectonics*, in press 1988.

ABSTRACT

Given a fault plane and its slip vector, the stress tensor which caused the displacement is sought. Two constraints are considered: first, a geometrical constraint that the shear stress applied to the fault plane is parallel to the slip [Wallace, 1951; Bott, 1959]; second, a frictional constraint that the shear to normal stress ratio equals $\tan\varphi_0$ [Coulomb, 1776]. This is done in two steps.

In a first step, the stress tensors that satisfy the geometrical constraint are sought. For tensors belonging to the vectorial space of solutions, shear and normal stress magnitudes become a function of the principal stress orientation $\vec{s1}$, $\vec{s2}$, $\vec{s3}$ and are mapped, extending a study by McKenzie [1969]. The relationship between Mohr's [1882] (σ_n,τ) plane and these maps is described.

In a second step, it is investigated which among these tensors also satisfy the frictional constraint. Within this more restricted vectorial space, there is a relationship between principal stress magnitudes, represented by $\delta = (\sigma_1 - \sigma_2)/(\sigma_1 - \sigma_3)$ and $s = (\sigma_1 - \sigma_3)/\sigma_1$, and the principal stress orientation $\vec{s1}$, $\vec{s2}$, $\vec{s3}$. Both the range of s and the spatial distribution of $\vec{s1}$, $\vec{s2}$, $\vec{s3}$ are more restricted than when the geometrical constraint alone is considered.

As when the geometrical constraint is solely considered [McKenzie, 1969], the principal stress orientations $\vec{s1}$, $\vec{s2}$, $\vec{s3}$ may lie significantly away from and up to right angle to the P, B, T axis. However, this can happen only in two cases: (1) either the effective stress difference, s, has reached a high value, which is unlikely to happen if enough pre-existing fractures are available to release the stress, or (2) σ_2 becomes close to either σ_1 or σ_3 and therefore barely distinguishable from it; in that case the delocalisation of the principal stress orientations is best described by a tendency for $\vec{s2}$ to exchange role with either $\vec{s1}$ or $\vec{s3}$.

When the stress difference remains small and σ_2 reasonably away from σ_1 and σ_3, $\vec{s1}$, $\vec{s2}$, $\vec{s3}$ approach positions that we define as the P_f, B, T_f axis and that are obtained from the P, B, T axis by a rotation of angle $\varphi_0/2$ around B and towards the slip vector. This explains why the P, B, T axis gives reasonable estimates of the principal stress orientations [Scheidegger, 1964] despite objections [McKenzie, 1969]. However, whenever the fault plane can be distinguished from the auxiliary plane, P_f, B, T_f should give a better estimate [Raleigh et al., 1972].

In an area where many fault planes are available and a uniform tensor is assumed, the scatter in the plane orientations contains information about both the relative position of σ_2, represented by δ, and the relative stress difference, s: the higher s or the closer δ to either 0 or 1, the more scatter. This information could then be extracted by inverse methods. Because a friction law would constrain these inverse methods more tightly, it may show the necessity of non-uniform tensor to explain scattered fault planes.

I

INTRODUCTION

To constrain the stress tensor, i.e., the principal stress orientations $\vec{s_1}$, $\vec{s_2}$, $\vec{s_3}$ and magnitudes $\sigma_1, \sigma_2, \sigma_3$ (Section II.2), that caused a displacement along an observed fault plane and slip direction requires some hypothesis about the failure mechanism. Two main cases can be distinguished.

First failure within intact rocks (Section IV.2). Using Coulomb's [1776] failure criteria, the stress orientations [Anderson, 1951] and the relative stress difference, s :

$$s = (\sigma_1 - \sigma_3) / \sigma_1 \qquad (1.1)$$

can be inverted for .

However in geological context a pre-existing plane of weakness is likely to be present within the rocks, and sliding on that plane may occur before a state of stress high enough to cause failure is reached [Wallace, 1951; Talobre, 1957; Bott, 1959; Jaeger, 1960; Donath, 1964; Handin, 1969; McKenzie, 1969; Section IV.3]. As a result in most geological cases, the failure model is of little use and other constraints must be sought [McKenzie, 1969].

Such a constraint can be found in the fact that the shear stress within the fault plane must parallel the slip vector [Wallace, 1951; Bott, 1959; McKenzie, 1969]. This will be referred to as the geometrical constraint in the rest of this paper. However, this sole constraint appears very weak since, for stress tensors satisfying it, the maximum principal stress direction, $\vec{s_1}$, can lie anywhere in the dilatational quadrant of a fault plane solution [McKenzie, 1969; Angelier and Mechler, 1977; Section III.9].

In practice, this problem is overcome by assuming that the same stress tensor is the cause of slip on many observed fault planes and that for each fault plane this constraint holds. Since the orientation of the shear stress depends only on the orientation of the principal stresses and on the ratio of the principal stress magnitudes differences, δ [Bott, 1959; Section III.3]:

$$\delta = (\sigma_1 - \sigma_2)/(\sigma_1 - \sigma_3) \qquad (1.2)$$

this approach invert only for these quantities. Theoretically four fault planes and their associated slips should determine the principal stresses orientations and δ. In practice more fault planes are used and a minimum misfit solution to this overdetermined system is sought [Carey and Brunier, 1974; Carey, 1976; 1979; Angelier, 1975, 1979a, 1979b, Armijo and Cisternas, 1978; Angelier and Goguel, 1979; Ellsworth and Zhonghuai, 1980; Etchecopar et al., 1981; Armijo et al., 1982; Angelier et al., 1982; Vasseur et al., 1983; Gephart and Forsyth, 1984] and in most cases, a regional uniform stress tensor solution is found acceptable.

However, the claim that no further constraint can be used in that case [McKenzie, 1969] seems unwarranted because frictional sliding requires a friction law to be satisfied [Palmer, 1949].

In fact, these methods allow mechanically unacceptable solutions, such as those producing a very small shear stress on a plane, that is parallel to the observed slip on that plane, but associated with a very large normal stress on that same plane. The question arises then, if these unacceptable solutions were thrown out, would a uniform stress tensor still be a possible solution?

An attempt to constrain this problem further considered that at rupture the shear stress τ must have reached a threshold τ_0 [Michael, 1984]. However this choice does not correspond to a realistic failure criterion and rather seems to be motivated by the simplification that it brings to the inversion technique by linearizing the equations. Another attempt introduced a friction law but only as an inequality that must be satisfied besides minimizing the misfit between shear stress and slip [Ellsworth, 1982; Sassi, 1985].

The work presented here follows a suggestion [Brace, personal communication] that some useful insight could be gained from applying Coulomb's [1776] law of friction to constrain this problem further (Section IV). This law is simple enough and reasonably independent of rock types [Byerlee, 1978]. The consequences of this extra constraint (referred to as the frictional constraint) in the case of a single fault plane are therefore derived in what follows. In a first step (Section III) the description of the stress tensors satisfying the geometrical constraint is extended from the initial work of McKenzie [1969] so as to facilitate, in subsequent steps, the recognition of those among them that also satisfy the friction law. In a second step (Section IV) the frictional constraint is introduced and combined with the geometrical constraint in simple cases. Finally, the general three dimensional inverse problem with both constraints together is solved (Section V). This will show that $\vec{s_1}$ is limited to a smaller range than the whole dilatational quadrant, that s is limited to values bigger than a critical value, s_c, and that not only δ, but also s could be inverted for in the case of multiple planes (Section VI).

II

SETTING THE PROBLEM

II.1. THE FAULT PLANE

The fault plane frame of reference E = ($\vec{e_1}$, $\vec{e_2}$, $\vec{e_3}$) is defined as in McKenzie [1969] (Fig. 2.1; symbols meaning in Table 2.1):

$\vec{e_1}$, $\vec{e_2}$, $\vec{e_3}$ are unit vectors;

$\vec{e_3}$ is normal to the fault plane;

$\vec{e_1}$ is the slip of the lower half space ($x_3 < 0$) relatively to the upper half space ($x_3 > 0$);

$\vec{e_2} = \vec{e_3} \times \vec{e_1}$.

There are in fact two frames satisfying this definition: if one is E = ($\vec{e_1}$, $\vec{e_2}$, $\vec{e_3}$) then the other is E' = ($-\vec{e_1}$, $\vec{e_2}$, $-\vec{e_3}$). Within that frame, A_1, A_2, A_3 are defined so that $\vec{OA_i} = \vec{e_i}$ and the P, T, B axis are defined as in seismology [Scheidegger, 1964].

II.2. THE EFFECTIVE STRESS TENSOR $\underline{\underline{T}}$

Failure or friction depends only on the effective stress tensor, $\underline{\underline{T}}$, which is represented in the E frame by the matrix T^E of components t_{ij}^E. A positive sign is chosen for compressive stresses as usually done in rock mechanics.

The six parameters that define the stress tensor $\underline{\underline{T}}$ can be broken into two categories:

- the 3 principal stress magnitudes: $\sigma_1, \sigma_2, \sigma_3$ that are the eigenvalues of $\underline{\underline{T}}$ ordered so that $\sigma_1 \geq \sigma_2 \geq \sigma_3$. σ_1 is then the maximum relative compression, σ_3 the maximum relative tension.

- the orientation of the frame of the principal stress direction: S = ($\vec{s_1}$, $\vec{s_2}$, $\vec{s_3}$) that is a direct set of unit eigenvectors of $\underline{\underline{T}}$ corresponding to the respective eigenvalue $\sigma_1, \sigma_2, \sigma_3$. This orientation depends on three parameters which will be taken as the Euler's [1767] angles (θ, φ, ψ) that transform E into S. The orientation of that frame will be represented by an equal area azimuthal projection [Lambert, 1772]. It can be noted that this frame is ambiguous: there are 4 possible such direct frames even in the case where the eigenvalues are all different from each other: if ($\vec{s_1}$, $\vec{s_2}$, $\vec{s_3}$) is one of them, ($\vec{s_1}$, $-\vec{s_2}$, $-\vec{s_3}$), ($-\vec{s_1}$, $-\vec{s_2}$, $\vec{s_3}$) and ($-\vec{s_1}$, $\vec{s_2}$, $-\vec{s_3}$) are the three others. By restricting $\vec{s_1}$ to the upper half space this indeterminacy is reduced and the projection facilitated. There remain an indeterminacy on the direction of $\vec{s_2}$ that will be reduced later on (Section III.4.3).

Because the effective stress tensor is deduced from the total stress tensor by subtraction of the isotropic pore pressure tensor, the effective principal stress orientations $\vec{s_1}$, $\vec{s_2}$, $\vec{s_3}$ coincide with the total principal stress orientations, and the effective stress magnitudes $\sigma_1, \sigma_2, \sigma_3$ are deduced from the total stress magnitudes by subtraction of the scalar pore pressure.

II.3. THE TRANSFORMATION MATRIX S^E

The matrix that transforms E into S is defined as S^E; its j^{th} column represents the coordinates of $\vec{s_j}$ in the E frame. S^E is a rotation matrix and therefore depends on only 3 parameters. Using Euler's [1767] angles, this rotation is decomposed into three elementary rotations, of respective angles θ, φ, and ψ and axis $\vec{e_3}$, $\vec{u_1}$, and $\vec{s_1}$ (Fig. 2.2), and the matrix S^E can be expressed as:

$$S^E = \begin{vmatrix} \sin\theta\sin\varphi, & \cos\theta\cos\psi - \sin\theta\cos\varphi\sin\psi, & -\cos\theta\sin\psi - \sin\theta\cos\varphi\cos\psi \\ -\cos\theta\sin\varphi, & \sin\theta\cos\psi + \cos\theta\cos\varphi\sin\psi, & -\sin\theta\sin\psi + \cos\theta\cos\varphi\cos\psi \\ \cos\varphi, & \sin\varphi\sin\psi, & \sin\varphi\cos\psi \end{vmatrix} \quad (2.1)$$

This shows that $\vec{s_1}$ depends only on two angles: θ and φ, while $\vec{s_2}$ and $\vec{s_3}$ require ψ. Finally, remembering that $\vec{s_1}$ is in the upper half space, the following intervals of definition are obtained for each angle:

$$\theta \in [0, 2\pi[\; ; \; \varphi \in [0, \pi/2] \; ; \; \psi \in [0, 2\pi[\quad (2.2)$$

II.4. ALTERNATE REPRESENTATION OF $\underline{\underline{T}}$

To facilitate the study, $\underline{\underline{T}}$ is decomposed in a fashion similar to that into pressure and deviatoric tensor, with the difference that tensional tensors must be avoided because of the friction law. Therefore the biggest isotropic tensor, $\sigma_3 \bullet \underline{\underline{I}}$, that still yields a compressive result is subtracted from $\underline{\underline{T}}$ and the result is scaled to 1 so as to define $\underline{\underline{T}}_d$:

$$\underline{\underline{T}}_d = \frac{1}{\sigma_1 - \sigma_3} \bullet [\underline{\underline{T}} - \sigma_3 \bullet \underline{\underline{I}}] \quad (2.3)$$

The shear and normal stress of these two tensors are related by:

$$\vec{\tau} = (\sigma_1 - \sigma_3) \bullet \vec{\tau_d} \quad (2.4)$$

$$\sigma_n = \sigma_3 + (\sigma_1 - \sigma_3) \bullet \sigma_{nd} \quad (2.5)$$

σ_1, σ_2, σ_3 are also scaled by defining:

$$\delta = (\sigma_1 - \sigma_2) / (\sigma_1 - \sigma_3) \qquad \delta \in [\,0, 1] \quad (2.6)$$

$$s = (\sigma_1 - \sigma_3) / \sigma_1 \qquad s \in [\,0, +\infty[\quad (2.7)$$

δ is also often more easily represented by θ_1 defined as:

$$\theta_1 = 2 \, \mathrm{Arctan}(\sqrt{\delta}) \qquad \theta_1 \in [\,0, \pi/2] \quad (2.8)$$

δ represents the relative position of σ_2 in respect to σ_1 and σ_3, i.e. the tensor aspect ratio, and s the relative stress difference; θ_1 can be graphically constructed (Fig. 2.3).

$\underline{\underline{T}}_d$ is represented in the E frame by:

$$T_d^E(\theta, \varphi, \psi, \delta) = S^E(\theta, \varphi, \psi) \bullet T_d^S(\delta) \bullet {}^tS^E(\theta, \varphi, \psi) \quad (2.9)$$

where:

$$T_d^S = \begin{vmatrix} 1 & 0 & 0 \\ 0 & 1-\delta & 0 \\ 0 & 0 & 0 \end{vmatrix} \qquad (2.10)$$

$\underline{\underline{T}}_d$ depends therefore on only 4 parameters: the principal stress orientation (θ, φ, ψ) and the aspect ratio, δ, yet it contains all the geometrical information about the shear stress (Eq. 2.4). This can be easily understood either because the Mohr's [1882] circles of $\underline{\underline{T}}_d$ are deduced from those of $\underline{\underline{T}}$ by a translation of $-\sigma_3$ along the σ_n axis and an similarity of ratio $1/(\sigma_1 - \sigma_3)$ centered on the origin, and are therefore similar to those of $\underline{\underline{T}}$ (Fig.2.3), or because these two tensors have the same eigenvectors, even though different eigenvalues.

T^E can then be recovered from T_d^E by:

$$T^E(\theta, \varphi, \psi, \sigma_1, s, \delta) = \sigma_1 \bullet (1-s) \bullet I + \sigma_1 \bullet s \bullet T_d^E(\theta, \varphi, \psi, \delta) \qquad (2.11)$$

II.5. THE STRESS $\vec{F}$ APPLIED TO THE FAULT PLANE

With the adopted sign convention (Section II.2), the stress $\vec{F}$ applied to the upper half space of the fault plane is given by:

$$\vec{F} = \underline{\underline{T}}(\vec{e_3}) \qquad (2.12)$$

and its matrix F^E in the E frame is:

$$F^E = \begin{vmatrix} t_{13}^E \\ t_{23}^E \\ t_{33}^E \end{vmatrix} \qquad (2.13)$$

The normal stress, $\vec{\sigma_n}$ and the shear stress, $\vec{\tau}$, are then (Fig. 2.1):

$$\vec{\sigma_n} = t_{33}^E \bullet \vec{e_3} \qquad (2.14)$$

$$\vec{\tau} = t_{13}^E \bullet \vec{e_1} + t_{23}^E \bullet \vec{e_2} \qquad (2.15)$$

Eq. 2.9 and 2.11 give the components of F^E as a function of $(\theta,\varphi,\psi,\sigma_1,\theta_1,s)$ (Table 2.2). These expressions display two symmetries: first

$$\vec{\tau}(\theta+\pi) = -\vec{\tau}(\theta) \qquad (2.16)$$

$$\vec{\sigma_n}(\theta+\pi) = \vec{\sigma_n}(\theta) \qquad (2.17)$$

allows to reduce the study to $\theta \in [\,0, \pi[$; and, second

$$\vec{\sigma_n}(\theta+\pi/2) = \vec{\sigma_n}(\theta) \qquad (2.18)$$

$$t_{13}^E(\theta+\pi/2) = -t_{23}^E(\theta) \qquad (2.19)$$

$$t_{23}^E(\theta+\pi/2) = t_{13}^E(\theta) \qquad (2.20)$$

The last two equations mean that $\vec{\tau}(\theta+\pi/2)$ is obtained by rotating $\vec{\tau}(\theta)$ by $\pi/2$ around $\vec{e_3}$ and

allow to deduct the study of t^E_{13} from that of t^E_{23}.

II.6. FRICTION

To apply the frictional constraint (Part IV.3) it is useful to define the scalar functions H and H_d as:

$$H = \tau - \tan\varphi_0 \bullet \sigma_n \tag{2.21}$$

$$H_d = \tau_d - \tan\varphi_0 \bullet \sigma_{nd} \tag{2.22}$$

II.7. THE PROBLEM

The relationship between the fault plane and slip orientations and the effective stress tensor, $\underline{\underline{T}}$, can be approached in two opposite fashions.

In the direct problem, the stress tensor is given and one looks for the orientation of the planes of failure and for the orientation of the slip, i.e., $E = (\vec{e_1}, \vec{e_2}, \vec{e_3})$, with respect to the principal stress referential $S = (\vec{s_1}, \vec{s_2}, \vec{s_3})$. This has been studied essentially for rock mechanics purposes where the stresses are controlled by the experimentalist [Wallace, 1951; Talobre, 1957; Jaeger, 1960; Jaeger and Rosengren, 1969]. Six parameters (defining the stress tensor) are given and three (defining the plane and slip orientation) are sought. This is usually solved by using Mohr's [1882] circles.

In tectonics, however, it is the inverse problem that is of interest, because the fault plane and slip frame $E = (\vec{e_1}, \vec{e_2}, \vec{e_3})$ is obtained from earthquake fault plane solution or structural geology and the stress tensor is sought. This problem, when limited to one given plane of failure and slip, is by nature underdetermined, and its study aims only at describing the set of acceptable solutions.

III

THE GEOMETRICAL CONSTRAINT ALONE: VARIATIONS ON A THEME BY MCKENZIE [1969]

III.1. INTRODUCTION

The goal of this section is to describe the stress tensors that satisfy the geometrical constraint that the shear stress is parallel to the observed slip on a given fault plane. This description will be made so as to facilitate the next task that is to distinguish among these stress tensors those that also satisfy a friction law (Section IV and V).

McKenzie [1969] showed that for stress tensors satisfying the geometrical constraint, the shear stress on the fault plane depends on the position of $\vec{s1}$ and the value of δ. Therefore, if δ is fixed, the shear stress, τ, can be mapped as a function of the position of $\vec{s1}$. Because the onset of slip is mechanically controlled by both shear, τ, and normal, σ_n, stress (Section IV), this mapping needs to be extended to σ_n and to the linear combination of τ and σ_n, H, that represents a friction law (Eq. 2.21).

The derivation of analytical instead of numerical representation is emphasized because critical cases can then be associated with precise relationships between the parameters, relationships that can be physically interpreted. The emphasis on $\vec{s1}$ is also relaxed so as to extend these maps to $\vec{s2}$ and $\vec{s3}$. Because using Euler's [1776] angles is a slightly different approach from that of McKenzie [1969], a preliminary task is to reformulate his results.

III.2. FORMULATION

The geometrical constraint is two fold:

(1) the shear stress $\vec{\tau}$ on the fault plane must be parallel to the slip vector $\vec{e1}$ [Wallace, 1951; Bott, 1959; McKenzie, 1969]. This can be expressed as (Fig. 2.1 or Eq. 2.15):

$$t^E_{23} = 0 \tag{3.1}$$

(2) $\vec{\tau}$ and $\vec{e1}$ must point in the same direction [McKenzie, 1969]:

$$t^E_{13} \geq 0 \tag{3.2}$$

III.3. OVERVIEW

$\underline{\underline{T}}$ depends on 6 parameters and is submitted to a linear constraint: the problem is then underdetermined and the set of solutions is the vectorial space of dimension 5 of the stress tensors whose matrices in E, T^E, satisfy $t^E_{23} = 0$. The general solution is then:

$$T^E = \begin{vmatrix} t^E_{11} & t^E_{12} & t^E_{13} \\ t^E_{12} & t^E_{22} & 0 \\ t^E_{13} & 0 & t^E_{33} \end{vmatrix} \tag{3.3}$$

where the t^E_{ij} are arbitrary.

This vectorial space structure can be used to reduce the problem in two ways [Carey and Brunier, 1974; Angelier, 1975]. First, because any isotropic tensor, $\alpha\underline{\underline{I}}$, belongs to that space, as one would expect since in that case $\vec{\tau} = \vec{0}$, it can be added to any solution to produce another solution. Second, a scaling factor on $\underline{\underline{T}}$ will not modify the problem. Therefore, the general solution can be written as:

$$\underline{\underline{T}}(\theta,\varphi,\psi,\sigma_1,s,\delta) = \sigma_1 \bullet (1\text{-}s) \bullet \underline{\underline{I}} + \sigma_1 \bullet s \bullet \underline{\underline{T}}_d\,(\theta,\varphi,\psi,\delta) \tag{3.4}$$

where σ_1 and s are arbitrary and $\underline{\underline{T}}_d$ satisfies the geometrical constraint (Eq. 3.1 and 3.2).

Therefore only $\underline{\underline{T}}_d$ need to be studied. This can be independently derived either by noticing that $\underline{\underline{T}}$ and $\underline{\underline{T}}_d$ have parallel shear stress (Eq. 2.4) or by noticing that the orientation of $\vec{\tau}$, i.e., the ratio $\underline{\underline{t}}^E_{23}/\underline{\underline{t}}^E_{13}$ (Table 2.2), depends only on θ, φ, ψ and δ. The dependence on δ of that orientation is the essence of Bott 's [1959] contribution. The only relevant parameters to this study are therefore θ,φ,ψ, and δ; σ_1 and s remain unconstrained.

III.4. SIGN AND ZEROS OF t^E_{d23}

Because of symmetries (Eq. 2.16 and 2.17), the study is limited to: $\theta \in [0,\pi]$; $\varphi \in [0, \pi/2]$; $\psi \in [0, 2\pi]$; Two particular cases where t^E_{23} does not depend on ψ are distinguished from the general case.

III.4.1. Particular case 1

$\delta = 1$ (then: $\sigma_2 = \sigma_3$ <u>and</u> $\theta_1 = \pi/2$). The stress coordinates (Table 2.2) become:

$$t^E_{d13} = \cos\varphi\sin\varphi\sin\theta \tag{3.5}$$

$$t^E_{d23} = -\cos\varphi\sin\varphi\cos\theta \tag{3.6}$$

$$t^E_{d33} = 1\text{-}\sin^2\varphi \tag{3.7}$$

Then $t^E_{d23} = 0$ if and only if $\varphi = 0$ or $\varphi = \pi/2$ or $\theta = \pi/2$. ψ remains a free parameter.

III.4.2. Particular case 2

$\vec{s_1} // \vec{e_2}$ (then $\varphi = \pi/2$ <u>and</u> $\theta=0$) and :

$$t^E_{d13} = \cos\theta_1\ \sin 2\psi/(1+\cos\theta_1) \tag{3.8}$$

$$t^E_{d23} = 0 \tag{3.9}$$

$$t^E_{d33} = 1 - (1+\cos\theta_1\cos 2\psi)/(1+\cos\theta_1) \tag{3.10}$$

Then $t^E_{d23} = 0$ regardless of the value of ψ.

III.4.3. General case

$\delta \neq 1$ and $\vec{s_1} \times \vec{e_2} \neq \vec{0}$. The functions:

$$K(\theta,\varphi) = \frac{\cos\varphi\cos\theta}{\sqrt{1-\sin^2\varphi\cos^2\theta}} \tag{3.11}$$

$$\chi(\theta,\varphi) = \text{Arcsin}[K(\theta,\varphi)] \tag{3.12}$$

are then defined and:

$$t^E_{d23} = \frac{\cos\theta_1}{1+\cos\theta_1} \bullet \sin\varphi \bullet \sqrt{1-\sin^2\varphi\cos^2\theta} \bullet [\sin(2\psi-\chi) - \frac{K}{\cos\theta_1}] \tag{3.13}$$

Except when $\varphi = 0$ ($\vec{s_1} = \vec{e_3}$), in which case $t^E_{d23} = 0$, the sign and zeros of t^E_{d23} are the same as those of f defined as:

$$f(\theta,\varphi,\psi,\theta_1) = \sin[2\psi-\chi(\theta,\varphi)] - K(\theta,\varphi)/\cos\theta_1 \tag{3.14}$$

Three regions in the (θ,φ) plane can then be distinguished (Fig. 3.1):

1 - a region R^+ where $K < -\cos\theta_1$ and then for any value of ψ, $t^E_{d23} > 0$

2 - a region R^- where $K > \cos\theta_1$ and then for any value of ψ, $t^E_{d23} < 0$

3 - a region R^0 where $-\cos\theta_1 < K < \cos\theta_1$. In that region the sign of t^E_{d23} depends on ψ once θ and φ are fixed and it is always possible to find ψ so that $t^E_{d23} = 0$; the only possible choices for that are ψ_1 and ψ_2:

$$\psi_1(\theta,\varphi,\delta) = \frac{\chi(\theta,\varphi)}{2} + \frac{1}{2} \bullet \text{Arcsin}[\frac{K(\theta,\varphi)}{\cos\theta_1}] + k\pi \tag{3.15}$$

$$\psi_2(\theta,\varphi,\delta) = \frac{\chi(\theta,\varphi)}{2} + \frac{\pi}{2} - \frac{1}{2} \bullet \text{Arcsin}[\frac{K(\theta,\varphi)}{\cos\theta_1}] + k\pi \tag{3.16}$$

where k is a signed integer that is taken as zero in what follows since the direction of $\vec{s_2}$ can be constrained (Section II.2).

III.5. CURVES C(α), D(α), D''(α), D'''(α)

C(α) is defined as the great circle that passes through A_2 and whose plane is at angle α with $\vec{e_3}$ (Fig. 3.2). Its equation, i.e., the condition for $\vec{s_1}$ to be on that circle, is:

$$\sin\theta = \tan\alpha / \tan\varphi \tag{3.17}$$

D(α) is the curve (Fig. 3.2) defined by the equation:

$$K^2(\theta,\varphi) = \cos^2\alpha \tag{3.18}$$

which can also be written as :

$$\cos\varphi = |\tan\theta/\tan\alpha| \qquad (3.19)$$

The shape of $D(\alpha)$ depends only on α which has two graphical interpretations: the projection of $D(\alpha)$ is tangent to $C(\alpha)$ in A_2 and to the line of slope $\pi/2-\alpha$ in A_3.

The boundary between the three regions R^-, R^0 and R^+ as defined before is $D(\theta_1)$. When $\vec{s_1}$ describes $D(\theta_1)$, the two stress tensor solutions of the geometrical constraint coincide because $\psi_1(\theta,\varphi,\delta) = \psi_2(\theta,\varphi,\delta)$. Therefore $\vec{s_2}$ and $\vec{s_3}$ also describe single curves that are defined as $D''(\theta_1)$ and $D'''(\theta_1)$.

III.6. STRESS COMPONENTS FOR A SOLUTION TENSOR

In the general case, for a stress tensor solution of $t^E_{d23} = 0$, ψ is either $\psi_1(\theta,\varphi,\delta)$ or $\psi_2(\theta,\varphi,\delta)$ and can then be eliminated from the expression of stress components of Table 2.2. The resulting expression of a component, t, that can be either τ_d, σ_{nd} or H_d are of the type (Table 3.1):

$$t(\theta,\varphi,\delta,\varepsilon) = A(\theta,\varphi)\bullet N(\theta,\varphi,\delta,\varepsilon) + B \qquad (3.20)$$

where $\varepsilon + 1$ if ψ_1 has been substituted and $\varepsilon = -1$ if ψ_2 has been substituted. The corresponding functions will be designated as t^+ (case $\varepsilon = +1$) and t^- (case $\varepsilon = -1$). $t^E_{d13}(\theta,\varphi,\delta,\varepsilon)$ is obviously positive (Table 3.1) in the domain of study: $\theta \in [0,\pi]$ and $\varphi \in [0,\pi/2]$. By symmetry it is negative in the other quadrant $\theta \in [0,-\pi]$, $\varphi \in [0,\pi/2]$. Therefore, once the first geometrical condition, $t^E_{d23} = 0$, is satisfied, the second condition, $t^E_{d13} \geq 0$ is satisfied if and only if $\vec{s_1}$ belongs to the dilatational quadrant. $\vec{s_1}$ is then restricted to the region R_G that is the intersection of the R^0 region with the dilatational quadrant (Fig. 3.1).

III.7. STRESS TENSOR SOLUTIONS

There are only 5 cases where $t^E_{d23} = 0$ [McKenzie, 1969]:

(1) $\underline{\underline{T}}$ is isotropic

(2) $\sigma_2 = \sigma_3$ (δ=1) and $\vec{s_1}$ belongs either to the $(\vec{e_1},\vec{e_3})$ plane (P, T plane) or to the fault plane $(\vec{e_1},\vec{e_2})$.

(3) $\vec{s_1} = \vec{e_2}$ ($\vec{s_1}$ within the fault plane and normal to the slip, hence along the B axis)

(4) $\vec{s_1} = \vec{e_3}$ ($\vec{s_1}$ normal to the fault plane)

(5) $\vec{s_1}$ belongs to R_G region, and the orientation of $(\vec{s_2}, \vec{s_3})$ is defined by either $\psi_1(\theta,\varphi,\delta)$ or $\psi_2(\theta,\varphi,\delta)$. The general solution is then

$$\underline{\underline{T}}\,(\theta,\varphi,\psi,\sigma_1,s,\delta) = \sigma_1 \bullet (1-s) \bullet \underline{\underline{I}} + \sigma_1 \bullet s \bullet \underline{\underline{T}}_d(\theta,\varphi,\psi=\psi_1 \text{ or } \psi_2,\delta) \qquad (3.21)$$

where σ_1 and s are arbitrary and $(\theta,\varphi) \in R_G$.

The shape of the R_G region (Fig. 3.1) which is bounded by the fault plane $(\vec{e_1},\vec{e_2})$ and $D(\theta_1)$, depends only on δ; it includes the positions of $\vec{s_1}$ obtained in cases (3) and (4) and its definition can be extended to include case (2) (δ=1). The general case can then be extended to include all the particular cases if one keeps in mind that in these cases ψ remains unconstrained.

III.8. MAPS OF THE STRESS COMPONENTS

III.8.1. Goal

For $\underline{T}_d$ satisfying the geometrical constraint and once δ and ε are fixed, the magnitude $t(\theta,\varphi,\delta,\varepsilon)$ (Table 3.1) of either τ_d, σ_{nd} or H_d, depends only on (θ,φ) which in turn determine the position of $\vec{s1}$, $\vec{s2}$ or $\vec{s3}$ through Eq. 2.1 and 3.15 or 3.16. In other words, the value of t can be mapped as a function of the position of either $\vec{s1}$ or $\vec{s2}$ or $\vec{s3}$. Such maps for $\underline{T}_d$ can be transferred to $\underline{T}$ through Eq. 2.4 and 2.5. To draw the V_0 level curve of such maps requires to solve for either θ or φ the equation:

$$t(\theta, \varphi, \delta, \varepsilon) = V_0 \tag{3.22}$$

Because of the new symmetry (Table 3.1):

$$t(\pi - \theta) = t(\theta) \tag{3.23}$$

the interval of study is reduced to that part of the R_G domain where $\theta \in [0,\pi/2]$ and $\varphi \in [0,\pi/2]$. This new domain will be called R_E.

Numerical solutions to Eq. 3.22 can be found, but analytical solutions are not obvious. However, a change of parameters overcome that problem.

III.8.2. Parameter change

A problem in solving Eq. 3.22 is that the curves θ = constant or φ = constant do not bear any simple relationship to the values of $t(\theta,\varphi,\delta,\varepsilon)$ (Table 3.1).

However, the circles $C(\alpha)$ are the level curves of the function $A(\theta,\varphi)$. Replacing then (θ,φ) by (θ,α) such as:

$$\tan\alpha = \tan\varphi \bullet \sin\theta \tag{3.24}$$

the curve α = constant is the circle $C(\alpha)$ (Eq. 3.17). The function $A(\theta,\varphi)$ becomes then a function of α only, $A(\alpha)$, and is very simplified (Table 3.1) while the new function $N(\theta,\alpha,\delta,\varepsilon)$ is not more complicated than the original $N(\theta,\varphi,\delta,\varepsilon)$.

N could also be simplified by using the fact that its level curve are the curves $D(\beta)$. However, the further simplification brought by a new parameterization (α,β) is somewhat offset by the more complicated expression of (θ,φ) as a function of (α,β); it is therefore not used.

III.8.3. Variations of $t(\theta,\alpha,\delta,\varepsilon)$ in R_E

Once δ (i.e., θ_1) is fixed, $t(\theta,\alpha,\delta,\varepsilon)$ is defined in the R_E domain. On $C(\alpha)$, i.e., when α is fixed, A is constant and N is a monotonous function of θ. Hence t is a monotonous of θ too. Because the family of circles $C(\alpha)$ spans the whole R_E domain the extreme values of the function t are reached on the boundary of that domain (Fig. 3.3). This boundary can be decomposed into four parts: (1): $D(\theta_1)$, (2): $C(\pi/2)$, (3): the singular point A_2, (4): the arc A_1A_3.

III.8.4. Extrema of $t(\theta,\alpha,\delta,\varepsilon)$

The extrema of $t(\theta,\alpha,\delta,\varepsilon)$ on each of the 4 boundaries of R_E are summed up in Table 3.2 where t^+ (ε=+1) and t^- (ε=-1) are separated. By comparing these relative extrema, the absolute extrema and their location are obtained (Table 3.3 and Fig. 3.3). Any function, t, is then

normalized into t_* (defined in Table 3.1) so that the absolute minimum is 0 and the absolute maximum 1.

The t_*^+ and t_*^- solutions differ both by the value and the location of their extrema. t_*^+ does span the full range of variation between 0 and 1, but t_*^- does not (Table 3.3). The absolute maximum of τ^- is reached at the intersection between $C(\pi/4)$ and $D(\theta_1)$ (Fig. 3.3) and two cases can be distinguished: either $\theta_1 \geq \pi/4$, and the maximum is reached within $D(\theta_1)$ or $\theta_1 \leq \pi/4$ and the maximum is in A_2. That of τ^+ is reached on the P axis which corresponds to a saddle for τ^-. H behaves like τ if one replaces $\pi/4$ by $\varphi_1 = \varphi_0/2 + \pi/4$, and P by the corresponding location that is defined as P_f (Section IV.2.2). As expected, the normal stress is maximum when $\vec{s_1}$ is on A_3 (normal to the plane) and minimum when it is on $C(\pi/2)$. Both locations correspond to the minimum of τ.

III.8.5. Parameterization of level curves

Solving:

$$t(\alpha, \theta, \theta_1, \varepsilon) = V_0 \tag{3.25}$$

with:

$$t = A(\alpha) \bullet N(\theta, \alpha, \theta_1, \varepsilon) + B \tag{3.26}$$

and:

$$N(\theta, \alpha, \theta_1, \varepsilon) = 1 + \varepsilon \bullet \cos\theta_1 \bullet R_D(\theta, \alpha, \theta_1)/(1 + \cos\theta_1) \tag{3.27}$$

yields:

$$\varepsilon \bullet R_D(\theta, \alpha, \theta_1) = G(V_0, \alpha, \theta_1) \tag{3.28}$$

where:

$$G(V_0, \alpha, \theta_1) = \frac{V_0 - B}{A(\alpha)} \bullet \frac{1 + \cos\theta_1}{\cos\theta_1} - \frac{1}{\cos\theta_1} \tag{3.29}$$

Squaring 3.28 put together the level curves corresponding both to a $\psi = \psi_1$ and $\psi = \psi_2$ solution. The limit between these two solutions occurs when $R_D = 0$, hence on the boundary $D(\theta_1)$. This yields:

$$R_D^2(\theta, \alpha, \theta_1) = G^2(V_0, \alpha, \theta_1) \tag{3.30}$$

which can be solved for θ:

$$\cos^2\theta = C(\alpha, \theta_1, V_0) \tag{3.31}$$

where:

$$C(\alpha, \theta_1, V_0) = \frac{1 - G^2(V_0,\alpha,\theta_1)}{1/\cos^2\theta_1 - G^2(V_0,\alpha,\theta_1)} \bullet \frac{1}{\cos^2\alpha} \tag{3.32}$$

φ can then be recovered through Eq. 3.24:

$$\tan\varphi = \tan\alpha\sqrt{1 - C(\alpha,\theta_1,V_0)} \qquad (3.33)$$

Eqs. 3.31 and 3.33 give then a parametric representation $\vec{s_1}(\theta(\alpha), \varphi(\alpha), \delta, \varepsilon)$ of the curves described by $\vec{s_1}$ when the constraint $t = V_0$ is fulfilled on top of the geometrical constraint $\vec{\tau} // \vec{e_1}$. The curves described by $\vec{s_2}$ and $\vec{s_3}$ under the same condition are obtained by: $\psi(\alpha) = \psi_1(\theta(\alpha), \varphi(\alpha), \delta)$ or $\psi(\alpha) = \psi_2(\theta(\alpha), \varphi(\alpha), \delta)$.

Because this parameterization has been using the substitution of ψ by $\psi_1(\theta,\varphi,\delta)$ or $\psi_2(\theta,\varphi,\delta)$ it is valid in the R_E domain except in two points: A_2 and A_3 (i.e. when $\vec{s_1}$ is parallel to either $\vec{e_2}$ or $\vec{e_3}$). For these two points one must then go back to the stress component expressions before that substitution (Table 2.2) and solve directly the equation:

$$t(\theta, \varphi, \psi, \theta_1) = V_0 \qquad (3.34)$$

with the simplification that either $\theta = \pi$ and $\varphi = \pi/2$ (for A_2) or $\varphi = 0$ (for A_3).

III.8.6. Critical cases

There are three independent ways of discussing the different shapes of the $t_* = V_0$ level curves which depend only on δ and V_0.

First, for Eq. 3.31, to have a solution in α the two following conditions must be met:

$$C(\alpha, \theta_1, V_0) \geq 0 \qquad (3.35)$$

and:

$$C(\alpha, \theta_1, V_0) \leq 1 \qquad (3.36)$$

If $C = 0$ then $\theta = \pi/2$ and $\varphi = \alpha$, therefore $\vec{s_1}$ is on the A_1A_3 arc; if $C = 1$ then $\theta = 0$ and $\varphi = \pi/2$, therefore $\vec{s_1}$ is on A_2 (the B axis). Therefore if θ_1 and V_0 are fixed, the value of α solutions of Eq. 3.31 will be bounded by critical α values for which $\vec{s_1}$ is either on the A_1A_3 arc or on A_2. These α critical values are a function of (θ_1,V_0) and the condition for their existence, which is also that for the existence of a α solution, translates into a condition on (θ_1,V_0). Finally, for whatever (α,θ_1,V_0) that is solution of Eq. 3.31, whether that solution corresponds to $\varepsilon = +1$ or $\varepsilon = -1$ can be determined by checking the sign of $G(V_0,\alpha,\theta_1)$ (Eq. 3.28).

Second, the type of a level curve depends on what boundaries of the R_E domain it will hit. A level curve $t = V_0$ will hit a boundary if and only if V_0 is between the extrema of t on that boundary. This discussion can be done separately for the ε=+1 and ε=-1 type of solution since the extrema are known in both cases (Table 3.2). The existence of the level curve can be discussed the same way by looking at the absolute extrema (Table 3.3); such a discussion shows that the $\varepsilon = -1$ type of solution will exist only for a narrower range of value of V_0 than the $\varepsilon = +1$ type which exists for any $0 \leq V_0 \leq 1$. Since all the extrema are only a function of δ, the whole discussion amounts to comparing V_0 and δ.

Third, Mohr's [1882] representation allows derivation of the same critical values for (V_0,δ) (Fig. 3.4). Only that part of Mohr's representation corresponding to positive shear stress is considered because of slip compatibility (Eq. 3.2). The problem is to know whether or not an $\vec{s_1}$ level curve hits one of the boundaries, A_2, $C(\pi/2)$, A_1A_3, or $D(\theta_1)$. These boundaries can be mapped on Mohr's representation:

- when $\vec{s_1}$ is in A_2 then in the fault plane, the inner left Mohr's circle is described;

- when $\vec{s_1}$ is on $C(\pi/2)$ but not in A_2, then either $\vec{s_2}$ or $\vec{s_3}$ are in A_3 in order to keep the shear stress, $\vec{\tau}$, parallel (in fact nought) to the slip, $\vec{e_1}$; this corresponds to the points of abscissa σ_2 or σ_3 on the σ_n axis;

- when $\vec{s_1}$ is on the arc A_1A_3, either $\vec{s_2}$ or $\vec{s_3}$ are in A_2, also in order to preserve the parallelism between $\vec{\tau}$ and $\vec{e_1}$, and therefore either the outer Mohr's circle or on the right inner Mohr's circle are described;

- finally, when $\vec{s_1}$ is on $D(\theta_1)$, the intermediate circle, that has the σ_n axis as diameter and passes through σ_1 and $(\sigma_2+\sigma_3)/2$ (i.e.: 1 and $(1+\delta)/2$ for T_d) on that axis (Figs. 2.3 and 3.4), is described and $\vec{s_2}$, $\vec{s_3}$ describe respectively $D''(\theta_1)$ and $D'''(\theta_1)$. This intermediate circle separate the $\varepsilon = +1$ or $\psi = \psi_1(\theta,\varphi,\delta)$ type of solution from the $\varepsilon = -1$ or $\psi = \psi_2(\theta,\varphi,\delta)$ type on Mohr's plane; the two corresponding range of orientations are superposed for $\vec{s_1}$, separated and filling the whole sphere for $\vec{s_2}$, neither separated nor totally superposed for $\vec{s_3}$.

Once this correspondence between the R_G domain for $\vec{s_1}$ and Mohr's circle is established (Fig 3.4), the whole discussion can be interpreted in terms of intersection between the line $t = V_0$ and the 4 critical circles mentioned (Fig. 3.5, 3.6 & 3.7 for τ_*, σ_{n*} and H_* respectively): the tangence with the outer circle corresponds to the highest value, $t_* = 1$, to $\vec{s_1}$, $\vec{s_2}$, $\vec{s_3}$ on P, B, T for τ_*, on positions defined as P_f, B, T_f (Table 2.1 & Section IV.2.2) for H_* and to $\vec{s_1}$ on $\vec{e_3}$ for σ_{n*}; the intersection with any inner circle will allow either $\vec{s_3}$ (right circle) or $\vec{s_1}$ (left circle) to reach the fault plane in A_2 (B axis); finally the intersection with the intermediate circle will allow the $\varepsilon = -1$ type of solution.

These three independent methods yield the same 6 critical cases for τ_*, 4 for σ_{n*} and 8 for H_*. Each of these critical cases corresponds to a relationship between V_0 and δ which is plotted in the (δ,V_0) plane for τ_*, σ_{n*} and H_* (Fig. 3.8, 3.9, and 3.10). Because the type of a V_0-level curve is determined by the position of V_0 with respect to the critical values, each polygon so delimited in the (δ,V_0) plane corresponds to one type of level curve. There are then 8 types for τ, 3 for σ_n and 13 for H.

III.8.7. Shear stress level curves types

All the 8 different types of shear stress level curves are shown through examples for $\delta = 0.3$ (Fig. 3.11) and $\delta = 0.55$ (Fig. 3.12). The evolution can be understood by concentrating on a fixed value of δ, which corresponds to a fixed set of Mohr's circles, and letting V_0 decrease from 1 to 0.

The case $\delta = 0.3$ is shown on Fig. 3.11. The maximum value of τ_*, $V_0 = 1$, corresponds to $\vec{s_1}$, $\vec{s_2}$, $\vec{s_3}$ on the P, B, T axis (Fig. 3.5). For smaller values that remain above the smaller circles, such as $V_0 = 0.75$, $\vec{s_1}$ and $\vec{s_3}$ describe trajectories around P and T while $\vec{s_2}$ describe a two parts trajectory which passes through A_2 (i.e.: the B axis). When the left inner circle is reached, such a when V_0=0.66, the $\vec{s_1}$ trajectory passes through A_2, the $\vec{s_2}$ trajectory intersects the A_1A_3 arc and is reunited in one part, and the $\vec{s_3}$ trajectory is split into two parts; as a result $\vec{s_1}$ appears to permute with $\vec{s_2}$. When the intermediate circle is reached ($V_0 = 0.64$) the $\varepsilon = -1$ type of trajectory starts appearing (dotted line). For $V_0 = 0.35$, which is below the intersection of the left inner with the intermediate circle, the $\varepsilon = -1$ $\vec{s_1}$ and $\vec{s_2}$ trajectories reach A_2 and A_1A_3 respectively. Finally, when the right inner circle is reached ($V_0 = 0.28$) the $\vec{s_3}$ trajectory reaches A_2, the $\vec{s_2}$ trajectory intersects the A_1A_3 axis in the compressional quadrant and splits into two parts again and the $\vec{s_1}$ trajectory splits into two parts; this time both $\vec{s_1}$ and $\vec{s_3}$ seem to permute with $\vec{s_2}$.

In the case $\delta = 0.55$ (Fig. 3.12), the transitions occur in a different order, giving rise to different trajectory types. The $\varepsilon = -1$ trajectories appear before any of the inner circles is reached, creating mixed trajectories ($\varepsilon = -1$ and $\varepsilon = +1$) ($V_0 = 0.6$) which look like higher value trajectories ($V_0 = 0.8$). Trajectories where $\vec{s_1}$ splits into two parts, $\vec{s_2}$ intersects A_1A_3 in the compressional

quadrant and unites in one part and $\vec{s_3}$ reaches A_2, appears next ($V_0 = 0.5$). Trajectories where $\vec{s_1}$ and $\vec{s_3}$ are split and reach A_2 while $\vec{s_2}$ is also split appear ($V_0 = 0.445$) before $\varepsilon = -1$ trajectories include A_2 for $\vec{s_1}$, A_1A_3 for $\vec{s_2}$ ($V_0 = 0.4$).

III.8.8. Normal stress level curves types

There are only 3 types of normal stress level curves and they are all displayed in the case $\delta = 0.3$ (Fig. 3.13).

The highest value, $V_0 = 1$, is reached for $\vec{s_1}$ in A_3 (i.e. normal to the fault plane, as expected) and $\vec{s_2}$, $\vec{s_3}$ within the fault plane (Fig. 3.6). For smaller values ($V_0 = 0.8$) $\vec{s_1}$ describes a closed trajectory within the dilatational quadrant while $\vec{s_2}$ and $\vec{s_3}$ describes trajectories that are located within the compressional quadrant and include A_2. As the value decreases ($V_0 = 0.6$), $\vec{s_1}$ and $\vec{s_2}$ describe trajectories including A_2 and within the dilatational quadrant while $\vec{s_3}$ describes a closed trajectory within the compressional quadrant. Finally, for even smaller values ($V_0 = 0.4$) the situation looks similar but the $\varepsilon = -1$ part of the trajectory no longer exists.

III.8.9. H_* level curves types

There are 13 types of H_* level curves. 12 of them are displayed by considering the cases $\delta = 0.2$ (Fig. 3.14), $\delta = 2/3$ (Fig. 3.15) and $\delta = 0.8$ (Fig. 3.16). The extra cases, when compared to τ, correspond to the further complication that the line $H_* = V_0$ may in part correspond to negative shear stress values, therefore in part not be solution. Beside that aspect, which mainly create new level curve types by removing these parts of the trajectories that correspond to negative shear stress, the types of curves are similar to those for $\tau_* = V_0$. A significant difference is that at maximum value, $V_0 = 1$, $\vec{s_1}$ $\vec{s_2}$ and $\vec{s_3}$ are located in P_f, B and T_f instead of P, B and T.

III.8.10. Maps

Maps of t^+ or t^- in the R_G domain are obtained by superposing the level curves for a fixed δ. Example of such maps are shown for different values of δ for τ_* (Fig. 3.17), σ_{n*} (Fig. 3.18) and H_* (Fig. 3.19).

Note that for any function t^+, the $\vec{s_1}$ map is independent of δ on the A_1A_3 axis. This corresponds to $\vec{s_2}$ within the fault plane (in A_2) and therefore to contacts with the outer Mohr's circle which are independent of δ (or σ_2).

The t^+ and t^- level curves connect on $D(\theta_1)$, $D''(\theta_1)$ and $D'''(\theta_1)$ for $\vec{s_1}$, $\vec{s_2}$, and $\vec{s_3}$ respectively. The $\vec{s_1}$ maps for t^+ and t^- cover the same domain, R_G, that is included in the dilatational quadrant and limited by the fault plane and $D(\theta_1)$. The $\vec{s_2}$ maps for t^+ and t^- cover different domains separated by $D''(\theta_1)$ and whose reunion is the whole space. The $\vec{s_3}$ maps are included in the compressional quadrant, and the reunion of the t^+ and t^- domain covers the area between the fault plane and $D(\theta_2)$ where:

$$\theta_2 = 2 \operatorname{Arctan}\sqrt{1- \delta} \qquad (3.37)$$

This reflects that the symmetry between $\vec{s_1}$ and $\vec{s_3}$ corresponds to that between δ and $1-\delta$.

The $\vec{s_1}$ maps for τ_* and H_* display again the difference between the $\varepsilon = +1$ and the $\varepsilon = -1$ case: τ_*^+ and H_*^+ reach their maximum, 1, in P and P_f respectively and the whole map represent a hill around that point; τ_*^- and H_*^- reach theirs, which is smaller than 1 (Table 3.3), either in A_2 (as τ in the case $\delta = 0.1$ or H in the case $\delta = 0.2$), or inside $D(\theta_1)$ (as τ in the case $\delta = 0.3$ or H in the case $\delta = 2/3$) and the P or P_f location corresponds to a saddle point. Also τ_*^+ and τ_*^- reach their minimum, zero, either in A_3 or on $C(\pi/2)$ while H_*^+ and H_*^- reach it only in A_3.

III.9. CONCLUSIONS

(1) The geometrical constraint constrains only $\underline{\underline{T}}_d$, therefore only δ and the orientation of $\vec{s1}$, $\vec{s2}$, $\vec{s3}$.

(2) When δ is fixed and the geometrical constraint is satisfied $\vec{s1}$ belongs to the R_G region within the dilatational quadrant and bounded by the fault plane and $D(\theta_1)$, $\vec{s3}$ belongs to the region within the compressional quadrant that is bounded by the fault plane and $D(\theta_2)$ where θ_2 corresponds to $1-\delta$ (Eq. 3.37), and $\vec{s2}$ can have any orientation in space.

(3) If δ is not known, the union of all the R_G regions for all possible δ values adds up to the whole dilatational quadrant: $\vec{s1}$ can therefore lie anywhere in it [McKenzie, 1969]. This sole result can be demonstrated much more rapidly by noticing that the scalar products $\vec{s1} \bullet \vec{e3}$ and $\vec{s1} \bullet \vec{\tau}$ have same sign [Angelier and Mechler, 1977]. For each position of $\vec{s1}$ within that dilatational quadrant, a whole range or orientations of ($\vec{s2}$, $\vec{s3}$) that correspond to the δ dependence of ψ_1 and ψ_2, is allowed.

(4) If δ is fixed, the magnitude of τ_{d*}, σ_{nd*}, and H_{d*} can be mapped as a function of the position of $\vec{s1}$, $\vec{s2}$, and $\vec{s3}$. Two cases ($\varepsilon = +1$ and $\varepsilon = -1$) must be distinguished. These maps can then be used to distinguish what solutions are mechanically acceptable. Section IV and V will concentrate on a friction law of the type $H = V_0$. The problem will then come to choose one of the H level-curves described here, thereby further constraining the solution tensor. This could however be extended to other failure criteria; for instance, the study of the τ level-curves would yield the solution tensors for a Tresca [1868] criteria: $\tau = V_0$.

IV

MECHANICAL CONSTRAINT

IV.1. INTRODUCTION

This section formulates the simplest realistic failure criterion [Coulomb, 1776] and recalls its consequences. Although this paper concentrates on frictional sliding on a pre-existing plane of weakness, it is useful to briefly review the constraint on stress tensor for failure in intact rocks. This mechanical constraint is then combined with the geometrical constraint in direct and inverse problems that can be solved simply. The remaining three dimensional inverse problem will be treated in Section V.

IV.2. FAILURE

Coulomb's [1776] failure criteria assumes that the failure envelope [Mohr, 1900] is a straight line in Mohr's [1882] (σ_n, τ) plane (Fig. 4.1a)[Handin, 1969, Jaeger and Cook, 1979]:

$$\tau = \tau_0 + \tan\varphi_0 \bullet \sigma_n \qquad (4.1)$$

where φ_0 is the angle of internal friction and τ_0 the cohesive shear stress. Even though experiments have shown that the failure envelope is concave [Byerlee, 1967], this linear approximation remains acceptable within limited stress ranges and attractive because of its simplicity.

IV.2.1. Direct problem

Failure occurs when there is a plane orientation for which the state of stress corresponds to the failure criterion (Eq. 4.1), therefore when the outer Mohr's [1882] circle is tangent to the straight line representing that failure criterion (Fig. 4.1.a). For any point on this outer circle, $\vec{s_2}$ is within the fault plane therefore:

$$\vec{s_2} \perp \vec{e_3} \qquad (4.2)$$

The tangence implies first that the angle α_1 between the fault plane normal $\vec{e_3}$ and $\vec{s_1}$ is:

$$\alpha_1 = \varphi_0/2 + \pi/4 \qquad (4.3)$$

and second that :

$$\frac{\sigma_1 - \sigma_3}{\sigma_1 + \tau_0/\tan\varphi_0} = \frac{2\sin\varphi_0}{1+ \sin\varphi_0} \qquad (4.4)$$

Finally, the slip vector $\vec{e_1}$ must be parallel to the shear stress on the fault plane [Wallace, 1951; Bott, 1959; McKenzie, 1969], so that :

$$\vec{e_1} \perp \vec{s_2} \qquad (4.5)$$

The constraints (4.2) and (4.3) define 2 conjugate fault planes and are the basis of Anderson's [1951] theory of faulting; (4.5) defines the orientation of the slip within each of these fault planes; (4.4) indicates the relative level of stress necessary to cause failure.

IV.2.2. Inverse problem

Starting from the fault plane and slip vector $\vec{e_1}$ the four former constraints uniquely define the principal stress orientations at failure: $\vec{s_1}$, $\vec{s_2}$, $\vec{s_3}$ are in positions that we define as P_f, B, T_f (Fig. 4.1.b). The angle $(\pi/4-\varphi_0/2)$ between P_f and the slip vector $\vec{e_1}$ is always much smaller than that of $\pi/4$ between the P axis and $\vec{e_1}$. The orientations of $\vec{s_1}$ and $\vec{s_3}$ at failure will be defined as P_f and T_f respectively. The position of these axes depends then only on the choice of φ_0. Moreover failure indicates that the parameters s' defined as:

$$s' = \frac{\sigma_1 - \sigma_3}{\sigma_1 + \tau_0/\tan\varphi_0} \qquad (4.6)$$

has reached a critical value, s_c, that depends only on φ_0:

$$s_c = \frac{2\sin\varphi_0}{1+\sin\varphi_0} = \frac{2\tan\varphi_0}{\tan(\varphi_0/2+\pi/4)} \qquad (4.7)$$

The parameter s' and the principal stress orientation are all the information that can be derived about the stress tensor. Neither σ_2, which does not play any role in this theory, nor absolute stress magnitudes can be evaluated. Finally, two problems may be encountered if one tries to apply these results to fault plane solutions:

(1) if the rocks that failed are not known, then φ_0 will be poorly constrained (Fig. 4.2) and so will be the orientations of $\vec{s_1}$ and $\vec{s_3}$ and the values of s';

(2) it will often be difficult to distinguish the auxiliary plane from the fault plane.

In seismology the P, B, and T axis are assumed to represent the positions of $\vec{s_1}$, $\vec{s_2}$, $\vec{s_3}$ because they display enough spatial regularity, and probably also because they do not necessitate to distinguish the fault plane from the other nodal plane [Honda and Masatuka, 1952; Scheidegger, 1964]. However this correspond to a maximum shear stress failure criterion (Fig. 4.3) which, if reasonable for metals [Tresca, 1868], is unrealistic for crustal rocks [Wallace, 1951; Jaeger and Cook, 1979].

IV.3. FRICTION

IV.3.1. Formulation

During slippage on a pre-existing plane of weakness the basic law of friction [Amonton, 1699; Coulomb, 1776] can also be written as:

$$\tau = \tau_0 + \tan\varphi_0 \bullet \sigma_n \qquad (4.8)$$

This looks like the failure criterion (Eq. 4.1) except that this law applies to the plane of weakness only, as opposed to any plane as in the case of failure. This results in three significant differences:

(1) φ_0 is now the angle of external friction, which is generally much smaller than the angle of internal friction (Fig 4.2).

(2) τ_0 has also a usually smaller value than for failure;

(3) The contact between the straight line representing Eq. 4.8 in the (σ_n, τ) plane does not necessarily occur on the outer Mohr's circle but generally below it (Fig. 4.4a), so that $\vec{s_2}$ is not necessarily within the fault plane.

As a consequence of (1) and (2) friction on a plane of weakness is likely to occur before a state of stress high enough to cause failure is reached; as expressed by (3) the orientation of the stresses and of the fault plane are not tightly related since the latter one is not, as in the case of failure, a consequence of the former [Wallace, 1951; Talobre, 1957; Bott, 1959; Jaeger, 1960, Donath, 1964; Handin, 1969; McKenzie, 1969].

The friction law holds only if the normal stress is compressive:

$$\sigma_n > 0 \tag{4.9}$$

which is guaranteed for all plane orientations as long as:

$$\sigma_3 > 0 \text{ or } s < 1 \tag{4.10}$$

There are, however, two aspects that are simpler in the case of friction: (1) actual measurements show this linear relationship to be accurate [Byerlee, 1967], and (2) at relatively high stresses ($\sigma_3 > 50$ bars or depth > 300 m if the pore pressure is hydrostatic) the coefficients τ_0 and φ_0 for maximum friction are fairly independent of the rock type except for clays [Byerlee, 1978]:

$$\varphi_0 = 40.4° \quad \text{and} \quad \tau_0 = 0 \quad \text{if } \sigma_n \leq 200 \text{ MPa} \tag{4.11}$$

$$\varphi_0 = 31° \quad \text{and} \quad \tau_0 = 60 \text{ MPa} \quad \text{if } \sigma_n \geq 200 \text{ MPa} \tag{4.12}$$

In-situ stress measurements are consistent with these laboratory results [Brace and Kohlstedt, 1980; Zoback and Healy, 1984].

IV.3.2. Two dimensional direct problem

Mohr's [1882] domain is reduced to the circle of diameter σ_1-σ_3 (Fig. 4.4a) and sliding occurs only at the two points of intersection with the friction line, then, using s' (Eq. 4.6):

$$s' = \frac{2\sin\varphi_0}{\sin\varphi_0 + \sin(2\alpha_1 - \varphi_0)} \tag{4.13}$$

and the two solutions to this equation, α_1 and α'_1, define the orientations of the only two planes on which friction can occur [Talobre, 1957; Jaeger, 1959, 1960, 1962, 1971; Donath, 1964; Raleigh et al., 1972; Jaeger and Cook, 1979].

IV.3.3. Three dimensional direct problem

The stress tensor being given, two elements are to be determined.

First the orientations of the fault planes that can slip, i.e., on which the friction law is satisfied. Wallace [1951] and, more comprehensively, Jaeger and Rosengren [1969] solved this

question and showed that these orientations display a strong dependence on the value of the ratio δ (Eq. 2.6).

Second the slip orientation within the fault plane, which according to the geometrical constraint, should be the same as that of the shear stress applied to that fault plane [Wallace, 1951; Bott, 1959]. Even once the principal stress directions are fixed, the slip spans a whole range of directions depending only on the value of the ratio δ [Bott, 1959]. The extreme possible directions correspond to the degenerate cases $\sigma_2=\sigma_1$ or $\sigma_2=\sigma_3$ (i.e., $\delta = 0$ or $\delta = 1$) which can be treated as a two dimensional case [Wallace, 1951; Bott, 1959].

IV.3.4. Two dimensional inverse problem

The slip vector $\vec{e_1}$ being given, for Eq.4.13 to have solutions it is necessary that:

$$s' \geq s_c \tag{4.14}$$

where s_c is defined as in Eq. 4.7. For the friction angle of Eq. 4.12:

$$s_c = 0.679 \tag{4.15}$$

For any s' satisfying Eq. 4.14, there are two possible positions for $\vec{s_1}$ that correspond to the two solutions α_1 and α'_1 of Eq. 4.13 and that satisfy:

$$\alpha_1 \geq \varphi_0 \tag{4.16}$$

$\vec{s_1}$ is therefore constrained to belong to a bounded domain (the shaded area of Fig. 4.4b) and s' is constrained to satisfy $s' \geq s_c$. Moreover, to each position of $\vec{s_1}$ within the authorized domain corresponds a unique value of s' given by Eq. 4.13 and at lowest stress difference, $s' = s_c$, $\vec{s_1}$ is on P_f, at $\varphi_1 = \varphi_0/2 + \pi/4$ from the normal.

IV.3.5. Degenerate three dimensional inverse problem

These cases are not only simple to study but also provides limiting cases for the general three dimensional case as inferred by Wallace [1951] and supported by this paper (Section V).

If $\sigma_2 = \sigma_3$ ($\delta = 1$), the geometrical constraint is satisfied only if $\vec{s_1}$ is either on the A_1A_3 arc or within the fault plane (Eq. 3.6). Because the second possibility corresponds to zero shear stress, it cannot satisfy the frictional constraint. Therefore $\vec{s_1}$ must be on the A_1A_3 arc and, because Mohr circle is identical to that of a two dimensional case the angle of $\vec{s_1}$ with $\vec{e_3}$ is then controlled by Eq. 4.13. To each position of $\vec{s_1}$ on that arc corresponds a value of s' and a whole great circle of pole $\vec{s_1}$ for $\vec{s_2}$ and $\vec{s_3}$, since they can be rotated freely around $\vec{s_1}$ (Fig. 4.5a). At the lowest value that allows sliding, $s' = s_c$, $\vec{s_1}$ is on the P_f axis.

Similarly, if $\sigma_2 = \sigma_1$ ($\delta = 0$) $\vec{s_3}$ is constrained by the slip to be in the A_1A_3 plane and $\vec{s_1}$ and $\vec{s_2}$ describe great circles around it (Fig. 4.5b). These circles are $C(\alpha_1)$ and $C(\alpha'_1)$ where α_1 and α'_1 are solutions of Eq. 4.13. When $s' = s_c$, $\vec{s_3}$ is on the T_f axis.

In both cases, s' can be contoured within the area spanned by $\vec{s_1}$, $\vec{s_2}$ and $\vec{s_3}$.

IV.4. REDUCTION TO $\tau_0 = 0$

The study of a Coulomb [1776] law can be reduced to the case $\tau_0 = 0$ since if $\underline{\underline{T}}$ is solution of the Eq. 4.1 or 4.8 then $\underline{\underline{T}}'$ defined as:

$$\underline{\underline{T}}' = \underline{\underline{T}} + \frac{\tau_0}{\tan\varphi_0} \bullet \underline{\underline{I}} \qquad (4.17)$$

is solution of the same constraint where $\tau_0 = 0$ [Jaeger and Rosengren, 1969].

IV.5. ISOTROPY

The fundamental difference between the two processes described above is not that between failure and friction, but that between isotropic and anisotropic material. A more rigorous terminology would replace "failure" and "friction" respectively by "failure within an isotropic material" and "failure within a material rendered anisotropic by a single plane of weakness" where failure would be taken in a broad sense that includes fresh failure as well as frictional sliding since the only difference between the two is the numerical values of τ_0 and φ_0. Indeed, an isotropic material that is fractured along all possible orientations behaves like a weak intact material because the fracturation did not remove the isotropy and it is then properly described by Section IV.2, while a layered, therefore anisotropic, intact material is properly described by Section IV.3 [Talobre, 1957; Jaeger and Cook, 1979].

V

THE THREE DIMENSIONAL INVERSE PROBLEM WITH GEOMETRICAL AND FRICTIONAL CONSTRAINTS TOGETHER

V.1. REDUCTION

For $\underline{\underline{T}}$ to satisfy the friction law (Eq. 4.8 and 4.10) and the geometrical constraint (Eq. 3.1 and 3.2) it is necessary and sufficient that $\underline{\underline{T}}'$ as defined in Eq. 4.17 satisfies the friction law with $\tau_0 = 0$ and that $\underline{\underline{T}}_d$ as defined in Eq. 2.3 satisfies the geometrical constraint. But because:

$$\underline{\underline{T}}_d = \underline{\underline{T}}_d' \tag{5.1}$$

for $\underline{\underline{T}}$ to satisfy both constraints, it is necessary and sufficient that $\underline{\underline{T}}'$ satisfies the same constraints with $\tau_0=0$.

We will therefore henceforth limit our study to the case $\tau_0 = 0$. Since in real situations τ_0 is small compared to σ_1, the results can be directly applied. However, if τ_0 is not negligible, it is sufficient to substitute in all what follows $\underline{\underline{T}}'$ for $\underline{\underline{T}}$ and s' for s with:

$$s' = (\sigma_1' - \sigma_3')/\sigma_1' = (\sigma_1 - \sigma_3)/(\sigma_1 + \tau_0/\tan\varphi_0) \tag{5.2}$$

In other terms the discussion for $\tau_0 = 0$ can be extended to $\tau_0 \neq 0$ simply by changing the definition of s originally given in Eq. 2.7 into the one given later in Eq. 4.6

V.2. OVERVIEW

Applying the frictional constraint (Eq. 4.8) on the fault plane when the geometrical constraint (Eq. 3.1 and 3.2) is already satisfied and when $\tau_0 = 0$ yields:

$$H = t^E_{13} - \tan\varphi_0 \bullet t^E_{33} = 0 \tag{5.3}$$

or:

$$H_d = t^E_{d13} - \tan\varphi_0 \bullet t^E_{d33} = (1/s - 1) \bullet \tan\varphi_0 \tag{5.4}$$

The set of solutions is a vectorial space of dimension 4:

$$T^E = \begin{vmatrix} t^E_{11} & t^E_{12} & \tan\varphi_0 \bullet t^E_{33} \\ t^E_{12} & t^E_{22} & 0 \\ \tan\varphi_0 \bullet t^E_{33} & 0 & t^E_{33} \end{vmatrix} \tag{5.5}$$

where the t^E_{ij} are arbitrary. This time, isotropic tensors, $\alpha\underline{\underline{I}}$, are <u>not</u> solutions because of the

frictional constraint.

If we consider the decomposition of $\underline{\underline{T}}$ into $\underline{\underline{I}}$ and $\underline{\underline{T}}_d$, the general solution is:

$$\underline{\underline{T}}(\theta, \varphi, \psi, \sigma_1, \delta) = \sigma_1 \bullet (1 - s) \bullet \underline{\underline{I}} + \sigma_1 \bullet s \bullet \underline{\underline{T}}_d (\theta, \varphi, \psi = \psi_1 \text{ or } \psi_2, \delta) \qquad (5.6)$$

with the only 3 requirements that:

(1) $(\theta,\varphi) \in R_G$;

(2) either $\psi_1(\theta,\varphi,\delta)$ or $\psi_2(\theta,\varphi,\delta)$ have been substituted for ψ in $\underline{\underline{T}}_d(\theta,\varphi,\psi,\delta)$; and

(3) $\underline{\underline{T}}_d(\theta,\varphi,\delta)$ satisfies the frictional constraint (Eq. 5.4).

Because of (1) and (2), $\underline{\underline{T}}_d(\theta,\varphi,\delta)$ already satisfies the geometrical constraint; it is therefore sufficient to find $\underline{\underline{T}}_d(\theta,\varphi,\delta)$ that satisfies (3).

Because the two constraints (Eq. 3.1 and 4.8) are homogeneous, a scaling factor on stress magnitudes doesn't affect the problem; this can be seen in Eq. 5.5 where the t^E_{ij} can be multiplied by any constant or in Eq. 5.6 where σ_1 remains unconstrained. There are then 5 relevant parameters to this problem: $(\theta,\varphi,\psi,s,\delta)$ and two constraints: Eq. 3.1 and 4.8. The number of degree of freedom is then not reduced compared to the geometrical constraint alone because adding the new frictional constraint requires to add a new parameter: s. Therefore we can only expect to express 2 parameters as a function of the 3 others. We can then express φ and ψ as a function of θ, s, and δ; this implies that once s and δ are fixed, $\vec{s_1}$, $\vec{s_2}$, $\vec{s_3}$, will each describe a trajectory parameterized by θ. There is then a relationship between magnitudes (i.e., s,δ) and orientations (i.e., θ,φ,ψ). We will describe this relationship by discussing the shape of these trajectories as a function of (s,δ), extending what was done in the two dimensional case where the position of $\vec{s_1}$ was described as a function of s (Section IV.3.4).

V.3. METHOD

Once the geometrical constraint is satisfied, H_d is a function of $(\theta,\varphi,\delta,\varepsilon)$ only (Table 3.1). Using H_*, that is a normalized version of H_d (Table 3.1), the frictional constraint (Eq. 5.4) becomes:

$$H_*(\theta,\varphi,\delta,\varepsilon) = s_c/s \qquad (5.7)$$

where, as in Eq. 4.7:

$$s_c = \frac{2\sin\varphi_0}{1+\sin\varphi_0} = \frac{2\tan\varphi_0}{\tan(\varphi_0/2+\pi/4)} \qquad (5.8)$$

This formulation has the advantage on Eq. 5.3 that s is already separated from the 3 other parameters (θ,φ,δ). In what follows, the discussion and figures are made for $\varphi_0 = 31°$ (Eq. 4.12) and therefore:

$$s_c = 0.679 \qquad (5.9)$$

V.4. SOLUTIONS AT δ AND s FIXED

Once s and δ are fixed, then to satisfy Eq. 5.7, $\vec{s_1}$, $\vec{s_2}$, $\vec{s_3}$ must be on the trajectories that correspond to the H level curve $H_* = V_0$ already described in Section III.4, with:

$$V_0 = s_c/s \tag{5.10}$$

We can then reformulate the discussion in (δ,V_0) done for H_* in terms of (δ, s) this time. The figure in Mohr's [1882] domain depends on only two parameters: the stress difference, s, which determine the friction line to be intersected and δ, which defines the relative size of the inner circles. By using $\underline{\underline{T}}_d$ instead of $\underline{\underline{T}}$, we are replacing a figure where the friction line would be fixed and Mohr's circles varying in position and size, with a fixed outer Mohr circle of diameter 1 and a friction line of varying position but constant slope; this makes superposition much easier. Using Eq. 5.10 the friction lines are labeled by their associated s value (Fig. 5.1) instead of V_0 (Fig. 3.7). The $\vec{s_1}$, $\vec{s_2}$, $\vec{s_3}$ solution trajectories correspond to that part of the straight line representing the friction law that is between the outer and inner Mohr's circles (Fig. 5.1).

V.5. CRITICAL CASES

If s is smaller than s_c, the friction line does not intersect the outer Mohr's circle, and therefore slip cannot occur. This corresponds to searching a level curve of H_* with $V_0 > 1$ that does not exist .

The smallest value of stress difference s for which the friction line intersects Mohr's circle is s_c. In other terms, for sliding to occur the stress difference must have reached the threshold s_c. For that value, $\vec{s_1}$, $\vec{s_2}$, $\vec{s_3}$, coincide with P_f, B, T_f (Fig. 5.1) unless the tensor is degenerate (cases $\delta = 0$ or $\delta = 1$). P_f, B, T_f is then the most efficient orientation of the principal stresses, that is, that which produces slip at minimum stress level.

As s increases, the friction line slices deeper into Mohr's circles, and the nature of the trajectories of $\vec{s_1}$, $\vec{s_2}$, and $\vec{s_3}$ changes. Two critical cases that correspond to the tangence of the friction line with the two inner circles occur (Fig. 5.1). Using Eq. 5.10, the corresponding critical relationships in the (δ, V_0) plane (Fig. 3.10) are transferred to the (δ, s) plane (Fig. 5.2).

Also, if the friction line does not intersect the intermediate circle that passes through $(1-\delta)/2$ and 1 on the σ_n axis, i.e., if the value of s is sufficiently small so that V_0 is greater than the absolute maximum of H_*^- (Table 3.3), then the trajectory is made only of an H_*^+ solution.

If the friction line does intersect the intermediate circle, i.e., if the value of s is large enough so that V_0 is smaller than the absolute maximum of H_*^-, then the trajectory is made in part of an H_*^+ solution and in part of an H_*^- solution; the two parts connect on $D(\theta_1)$ for $\vec{s_1}$ and on the corresponding curves, $D''(\theta_1)$ and $D'''(\theta_1)$, for $\vec{s_2}$ and $\vec{s_3}$ (Fig. 5.3). For $\vec{s_1}$, one solution is "reflected" into the other at the contact of $D(\theta_1)$. For $\vec{s_2}$, "refraction" occurs and $D''(\theta_1)$ separates the domain of each solution. For $\vec{s_3}$, crossing $D'''(\theta_1)$ may or may not result in a change of solution type. Because this difference does not seem to have physical meaning, even though it has to be taken into account in the substitution of ψ for correct results, the discussion can be simplified if $\varepsilon = +1$ ($\psi = \psi_1$) and $\varepsilon = -1$ ($\psi = \psi_2$) types of solution are not distinguished.

Finally, because applying a friction law requires a compressive environment:

$$0 \le s < 1 \tag{5.11}$$

V_0 must satisfy:

$$s_c < V_0 \tag{5.12}$$

This adds a fifth critical case: the lowest friction line that corresponds to $s = 1$ or $V_0 = s_c$ and passes through the origin. This is expected since the Mohr circle of a compressive tensor i.e.: $\sigma_3 \ge 0$, will never be intersected by a friction line below the point $(\sigma_3, 0)$ in the (σ_n, τ) plane. As a

result there are fewer cases to discuss than for H_* and we are left with only 8 domains in the (δ, s) plane (Fig. 5.2) from the original 13 domains in the (δ,V_0) plane of H_* (Fig. 3.10). The corresponding 8 types of solution trajectories are a subset of the 13 types described for H_* (Fig. 3.14 to 3.16 and 3.19).

By not distinguinshing the $\varepsilon = +1$ from the $\varepsilon = -1$ ($\psi = \psi_2$) types of solution, we are left with only four critical cases, each of which corresponds to a relationship between s and δ. Figure 5.4 shows these limiting cases in Mohr's domain for the stress magnitudes and on Lambert's [1772] projection for the corresponding orientations of $\vec{s_1}$, $\vec{s_2}$, $\vec{s_3}$. The corresponding relationships divide the (δ, s) plane into five areas (Fig. 5.5), four of which correspond to the four types of $\vec{s_1}$, $\vec{s_2}$, $\vec{s_3}$ trajectories. The evolutions between these types of trajectories can be easily understood if one concentrates on cross sections of the (δ, s) planes at either δ or s constant.

V.6. TRAJECTORIES AT δ FIXED

The representation at fixed δ has the advantage that Mohr's circles are fixed, that therefore as s varies, only the friction envelope moves (Fig. 5.1, 5.4, 5.6, 5.7), and that the $\vec{s_2}$ trajectories for different s do not cross each other (Fig. 5.8), but the drawback that the $\vec{s_1}$ and $\vec{s_3}$ trajectories for different s do cross each other.

As the friction envelope slices more and more deeply into Mohr's circles, the corresponding solution orientations of $\vec{s_1}$, $\vec{s_2}$, $\vec{s_3}$ for 2 cases: $\delta = 0.2$ (Fig. 5.6) and $\delta = 0.8$ (Fig. 5.7) are described.

The smallest value of stress differences, s, for which the friction line intersect Mohr's circle is s_c (Eq. 5.8). Below that value there cannot be any movement on the fault plane. For that value, $\vec{s_1}$, $\vec{s_2}$, $\vec{s_3}$, coincide with P_f, B, T_f (Fig. 5.4).

As s increases above s_c, the friction line slices deeper into Mohr's circle and $\vec{s_1}$, $\vec{s_2}$, $\vec{s_3}$ start moving away from P_f, B, T_f. $\vec{s_2}$ starts then to move away from the fault plane (Fig. 5.6 with $s = 0.7$ and Fig. 5.7 with $s = 0.8$).

If s increases more the friction line will start intersecting one of the two lower circles and this will have different effects according to which circle is intersected.

If the circle of diameter $\sigma_2 - \sigma_3$ is hit then $\vec{s_1}$ reaches the fault plane in A_2 and $\vec{s_2}$ replaces $\vec{s_1}$ on A_1A_3, $\vec{s_3}$ keeping its position on A_1A_3 (Fig. 5.6 with $s = 0.9$). This happens if and only if (Fig. 5.4 and 5.5):

$$s \geq s_c/[1-(1-s_c)\delta] \qquad (5.13)$$

When that circle is not intersected, the closer to it the friction line approaches, the more $\vec{s_1}$ and $\vec{s_2}$ tend to exchange roles.

If the circle of diameter $\sigma_1 - \sigma_2$ is hit then $\vec{s_3}$ reaches the fault plane and $\vec{s_2}$ and replaces $\vec{s_3}$ on the A_1A_3 plane, $\vec{s_1}$ keeping its position on A_1A_3 (Fig. 5.7 with $s = 0.9$); this happens if and only if (Fig. 5.4 and 5.5):

$$s \geq s_c/\delta \qquad (5.14)$$

The closer to that circle the friction line approaches, the more $\vec{s_3}$and $\vec{s_2}$ tend to exchange roles.

The order in which theses events occur as s increases depends only on the size ratio of the different inner circles, then on δ. In general the higher the stress difference, the further away from

P_f, B and T_f must $\vec{s_1}$, $\vec{s_2}$ and $\vec{s_3}$ be. In other words if the stress difference is high, $\vec{s_1}$, $\vec{s_2}$, $\vec{s_3}$ must have been poorly oriented for the movement not to occur earlier (at lower s), and according to which inner circle is bigger, $\vec{s_2}$ will tend to exchange roles with either $\vec{s_1}$ or $\vec{s_3}$. The highest value that s can reach in a compressive environment is 1, which corresponds to a friction envelope going through σ_3 on the σ_n axis (Fig. 5.4).

Globally, since the orientations satisfying our requirement (Fig. 5.8, 5.6c and 5.7c) satisfy the geometrical constraint, $\vec{s_1}$ is limited to the region defined as R_G, as demonstrated by McKenzie [1969]. Furthermore, the frictional constraint forbids some of this region, as can be seen by splitting it into 3 areas (Fig. 5.9):

- an area where both solution $\varepsilon = +1$ and $\varepsilon = -1$ are allowed. For any location of $\vec{s_1}$ within that area, two orientations of $\vec{s_2}$, $\vec{s_3}$, corresponding to ψ_1 and ψ_2, around it are then allowed;

- an area where only $\varepsilon = +1$ solutions are allowed and where to any location of $\vec{s_1}$ corresponds only one acceptable orientation of $\vec{s_2}$, $\vec{s_3}$ corresponding to ψ_1;

- an area where no solutions exist and where the tensors that satisfy the geometrical constraint do not satisfy the frictional constraint. This area corresponds to the solutions that would be accepted by an inversion based on the simple geometrical constraint but that are mechanically unsound because they would yield too small a shear stress compared to the normal stress across the fault plane to produce any sliding.

These areas are limited by the contour corresponding to:

$$s = 1 \quad \text{or} \quad V_0 = s_c \tag{5.15}$$

$$s = s_c \quad \text{or} \quad V_0 = 1 \tag{5.16}$$

V.7. TRAJECTORIES AT s FIXED

This representation has qualities that are converse of those at constant δ: the drawback is that as δ varies, so do the Mohr's circles (Figs. 5.10 and 5.11) and that the $\vec{s_2}$ trajectories tend to cross each other (Fig. 5.12); the advantage is that the $\vec{s_1}$ and $\vec{s_3}$ trajectories for different δ do not cross, a fact that allows to superpose them.

If $s < s_c$ no slippage can occur.

If $s = s_c$, (Fig. 5.12 for $s = 0.68$) the least stress difference for which slippage can occur, three cases can be distinguished:

either $\delta \neq 0$ and $\delta \neq 1$ (i.e., $\sigma_1 \neq \sigma_2$ and $\sigma_3 \neq \sigma_2$) and then $\vec{s_1}$ lies on the P_f axis (Fig. 5.4), a position already recommended by Raleigh et al. [1972], while $\vec{s_2}$ and $\vec{s_3}$ are in B and T_f respectively;

or $\delta = 0$ (i.e., $\sigma_1 = \sigma_2$) and then $\vec{s_1}$ and $\vec{s_2}$ describe the great circle going through P_f and B while $\vec{s_3}$ is in T_f (Fig. 4.5b);

or $\delta = 1$ (i.e. $\sigma_3 = \sigma_2$) and then $\vec{s_2}$ and $\vec{s_3}$ describe the great circle going through T_f and B while $\vec{s_1}$ is in P_f (Fig. 4.5a).

For $s_c < s \leq s_c(2-s_c)$, (Fig. 5.10 and 5.12 for any value $0.68 < s < 0.9$) two cases can be distinguished according to the values of δ: (1) either the inner Mohr's circles are not intersected and the principal stress orientations $\vec{s_1}$, $\vec{s_2}$, $\vec{s_3}$ stay reasonably close from where they are classically

expected, i.e., close to P_f, B, T_f or (2) one of the inner circles is intersected and $\overrightarrow{s_2}$ may interchanges position with either $\overrightarrow{s_1}$ or $\overrightarrow{s_3}$. But, because both inner circles cannot be intersected for any given value of δ, $\overrightarrow{s_2}$ can never exchanges roles with both $\overrightarrow{s_1}$ and $\overrightarrow{s_3}$. Therefore if one of $\overrightarrow{s_1}$ or $\overrightarrow{s_3}$ tends to be delocalized and away from where classically expected, the other one will tend to be localized around its classical position.

For $s_c(2-s_c) \leq s < 1$, (Fig. 5.11 and 5.12 for any value $s \geq 0.9$) the same behavior is observed but there is also a range of value of δ for which both inner circles are intersected and therefore $\overrightarrow{s_2}$ can exchange position with either $\overrightarrow{s_1}$ or $\overrightarrow{s_3}$, i.e., slip can occur on both modes of unexpected stress orientations.

If $s = 1$, the area where $\overrightarrow{s_1}$ can be reaches its maximum extent (Fig. 5.12); its is bounded by a great circle at angle φ_0 from the fault plane normal and by the fault plane itself. However this is a limiting case because it violates a condition of applicability of the friction law: positive normal stress (Eq. 4.10). It corresponds to either $\sigma_1 = \infty$ or $\sigma_3 = 0$. The first case can be safely ruled out because of the finite strength of rocks; the second case, since it applies to effective stress, can correspond to a case where pore pressure is equal to the least principal stress magnitude and is appropriately described by hydrofracturing or tensional cracking as opposed to frictional sliding.

The domains spanned by $\overrightarrow{s_1}$, $\overrightarrow{s_2}$, $\overrightarrow{s_3}$ when s is fixed can be described as follow (Fig. 5.12):

- the set of $\overrightarrow{s_1}$ trajectories which correspond to various values of δ is bounded by two great circles that correspond to the degenerate case $\delta = 0$ ($\sigma_2 = \sigma_1$) (Fig. 4.5b); these are the two great circles $C(\alpha_1)$ and $C(\alpha_1')$, where α_1 and α_1' are the solutions of Eq. 4.13 (Section IV.3.5);

- the limits for $\overrightarrow{s_3}$ can be obtained in the same fashion by the case $\delta = 1$ ($\sigma_2 = \sigma_3$) (Fig. 4.5a);

- the maximum area allowed to $\overrightarrow{s_2}$ is larger than the union of the area for $\overrightarrow{s_1}$ and $\overrightarrow{s_3}$ especially around A_2 (or B axis); its exact boundary is therefore not as simple.

The area spanned by $\overrightarrow{s_1}$, $\overrightarrow{s_2}$, $\overrightarrow{s_3}$ for any value of s includes the area spanned for any smaller value of s. This means the higher the stress difference the worse oriented the principal stresses can afford to be in respect to the fault plane and still cause slippage. The maximum range is therefore obtained for $s = 1$.

The role of σ_2 (or δ) [Bott, 1959; Jaeger and Rosengren, 1969] in the $\overrightarrow{s_1}$ orientation is obvious through the δ dependence of our trajectories at s fixed. As δ goes to 0 (σ_2 becomes close to σ_1) $\overrightarrow{s_1}$ and $\overrightarrow{s_2}$ tend to exchange roles, while as δ goes to 1 (σ_2 becomes close to σ_3) $\overrightarrow{s_3}$ and $\overrightarrow{s_2}$ tend to exchange roles. For $s = s_c$ the only cases where $\overrightarrow{s_2}$ can exchange roles with $\overrightarrow{s_3}$ or $\overrightarrow{s_1}$ are $\delta = 0$ and $\delta = 1$; as s increases above s_c such cases occur for δ further and further away from 0 or 1 (Fig. 5.5).

Therefore, the orientations allowed for $\overrightarrow{s_1}$ and $\overrightarrow{s_3}$ can be globally described as controlled in width by s, and in span by δ.

Within the allowed domain for $\overrightarrow{s_1}$ and $\overrightarrow{s_3}$ each point is reached by one and only one trajectory which simply means that the trajectories do not cross each other. Also, the two types of solutions, $\varepsilon = +1$ and $\varepsilon = -1$ connect nicely and therefore the distinction between them, which correspond to the use of different formulae, doesn't seem physically very important and can be dropped in most discussions.

VI

CONCLUSIONS

(1) When both the geometrical and frictional constraint are required, there are still 4 degrees of freedom among the solution tensors $\underline{\underline{T}}$. One such degree, the scaling factor σ_1, can be removed and the resulting tensor $(1/\sigma_1) \bullet \underline{\underline{T}}$ depends on 5 parameters, θ, φ, ψ, δ, s, and exhibits 3 degrees of freedom. There is then a whole family of solution tensors, but for these tensors there is an interrelation between principal stress magnitudes, δ and s, and orientations, θ, φ, ψ; to a fixed orientation corresponds a relationship between δ and s (Eq. 5.7), and to fixed relative magnitudes, δ and s, corresponds a trajectory for each of $\vec{s1}$, $\vec{s2}$ and $\vec{s3}$

(2) If the lithosphere is isotropically fractured, as assumed by Brace and Kohlstedt [1980], there is always a plane of weakness along the most favorable orientation for frictional sliding, and when failure occurs, it occurs along that plane; it therefore behaves like a weak intact material [Talobre, 1957; Jaeger, 1962]. This is then a "failure" problem and $\vec{s1}$, $\vec{s2}$, $\vec{s3}$ are tightly constrained to be on the P_f, B and T_f axis and s to be equal to s_c, the minimal stress difference that can cause sliding, $s_c = 0.679$ (Eq. 4.15), corresponds exactly to $\sigma_1 \approx 3\sigma_3$ proposed by Brace and Kohlstedt [1980] if one considers, as they did, Byerlee's [1978] friction coefficient (Eq. 4.12). The only exception would be a degenerate tensor where a whole circle would be allowed for either $\vec{s2}$ and $\vec{s1}$ (case $\sigma_2 = \sigma_1$) or $\vec{s2}$ and $\vec{s3}$ (case $\sigma_2 = \sigma_3$).

(3) If the planes of weakness do not span all orientations, but that any orientation is at a small angle to a plane of weakness, then the stress difference, s, is unlikely to reach too high values; then, unless the stress tensor is close to a degenerate case (i.e., unless σ_2 is close to σ_1 or σ_3), $\vec{s1}$, $\vec{s2}$ and $\vec{s3}$ will remain reasonably close to P_f, B and T_f. This explains why the classical P, B, T axes, which are only 15° away from these orientations give reasonable answers [Scheidegger, 1964] despite objections [McKenzie, 1969]. However if the fault plane can be identified, P_f, B and T_f give more accurate estimates, as already suggested by Raleigh et al. [1972] on the basis of a two dimensional study.

(4) In areas where a few major faults are known to be reactivated over and over again the former assumptions might not hold true and s may be limited only by the strength of the rocks. As s increases, $\vec{s1}$ and $\vec{s3}$ may move away from P_f and T_f within the A_1A_3 plane. Furthermore, according to the value of δ, $\vec{s1}$ and $\vec{s3}$ may also go significantly away from that A_1A_3 plane toward the fault plane in A_2, i.e.,the B axis, where $\vec{s2}$ would be expected, while $\vec{s2}$ may go out of the fault plane toward the A_1A_3 plane where $\vec{s1}$ and $\vec{s3}$ would be expected. There is then a tendency for $\vec{s2}$ to exchange role with either $\vec{s1}$ or $\vec{s3}$. The conditions on (δ,s) for such exchanges to be possible are summarized in Fig. 5.5.

(5) If the only available data is a single fault plane, then the stress tensor must verify $s \geq s_c$ and $\vec{s1}$, $\vec{s2}$ $\vec{s3}$ may lie anywhere in the regions allowed for s = 1 (Fig. 6.1a). These areas are significantly smaller than those obtained obtained by considering the geometrical constraint alone [McKenzie, 1969; Angelier and Mechler, 1977]. Moreover, fresh failure is expected to limit the stress difference so as $s \leq s_c' < 1$, where s_c' is determined by the failure properties for intact rocks as opposed to the frictional ones. Data for quartz rheologies [Ohnaka, 1973] suggest that fresh

failure is likely to occur for s above the critical value $s_c' \approx 0.8$. As a result, the principal stress orientations are limited to the more restricted domains obtained for s = 0.8 (Fig 6.1b). It may be useful to remember that that the simple two-dimensional analysis for $\sigma_2 = \sigma_1$ and $\sigma_2 = \sigma_3$ (Fig. 4.5) gives the extreme bounds for the orientation of $\vec{s_1}$ and $\vec{s_3}$ respectively, as suggested by Wallace [1951]. Also, if by other means the orientation of $\vec{s_1}$ is determined, then s and δ are linked (Eq. 5.7) and therefore an estimate of the stress difference, s, can be translated into an estimate of the aspect ratio δ.

(6) If multiple fault planes are available and one assumes that the same stress tensor is responsible for the movement on all of them, two methods can be implemented:

(a) Graphic method: one could intersect the areas allowed to $\vec{s_1}$, $\vec{s_2}$ and $\vec{s_3}$ for each fault plane and so localize the principal stresses orientations. This is an improvement on the dihedra method [Angelier and Mechler, 1977] because the areas to intersect are smaller. Then going back into each fault plane, the determined position of $\vec{s_1}$, would yield an equation in (s, δ) and the resulting overdetermined system in (s, δ) could be solved.

(b) Inverse method: it seems that the extra constraint brought by the friction law allows to invert for s on top of δ, $\vec{s_1}$, $\vec{s_2}$ and $\vec{s_3}$. Unless the tensor is close to a degenerate one, at reasonable stress level $\vec{s_1}$ and $\vec{s_3}$ cannot have a wide range of variation; therefore, in that case, widely different plane orientations would require a higher stress difference than clustered ones. The fault plane orientations therefore contains information not only about δ but also about s and this information could be extracted.

For both methods, the extra frictional constraint reduces the chances of finding an acceptable uniform tensor solution, while it increases the chances of demonstrating the necessity of a spatially or temporally varying tensor.

ACKNOWLEDGMENTS

This work was initiated by W.F. Brace's suggestion to add a frictional law to the commonly used geometrical constraint to further constrain this problem; his course provided also many sources of inspiration. I am grateful to K. Aki, P. Molnar and J.G. Sclater for encouragements and comments, to Mark Gordon for comments on style, to M. McNutt and B. Parsons for free computer access, and to K. Craeger and D. Krowitz for help with the computer system. I am also indebted to D. Forsyth for a very helpful and thorough review. Writing this report was partially funded by a Shell Professorship to J.G. Sclater.

REFERENCES

Amontons, G., De la résistance causée dans les machines, *Mem. Acad. R. Sci. Paris*, 206-222, 1699.

Anderson, E.M., *The dynamics of faulting and dyke formation with applications to Britain*, 2nd ed., 206 pp., Oliver and Boyd, Edinburgh, 1951.

Angelier, J., Sur l'analyse de mesures recueillies dans des sites faillés: l'utilité d'une confrontation entre les méthodes dynamiques et cinématiques, *C. R. Acad. Sci., Ser. D, 281,* 1805-1808, 1975.

Angelier, J., Determination of the mean principal directions of stresses for a given fault population, *Tectonophysics, 56*, T17-T26, 1979a.

Angelier, J., Néotectonique de l'arc egéen, *Spec. Publ. Soc. Geol. Nord., 3*, 418 pp., 1979b.

Angelier, J., and J. Goguel, Sur une méthode simple de détermination des axes principaux des contraintes pour une population de failles, *C. R. Acad. Sci., Ser. D, 288*, 307-310, 1979.

Angelier, J., and P. Mechler, Sur une méthode graphique de recherche des contraintes principales également utilisable en tectonique et en sismologie: la méthode des dièdres droits, *Bull. Soc. Geol. Fr., XIX(6)*, 1309-1318, 1977.

Angelier, J., A. Tarantola, B. Valette, and S. Manoussis, Inversion of field data in fault tectonics to obtain the regional stress, I, Single phase fault populations: a new method of computing the stress populations, *Geophys. J. R. Astron. Soc., 69*, 607-621, 1982.

Armijo, R., and A. Cisternas, Un problème inverse en microtectonique cassante, *C. R. Acad. Sci., Ser. D, 287*, 595-598, 1978.

Armijo, R., E. Carey, and A. Cisternas, The inverse problem in microtectonics and the separation of tectonic phases, *Tectonophysics, 82*, 145-160, 1982.

Bott, M.H.P., The mechanics of oblique slip faulting, *Geol. Mag., 96*, 109-117, 1959.

Brace, W.F., and D.L. Kohlstedt, Limits on lithospheric stress imposed by laboratory experiments, *J. Geophys. Res., 85*, 6248-6252, 1980.

Byerlee, J.D., Frictional characteristics of granite under high confining pressure, *J. Geophys. Res., 72*, 3639-3648, 1967.

Byerlee, J.D., Friction of rocks, *Pure Appl. Geophys., 116*, 615-626, 1978.

Carey, E., Analyse numérique d'un modèle mécanique élémentaire appliqué à l'étude d'une population de failles: calcul d'un tenseur moyen des contraintes à partir des stries de glissement, thèse, 138 pp., Univ. de Paris Sud, 1976.

Carey, E., Recherche des directions principales de constraintes associées au jeu d'une population de failles, *Rev. Geol. Dyn. Geogr. Phys., 21*, 57-66, 1979.

Carey, E., and B. Brunier, Analyse théorique et numérique d'un modèle mécanique élémentaire appliqué à l'étude d'une population de failles, *C. R. Acad. Sci., Ser. D, 279*, 891-894, 1974.

Coulomb, C.A., Sur une application des règles maximis et minimis à quelques problèmes de statique relatifs à l'architecture, *Acad. Sci. Paris Mém. Math. Phys., 7*, 343-382, 1776.

Donath, F.A., Strength variation and deformational behaviour in anisotropic rock, in *State of stress in the earth's crust*, edited by W.R. Rudd, pp. 280-298, American Elsevier, New York, 1964.

Ellsworth, W.L., A general theory for determining state of stress in the earth from fault slip measurements, *Terra Cognita, 2*, 170-171, 1982.

Ellsworth, W.L., and X. Zhonghuai, Determination of the stress tensor from focal mechanism data, *Eos Trans. AGU, 61*, 1117, 1980.

Etchecopar, A., G. Vasseur, and M. Daignieres, An inverse problem in microtectonics for the determination of stress tensors from fault striation analysis, *J. Struct. Geol., 3*, 51-65, 1981.

Euler, L., Du mouvement d'un corps solide quelconque lorsqu'il tourne autour d'un axe mobile, *Mém. Acad. Sci. Berlin*, [16](1760), 176-227, 1767.

Gephart, J.W., and D.W. Forsyth, An improved method for determining the regional stress tensor using earthquake focal mechanism data: application to the San Fernando earthquake sequence, *J. Geophys. Res., 89*, 9305-9320, 1984.

Handin, J., Strength and ductility, in *Handbook of physical constants*, edited by S.P. Clark, Mem. Geol. Soc. Am., vol. 97, 223-289, 1966.

Handin, J., On the Coulomb-Mohr failure criterion, *J. Geophys. Res., 74*, 5343-5348, 1969.

Honda, H., and A. Masatuka, On the mechanisms of the earthquakes and the stresses producing them in Japan and its vicinity, *Sci. Rep. Tohohu Univ., Ser. 5, 4*, 42-60, 1952.

Jaeger, J.C., The frictional properties of joints in rock, *Geofis. Pura Appl., 43*, 148-158, 1959.

Jaeger, J.C., Shear fracture of anisotropic rocks, *Geol. Mag., 97*, 65-72, 1960.

Jaeger, J.C., *Elasticity, fracture and flow*, 2nd ed., 268 pp., Methuen, London, 1962.

Jaeger, J.C., Friction of rocks and stability of rock slopes, *Geotechnique, 21*, 97-134, 1971.

Jaeger, J.C., and N.C. Cook, *Fundamentals of rock mechanics*, 3rd ed., 593 pp., Chapman and Hall, London, 1979.

Jaeger, J.C., and K.J. Rosengren, Friction and sliding of joints, *Proc. Aust. Inst. Min. Metall., 229*, 93-104, 1969.

Lambert, J.H., *Beiträge zum Gebrauche der Mathematik und deren Anwendung, part III*, section 6, Anmerkungen und Zusätze zur Entwerfung der Land- und Himmelscharten, pp. 105-199, Berlin, 1772.

McKenzie, D.P., The relation between fault plane solutions for earthquakes and the directions of the principal stresses, *Bull. Seismol. Soc. Am., 59*, 591-601, 1969.

Michael, A.J., The determination of stress from slip data, faults and folds, *J. Geophys. Res., 89*, 11,517-11,526, 1984.

Mohr, O., Über die Darstellung des Spannungzustandes eines Korperelementes, *Civilingenieure, 28*, 113-156, 1882.

Mohr, O., Welche Umstände bedingen die Elastizitätsgrenze und den Bruch eines Materials, *Z. Ver. Dtsch. Ing., 44*, 1524-1530, 1572-1577, 1900.

Ohnaka, M., The quantitative effect of hydrostatic confining pressure on the compressive strength of crystalline rocks, *J. Phys. Earth, 21*, 125-140, 1973.

Palmer, F., What about friction?, *Am. J. Phys., 17*, 181-187, 327-342, 1949.

Rabinowicz, E., Resource Letter F-1 on friction, *Am. J. Phys., 31*, 897-900, 1963.

Raleigh, C.B, J.H. Healy, and J.D. Bredehoeft, Faulting and crustal stress at Rangely, Colorado, in *Flow and fracture of rocks*, edited by H.C. Heard, I.Y. Borg, N.L. Carter, and C.B. Raleigh, pp. 275-284, Geophys. Monogr. Ser., vol. 16, AGU, Washington, D.C., 1972.

Sassi, W., Analyse numérique de la déformation cassante, thèse de 3ème cycle, 229 pp., Univ. de Paris Sud à Orsay, 1985.

Scheidegger, A.E., The tectonic stress and tectonic motion direction in Europe and Western Asia as calculated from earthquake fault plane solutions, *Bull. Seismol. Soc. Am., 54*, 1519-1528, 1964.

Talobre, J.A., *La mécanique des roches appliquée aux travaux publics*, 444 pp., Dunod, Paris, 1957.

Tresca, Mémoires sur l'écoulement des corps solides, *Mémoires présentés par divers savants*, Acad. Sci., Paris, vol. 18, 733-799, 1868.

Vasseur, G., A. Etchecopar, and H. Philip, Stress state inferred from multiple focal mechanisms, *Ann. Geophys., 1*, 291-298, 1983.

Wallace, R.E., Geometry of shearing stress and relation to faulting, *J. Geol., 59*, 118-130, 1951.

Zoback, M.D., and J.H. Healy, Friction, faulting, and in situ stress, *Ann. Geophys., 2*, 689-698, 1984.

TABLES

TABLE 2.1

SYMBOLS

Symbols	Comments
	General conventions
$\underline{\underline{A}}$	operator
$\underline{\underline{A}}^B$	matrix of operator $\underline{\underline{A}}$ (or frame A) in frame B
a_{ij}^B	components of matrix A in frame B
$\vec{v}$	vector
v	magnitude of $\vec{v}$
	Fault plane frame (Section II.1)
$E = (\vec{e_1}, \vec{e_2}, \vec{e_3})$	Slip and fault plane frame (Fig. 2.1)
A_1, A_2, A_3	endpoints of unit vectors: $\vec{OA_i} = \vec{e_i}$ (Fig. 2.1)
P, B, T	defined as in seismology [Scheidegger, 1964] (Fig. 4.3)
	Stress tensor (Section II.2-5)
$\underline{\underline{T}}$	effective stress tensor
$\underline{\underline{T}}_d$	reduced stress tensor (Eq. 2.3)
$S = (\vec{s_1}, \vec{s_2}, \vec{s_3})$	principal stresses frame (eigenvectors of $\underline{\underline{T}}$) (Fig. 2.2)
$\sigma_1 \geq \sigma_2 \geq \sigma_3$	magnitudes of the principal effective stresses (eigenvalues of $\underline{\underline{T}}$)
$s = (\sigma_1 - \sigma_3)/\sigma_1$	relative stress difference (Eq. 1.1 & 2.7)
$\delta = (\sigma_1 - \sigma_2)/(\sigma_1 - \sigma_3)$	tensor aspect ratio or relative position of σ_2 (Fig. 2.3b; Eq. 1.2 & 2.6)
θ_1	angular representation of δ (Fig. 2.3; Eq. 2.8)
$\vec{F}$	stress applied to the fault plane of normal $\vec{e_3}$(Fig. 2.1; Eq. 2.12 & 2.13)
$\vec{\tau}$	shear stress on the fault plane (Fig. 2.1; Eq. 2.15)
$\vec{\sigma_n}$	normal stress on the fault plane (Fig. 2.1; Eq. 2.14)
	Coulomb's criterion (Section IV)
τ_0	cohesion (Fig. 4.1 & 4.2; Eq. 4.1)
φ_0	friction angle (Fig. 4.1 & 4.2; Eq. 4.1); in the figures $\varphi_0 = 31°$ (Eq. 5.9)
$H = \tau - \tan\varphi_0 \bullet \sigma_n$	$H = \tau_0$ is Coulomb's criteria (Eq. 2.21 & 4.1)
$s' = (\sigma_1-\sigma_3)/(\sigma_1+\tau_0/\tan\varphi_0)$	modified stress difference (if $\tau_0 = 0$ then $s' = s$) for the failure criteria (Eq. 4.6)
$s_c = 2\tan\varphi_0/\tan\varphi_1$	minimum stress difference for slip (Eq. 4.7); for $\varphi_0 = 31°$, $s_c = 0.679$
P_f, B, T_f	most efficient orientation of $\vec{s_1}$, $\vec{s_2}$, $\vec{s_3}$ to produces sliding (Fig. 4.1)
$\varphi_1 = \varphi_0/2 + \pi/4$	angle between P_f and $\vec{e_3}$ and between $-\vec{e_1}$ and T_f (Fig. 4.1; Eq. 4.3)
	Other variables
θ,φ,ψ	Euler's angles transforming E into S (Fig. 2.2)
R_G	area where $\vec{s_1}$ must be to satisfy the geometrical constraint (Fig. 3.1b)
$D(\theta_1)$, $D''(\theta_1)$, $D'''(\theta_1)$	$\vec{s_1}$, $\vec{s_2}$, $\vec{s_3}$ trajectories when $\psi_1(\theta,\varphi,\delta) = \psi_2(\theta,\varphi,\delta)$ (Fig. 3.4)
$\varepsilon = \pm 1$	+1 or -1 if ψ_1 or ψ_2 (Eq. 3.15 or 3.16) are respectively substituted for ψ (Eq. 3.20)
$C(\alpha)$	great circle in plane at angle α from $\vec{e_3}$ (Fig. 3.2; Eq. 3.17)
α_i	angle $(\vec{s_i}, \vec{e_3})$ (Section IV)

TABLE 2.2

COMPONENTS OF THE STRESS APPLIED TO THE FAULT PLANE

Component		Value
t^E_{13}	=	$\sigma_1 \bullet s \bullet t^E_{d13}$
t^E_{23}	=	$\sigma_1 \bullet s \bullet t^E_{d23}$
t^E_{33}	=	$\sigma_3 + \sigma_1 \bullet s \bullet t^E_{d33}$
t^E_{d13}	=	$\frac{\sin\varphi}{1+\cos\theta_1} \bullet [(1+\cos\theta_1\cos2\psi)\cos\varphi\sin\theta + \cos\theta_1\sin2\psi\cos\theta]$
t^E_{d23}	=	$\frac{-\sin\varphi}{1+\cos\theta_1} \bullet [(1+\cos\theta_1\cos2\psi)\cos\varphi\cos\theta - \cos\theta_1\sin2\psi\sin\theta]$
t^E_{d33}	=	$1-\frac{\sin^2\varphi}{1+\cos\theta_1} \bullet (1+\cos\theta_1\cos2\psi)$

TABLE 3.1

COMPONENTS OF THE STRESS APPLIED TO THE FAULT PLANE WHEN $\vec{\tau} // \vec{e_1}$

Function	Definition	Value	B
	Shear Stress		
τ	$= t^E_{13}$	$= \sigma_1 \bullet s \bullet A_\tau \bullet N$	
τ_d	$= t^E_{d13} = \tau/(\sigma_1-\sigma_3)$	$= A_\tau \bullet N + B_\tau$	$B_\tau = 0$
τ_*	$= 2\tau_d$	$= 2 \bullet A_\tau \bullet N$	
	Normal Stress		
σ_n	$= t^E_{33}$	$= \sigma_1 \bullet (1 + s \bullet A_\sigma \bullet N)$	
σ_{nd}	$= t^E_{d33} = \dfrac{\sigma_n - \sigma_3}{\sigma_1 - \sigma_3}$	$= B_\sigma + A_\sigma \bullet N$	$B_\sigma = 1$
σ_{n*}	$= \sigma_{nd}$	$= 1 + A_\sigma \bullet N$	
	Friction Law		
H	$= \tau - \tan\varphi_0 \bullet \sigma_n$	$= \sigma_1 \bullet (s \bullet A_H \bullet N - \tan\varphi_0)$	
H_d	$= \tau_d - \tan\varphi_0 \bullet \sigma_{nd}$	$= A_H \bullet N + B_H$	$B_H = -\tan\varphi_0$
H_*	$= 2 \bullet (H_d+\tan\varphi_0)/\tan\varphi_1$	$= 2 \bullet A_H \bullet N/\tan\varphi_1$	

Function	Expression in (θ,ϕ)	Expression in (θ,α)
R_D	$= \sqrt{1 - \cos^2\varphi \dfrac{\tan^2\theta_1}{\tan^2\theta}}$	$= \sqrt{\dfrac{1 - \cos^2\alpha\cos^2\theta/\cos^2\theta_1}{1 - \cos^2\alpha\cos^2\theta}}$
N	$= \dfrac{1 + \varepsilon\cos\theta_1 R_D(\theta,\varphi,\theta_1)}{1 + \cos\theta_1}$	$= \dfrac{1 + \varepsilon\cos\theta_1 R_D(\theta,\alpha,\theta_1)}{1 + \cos\theta_1}$
A_τ	$= \dfrac{1}{2}\dfrac{\sin2\varphi\sin\theta}{1 - \sin^2\varphi\cos^2\theta}$	$= \dfrac{1}{2}\sin2\alpha$
A_σ	$= -\dfrac{\sin^2\varphi\sin^2\theta}{1 - \sin^2\varphi\cos^2\theta}$	$= -\sin^2\alpha$
A_H	$= \dfrac{\sin\theta\sin\varphi[\cos\varphi + \tan\varphi_0\sin\varphi\sin\theta]}{1 - \sin^2\varphi\cos^2\theta}$	$= \dfrac{\sin(2\alpha-\varphi_0) + \sin\varphi_0}{2\cos\varphi_0}$

TABLE 3.2

FORMULAE AND EXTREMA ON THE BOUNDARIES

Functions	Boundaries		
	A_1A_3	$D(\theta_1)$	A_2
$N(\theta,\alpha,\theta_1)$	$\frac{1+\varepsilon\cos\theta_1}{1+\cos\theta_1}$	$\frac{1}{1+\cos\theta_1}$	$\frac{1+\varepsilon\sqrt{1-\sin^2\theta_1/\sin^2\alpha}}{1+\cos\theta_1}$
τ_*^+ Maximum	1 $[\alpha=\pi/4]$	$\theta_1\le\pi/4$: $2\sqrt{\delta}(1-\delta)/(1+\delta)$ $[\alpha=\theta_1]$ $\theta_1\ge\pi/4$: $(1+\delta)/2$ $[\alpha=\pi/4]$	$1-\delta$ $[\alpha=\mathrm{Arcsin}(1/\sqrt{1+\cos^2\theta})]$
τ_*^+ Minimum	0 $[\alpha=0;\pi/2]$	0 $[\alpha=0]$	0 $[\alpha=\pi/2]$
σ_{n*}^+ Maximum	1 $[\alpha=0]$	1 $[\alpha=0]$	$(1-\delta)/(1+\delta)$ $[\alpha=\theta_1]$
σ_{n*}^+ Minimum	0 $[\alpha=\pi/2]$	$(1-\delta)/(1+\delta)$ $[\alpha=\theta_1]$	0 $[\alpha=\pi/2]$
H_*^+ Maximum	1 $[\alpha=\varphi_1]$	$\theta_1\le\varphi_1$: $s_c\sqrt{\delta}\frac{\cos(\theta_1-\varphi_0)}{\sin\varphi_0}$ $[\alpha=\theta_1]$ $\theta_1\ge\varphi_1$: $(1+\delta)/2$ $[\alpha=\varphi_1]$	$1-(1-s_c)\delta$ $[\alpha=\theta_1]$
H_*^+ Minimum	0 $[\alpha=0]$	0 $[\alpha=0]$	$\theta_1\le2\varphi_0$: $s_c\sqrt{\delta}\frac{\cos(\theta_1-\varphi_0)}{\sin\varphi_0}$ $[\alpha=\theta_1]$ $\theta_1\ge2\varphi_0$: s_c $[\alpha=\pi/2]$
τ_*^- Maximum	δ $[\alpha=\pi/4]$	$\theta_1\le\pi/4$: $2\sqrt{\delta}(1-\delta)/(1+\delta)$ $[\alpha=\theta_1]$ $\theta_1\ge\pi/4$: $(1+\delta)/2$ $[\alpha=\pi/4]$	$2\sqrt{\delta}(1-\delta)/(1+\delta)$ $[\alpha=\theta_1]$
τ_*^- Minimum	δ $[\alpha=0,\pi/2]$	0 $[\alpha=0]$	0 $[\alpha=\pi/2]$
σ_{n*}^- Maximum	1 $[\alpha=0]$	1 $[\alpha=0]$	$1-\delta$ $[\alpha=\pi/2]$
σ_{n*}^- Minimum	$1-\delta$ $[\alpha=\pi/2]$	$(1-\delta)/(1+\delta)$ $[\alpha=\theta_1]$	$(1-\delta)/(1+\delta)$ $[\alpha=\theta_1]$
H_*^- Maximum	δ $[\alpha=\varphi_1]$	$\theta_1\le\varphi_1$: $s_c\sqrt{\delta}\frac{\cos(\theta_1-\varphi_0)}{\sin\varphi_0}$ $[\alpha=\theta_1]$ $\theta_1\ge\varphi_1$: $(1+\delta)/2$ $[\alpha=\varphi_1]$	$s_c\sqrt{\delta}\frac{\cos(\theta_1-\varphi_0)}{\sin\varphi_0}$ $[\alpha=\theta_1]$
H_*^- Minimum	0 $[\alpha=0]$	0 $[\alpha=0]$	$s_c\delta$ $[\alpha=\pi/2]$

+ and − superscript corresponds to $\varepsilon = +1$ ($\psi=\psi_1$; Eq. 3.15) and $\varepsilon = -1$ ($\psi=\psi_2$; Eq. 3.16) respectively. The value of the extremum is given first , followed by the α-value corresponding to its locations between brackets.

TABLE 3.3

ABSOLUTE EXTREMA

	MAXIMUM		MINIMUM	
	value	location of $\vec{s_1}$	value	location of $\vec{s_1}$
τ_*^+	1	P $[\alpha=\pi/4]$	0	$A_3; C\left(\frac{\pi}{2}\right)$ $[\alpha=0;\pi/2]$
σ_{n*}^+	1	A_3 $[\alpha=0]$	0	$C\left(\frac{\pi}{2}\right)$ $[\alpha=\pi/2]$
H_*^+	1	P_f $[\alpha=\varphi_1]$	0	A_3 $[\alpha=0]$
τ_*^-	$\theta_1\le\pi/4$: $2\sqrt{\delta}(1-\delta)/(1+\delta)$ $\theta_1\ge\pi/4$: $(1+\delta)/2$	A_2 $[\alpha=\theta_1]$ $D(\theta_1)$ $[\alpha=\pi/4]$	0	$A_3; C\left(\frac{\pi}{2}\right)$ $[\alpha=0;\pi/2]$
σ_{n*}^-	1	A_3 $[\alpha=0]$	$(1-\delta)/(1+\delta)$	A_2 $[\alpha=\theta_1]$
H_*^-	$\theta_1\le\varphi_1$: $s_c\sqrt{\delta}\cos(\theta_1-\varphi_0)/\sin\varphi_0$ $\theta_1\ge\varphi_1$: $(1+\delta)/2$	A_2 $[\alpha=\theta_1]$ $D(\theta_1)$ $[\alpha=\varphi_1]$	0	A_3 $[\alpha=0]$

+ and − superscript corresponds to $\varepsilon = +1$ ($\psi=\psi_1$; Eq. 3.15) and $\varepsilon = -1$ ($\psi=\psi_2$; Eq. 3.16) respectively.

FIGURE CAPTIONS

Fig. 2.1 The fault plane frame of reference $E = (\vec{e_1}, \vec{e_2}, \vec{e_3})$. $\vec{e_3}$ is normal to the fault plane. $\vec{e_1}$ is the slip of the lower half space ($x_3 < 0$) relatively to the upper half space ($x_3 > 0$). $\vec{F} = \underline{\underline{T}}(\vec{e_3}) = (t_{13}^E, t_{23}^E, t_{33}^E)$ is the stress applied to the upper half space. Other symbols are defined in Table 2.1.

Fig. 2.2 The fault plane frame $E = (\vec{e_1}, \vec{e_2}, \vec{e_3})$ is transformed into the principal stress frame $S = (\vec{s_1}, \vec{s_2}, \vec{s_3})$ by three successive rotations [Euler, 1767]. The intermediate stages are $\vec{u_1}$, $\vec{u_2}$, $\vec{u_3}$ and $\vec{v_1}$, $\vec{v_2}$, $\vec{v_3}$. **(a)** View in space **(b)** The upper half sphere is projected onto the plane by an azimuthal equal area projection [Lambert, 1772].

Fig. 2.3 Mohr's [1882] circles. To the classical outer and inner circles is added an intermediate circle that is centered on the σ_n axis, goes through the center of the left inner circle and through the point of coordinates $(\sigma_1,0)$. θ_1 can be graphically constructed from the intersection of the left inner circle with that intermediate circle. **(a)** $\underline{\underline{T}}$. **(b)** $\underline{\underline{T}}_d$. The outer circle has diameter 1 and goes through the origin.

Fig. 3.1 **(a)** R^-, R^0 and R^+ regions for $\vec{s_1}$. The upper half sphere ($x_3 \geq 0$) is projected into the $(\vec{e_1}, \vec{e_2})$ plane by an azimuthal equal area projection [Lambert, 1772]. $\vec{s_1}$ represents any couple (θ,φ). The boundary between these 3 regions is the curve $D(\theta_1)$. R_G is the dilatational part, i.e., the right side, of R^0. **(b)** R_G regions for $\theta_1 = 0°$ to $90°$ by increment of $10°$.

Fig. 3.2 $C(\alpha)$ and $D(\alpha)$. $C(\alpha)$ is the great circle at angle α from $\vec{s_3}$ that passes through A_2. $D(\alpha)$ is the locus of $\vec{s_1}$ satisfying Eq 3.19.

Fig. 3.3 Variations of τ, σ_n and H in the R_E domain as a function of the position of $\vec{s_1}$. The arrows on the circles $C(\alpha)$ point in the direction of increasing values. Note that the P axis corresponds to the absolute maximum for τ^+, but to a saddle for τ^-. The corresponding location for H is defined as P_f.

Fig. 3.4 Correspondence between Mohr's representation and the principal stress orientations for stress tensor satisfying the geometrical constraint. **(a)** Mohr's representation. **(b)** $\vec{s_1}$ orientations in azimuthal equal area projection [Lambert, 1772]. **(c)** $\vec{s_2}$ orientations. **(d)** $\vec{s_3}$ orientations. The symbols laid on Mohr's diagram are shown on the corresponding orientations projection: the thick line corresponds to the intermediate circle and to $D(\theta_1)$, $D''(\theta_1)$ and $D'''(\theta_1)$ for $\vec{s_1}$, $\vec{s_2}$, $\vec{s_3}$; the "+" area corresponds to $\varepsilon = +1$ or $\psi = \psi_1(\theta,\varphi,\delta)$ while the lined area corresponds to $\varepsilon = -1$ or $\psi = \psi_2(\theta,\varphi,\delta)$; the open symbols correspond to Mohr's circles and the filled symbols to zero shear stress.

Fig. 3.5 Tangence of the line $\tau_* = V_0$ with the 4 critical circles. These tangences correspond to cases across which the $\vec{s_1}$, $\vec{s_2}$ or $\vec{s_3}$ trajectories undergo significant changes. The principal stress orientations corresponding to these critical cases are shown in azimuthal equal area projection [Lambert, 1772]. Each critical case corresponds to a relationship between V_0 and δ that is

consistent with Table 3.2.

Fig. 3.6 Tangence of the line $\sigma_{n*} = V_0$ with the 4 critical circles.

Fig. 3.7 Tangence of the line $H_* = V_0$ with the 4 critical circles.

Fig. 3.8 Critical boundaries in the (δ, V_0) plane for τ_*. The critical V_0 values (Table 3.2 or Fig. 3.5) are plotted as a function of δ. Each polygon correspond to a level curve type. The star symbol corresponds to level curves displayed in Fig. 3.11 and 3.12.

Fig. 3.9 Critical boundaries in the (δ, V_0) plane for σ_{n*} (Table 3.2 and Fig. 3.6). Stars correspond to level curves of Fig. 3.13.

Fig. 3.10 Critical boundaries in the (δ, V_0) plane for H_* (Table 3.2 and Fig. 3.7). Stars correspond to level curves of Fig. 3.14, 3.15, and 3.16.

Fig. 3.11 Typical τ_* level curves for $\delta = 0.3$. The $\overrightarrow{s1}$, $\overrightarrow{s2}$, $\overrightarrow{s3}$ trajectories are shown as well as the corresponding lines in Mohr's representation for typical values of V_0. The solid lines correspond to the $\varepsilon = +1$ type of solutions while the dotted lines correspond to the $\varepsilon = -1$ type of solutions. The thick points correspond to P and T.

Fig. 3.12 Typical τ_* level curves for $\delta = 0.55$.

Fig. 3.13 Typical σ_{n*} level curves for $\delta = 0.3$.

Fig. 3.14 Typical H_* level curves for $\delta = 0.2$. The thick points correspond to P_f and T_f.

Fig. 3.15 Typical H_* level curves for $\delta = 2/3$.

Fig. 3.16 Typical H_* level curves for $\delta = 0.8$.

Fig. 3.17 Map of shear stress for $\delta = 0.1$ and $\delta = 0.3$. 10 level curves, $\tau_* = 0$ to $\tau_* = 1.0$ by increment of 1/10, are shown. Left: $\overrightarrow{s1}$ (in the dilatational quadrant) and $\overrightarrow{s3}$ (in the compressional quadrant) trajectories for ε - +1 (solid lines); center: $\overrightarrow{s1}$, $\overrightarrow{s3}$ trajectories for $\varepsilon = -1$ (dotted lines); right: $\overrightarrow{s2}$ trajectories for both $\varepsilon = +1$ (solid line) and $\varepsilon = -1$ (dotted line). The curves $D(\theta_1)$, $D''(\theta_1)$ and $D'''(\theta_1)$ are shown in solid line (best seen among the dotted trajectories for $\overrightarrow{s3}$, and clearly crosscutting the level for $\overrightarrow{s2}$ at the location where dotted and continuous lines connect). The thick points represent the locations of the maxima of τ_*^+ and τ_*^-. There are not always 10 level curves for τ_*^- because its maximum is smaller than 1 (Table 3.3). Note that the P axis is a saddle point for the $\overrightarrow{s1}$ levels of τ_*^- and a summit for those of τ_*^+.

Fig. 3.18 Map of normal stress for $\delta = 0.3$ and $\delta = 2/3$.

Fig. 3.19 Map of H_* for $\delta = 0.2$ and $\delta = 2/3$. Similarly to τ, P_f is a summit for the $\overrightarrow{s1}$ levels of H_*^+, a saddle for those of H_*^-.

Fig. 4.1 Coulomb [1776] failure. **(a)** Mohr's circles. **(b)** Principal stress orientations. The upper half sphere is projected by azimuthal equal area projection [Lambert, 1772]. The fault plane is horizontal; the second nodal plane contains A_2 and A_3. P, T and B are as in seismology [Scheidegger, 1964]. The positions of $\overrightarrow{s1}$ and $\overrightarrow{s3}$ at failure are defined as P_f and T_f.

Fig 4.2 Experimental values of failure and friction coefficients.

Fig. 4.3 Maximum shear stress failure [Tresca, 1868]. **(a)** Mohr's circles. **(b)** Principal stress orientations: $\vec{s_1}$, $\vec{s_2}$, $\vec{s_3}$ coincide with P, B, T.

Fig. 4.4 Two dimensional frictional sliding. The two principal stresses are σ_1 and σ_3. **(a)** Mohr's (σ_n,τ) domain is reduced to the circle of diameter $\sigma_1 - \sigma_3$. Friction may occur on the two planes that correspond to A and A'. **(b)** Principal stress orientations. $\vec{e_1}$ and $\vec{e_3}$ are the slip and normal to the plane respectively. The stippled area represent the possible orientations of $\vec{s_1}$. To each orientation of $\vec{s_1}$ in the allowed domain corresponds one and only one value of s represented by the length OA.

Fig. 4.5 Three dimensional frictional sliding in degenerate cases. The acceptable positions of $\vec{s_1}$, $\vec{s_2}$, $\vec{s_3}$ are represented in azimuthal equal area projection [Lambert, 1772]. **(a)** case $\sigma_3 = \sigma_2$. The orientations of $\vec{s_1}$ on A_1A_3 and the circles described by $\vec{s_2}$ and $\vec{s_3}$ corresponding to $s = s_c$; 0.7; 0.8; 0.9; 1.0 are shown labelled in s. **(b)** case $\sigma_1 = \sigma_2$.

Fig. 5.1 Tangence of the friction lines $H_* = s_c/s$ with the critical circles. The figure is similar to Fig. 3.7 but in two respects: first the friction lines are labeled in s instead of V_0, second only the friction lines above the origin are allowed. The region below the σ_n axis is omitted since the known direction of movement, requires that $\tau \geq 0$. In this and all subsequent figures, $\varphi_0 = 31°$ (Eq. 4.12) and therefore $s_c = 0.679$ (Eq. 4.15).

Fig. 5.2 Critical boundaries in the (δ, s) plane. The critical relationships (Fig. 5.1) are plotted in the (δ, s) plane. All the tensors within the same polygon exhibit the same type of principal stress trajectories. There are 8 cases:

(1) Only the $\varepsilon = +1$ type of trajectory exists. Therefore $\vec{s_2}$ and $\vec{s_3}$ are obtained by $\psi_1(\theta,\varphi,\delta)$. $\vec{s_1}$ reaches A_2 (B axis) but $\vec{s_3}$ does not.

(2) Same as (1) except that neither $\vec{s_1}$ nor $\vec{s_3}$ reaches A_2.

(3) Both types of solution are possible, therefore on part of the trajectories $\vec{s_2}$ and $\vec{s_3}$ are obtained by $\psi_1(\theta,\varphi,\delta)$ $(\varepsilon = +1)$ and on other part by $\psi_2(\theta,\varphi,\delta)$ $(\varepsilon = -1,)$. Neither $\vec{s_1}$ nor $\vec{s_3}$ reaches A_2.

(4) Same as (3) except that $\vec{s_3}$ reaches A_2 while $\vec{s_1}$ does not.

(5) Same as (3) except that $\vec{s_1}$ reaches A_2 only on $\varepsilon = +1$ type of solution while $\vec{s_3}$ doesn't reach A_2.

(6) Same as (3) except that $\vec{s_1}$ reaches A_2 only on $\varepsilon = +1$ type of solution and $\vec{s_3}$ also reaches A_2.

(7) Same as (3) except that $\vec{s_1}$ reaches A_2 on both $\varepsilon = +1$ and $\varepsilon = -1$ type of solution while $\vec{s_3}$ doesn't reach A_2.

(8) Same as (3) except that $\vec{s_1}$ reaches A_2 on both $\varepsilon = +1$ and $\varepsilon = -1$ type of solution and $\vec{s_3}$ also reaches A_2.

Fig. 5.3 $\vec{s_1}$, $\vec{s_2}$, $\vec{s_3}$ trajectories for a solution tensor with $\delta = 0.795$ and $s = 0.8$. The solid line corresponds to $\varepsilon = +1$ $(\psi = \psi_1(\theta,\varphi,\delta))$ while the dotted line corresponds to $\varepsilon = -1$ $(\psi = \psi_2(\theta,\varphi,\delta))$. $D''(\theta_1)$ and $D'''(\theta_1)$ are the curves described by $\vec{s_2}$ and $\vec{s_3}$ when $\vec{s_1}$ describes $D(\theta_1)$. The connection between the two types of solutions occurs on these curves.

Fig. 5.4 Tangence of the friction lines $H_* = s_c/s$ with Mohr's circles. These tangences correspond to the three critical cases where the $\vec{s_1}$, $\vec{s_2}$ $\vec{s_3}$ orientations undergo significant physical changes. The orientations of the principal stresses corresponding to each case are shown in azimuthal equal area projection [Lambert, 1772].

Fig. 5.5 Critical boundaries in the (δ, s) plane corresponding to the critical cases of Fig 5.4. To each curved polygon correspond a type of $\vec{s_1}$, $\vec{s_2}$, $\vec{s_3}$ trajectories; the lined area corresponds to tensors that satisfy the geometrical and frictional constraint and for which $\vec{s_1}$ can lie in the fault plane along the B axis, therefore totally exchanging roles with $\vec{s_2}$; the dotted area corresponds to tensors that satisfy the geometrical and frictional constraint and for which $\vec{s_3}$ can lie in the fault plane along the B axis, therefore totally exchanging roles with $\vec{s_2}$. The white area where $s \geq s_C$ corresponds to those tensors for which neither $\vec{s_1}$ nor $\vec{s_3}$ can lie on the B axis once the constraints are satisfied. The white area where $s \leq s_C$ corresponds to tensors that cannot satisfy the frictional constraint because their stress difference is too small to cause sliding. The squares designate the trajectories that are displayed in Fig. 5.6, 5.7, 5.10 & 5.11.

Fig. 5.6 Solution tensor with $\delta = 0.2$. **(a)**: Mohr's circle.The dotted area, limited by the friction line $s = 1$, corresponds to all the acceptable solutions. There are only 2 typical cases: the friction line intersects either the outer circle only ($s = 0.7$) or both the outer and the left inner circle ($s = 0.9$). **(b)**: Principal stress trajectories corresponding to the friction lines shown in (a). Left side: $\vec{s_1}$ and $\vec{s_3}$ trajectories in the dilatational and compressional quadrant respectively. Right side: $\vec{s_2}$ trajectories. **(c)**: The dotted area represents the orientations spanned by the principal stress; it corresponds to the dotted area in (a). Note that $\vec{s_1}$ does not fill up the whole R_G area.

Fig. 5.7 Solution tensor with $\delta = 0.8$. Same conventions as Fig. 5.6. The dotted trajectories and friction lines correspond to $\varepsilon = -1$, the solid ones to $\varepsilon = +1$. Besides the typical cases already seen for $\delta = 0.2$, appears a new one: the friction line can intersect both inner circles at once ($s = 0.95$) therefore $\vec{s_2}$ can exchange positions with both $\vec{s_1}$ or $\vec{s_3}$. As a result the domain covered by $\vec{s_2}$ is greatly extended.

Fig. 5.8 $\vec{s_1}$, $\vec{s_2}$, $\vec{s_3}$ trajectories at fixed δ. The trajectories from $s = s_C$ to $s = 1$ by increment of $(1-s_C)/10$ are labeled from 0 to 10 in that order. Solid lines: $\varepsilon = +1$; Dotted lines: $\varepsilon = -1$.

Fig. 5.9 Area covered by $\vec{s_1}$, $\vec{s_2}$, $\vec{s_3}$ at fixed δ. From Fig. 5.8, the areas covered by the principal stresses can be split into 3 groups:
(1) Areas covered only by $\varepsilon = +1$ type of solution only (+ symbols);
(2) Areas covered only by $\varepsilon = -1$ type of solution only (stippled);
(3) Areas covered by both type of solution (dot pattern).

Note that the R_G region that is allowed to $\vec{s_1}$ by the geometrical constraint [McKenzie, 1969], is not filled up by these 3 domains. For $\delta = 0.2$, there is no $\varepsilon = -1$ type of solution; for $\delta = 2/3$ both types of solution exist; and for $\delta = 0.8$ the $\varepsilon = -1$ type of solution reaches the A_1A_3 arc.

Fig. 5.10 Typical solution tensors with $s = 0.8$. **(a)** Mohr's circles **(b)** Trajectories of the principal stresses. The symbols correspond to those in (a).

Fig. 5.11 Typical solution tensors with $s = 0.95$.

Fig. 5.12 $\vec{s_1}$, $\vec{s_2}$, $\vec{s_3}$ trajectories at fixed s. The trajectories for δ varying from 0 to 1 by increment of 1/10 are labeled from 0 to 10 in that order. Solid lines: $\varepsilon = +1$; Dotted lines: $\varepsilon = -1$.

Fig. 6.1 Range of orientations for $\vec{s_1}$, $\vec{s_2}$, $\vec{s_3}$ when neither δ, nor s are known and **(a)** one does not assume anything about s or **(b)** one assumes that s is limited by failure on intact plane to $s \leq s_C' = 0.8$.

(a)

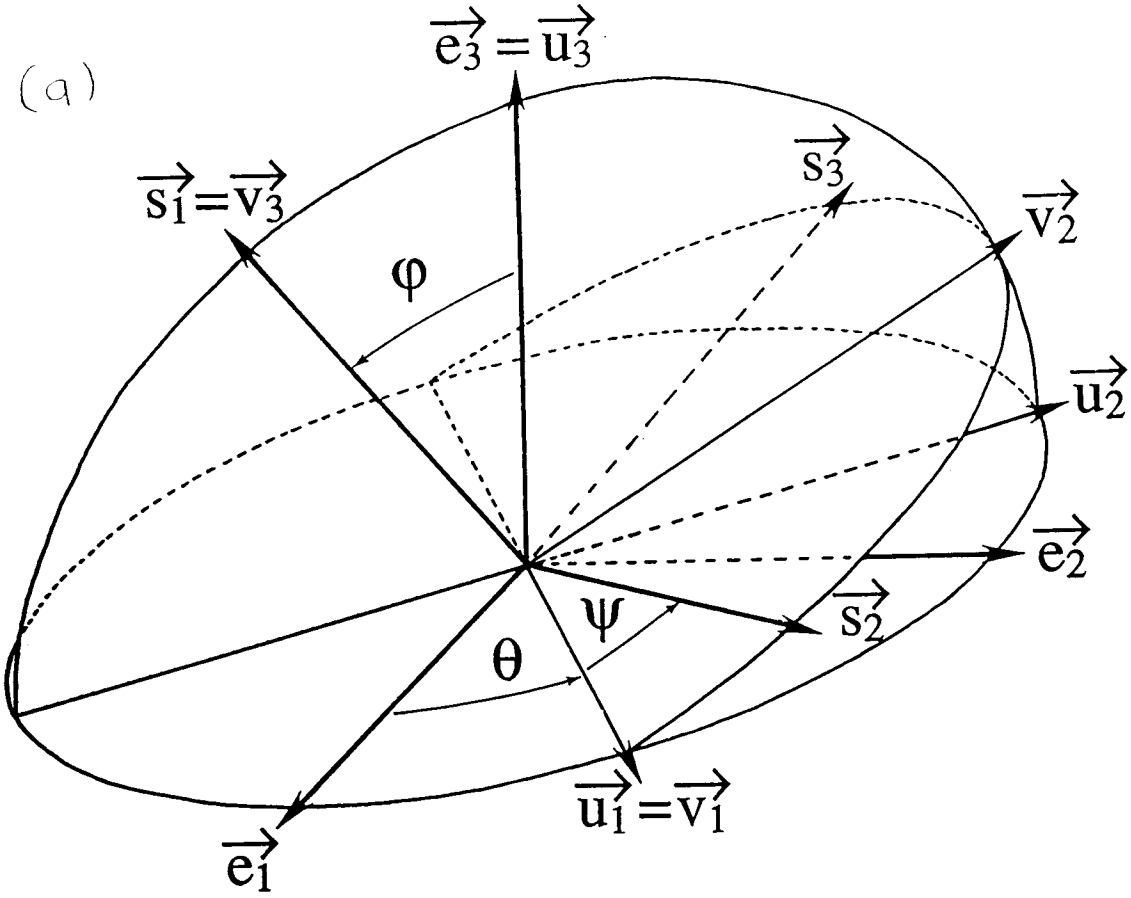
$\vec{e_3} = \vec{u_3}$
$\vec{s_1} = \vec{v_3}$
$\vec{s_3}$
$\vec{v_2}$
φ
$\vec{u_2}$
$\vec{e_2}$
ψ
$\vec{s_2}$
θ
$\vec{u_1} = \vec{v_1}$
$\vec{e_1}$

(b)

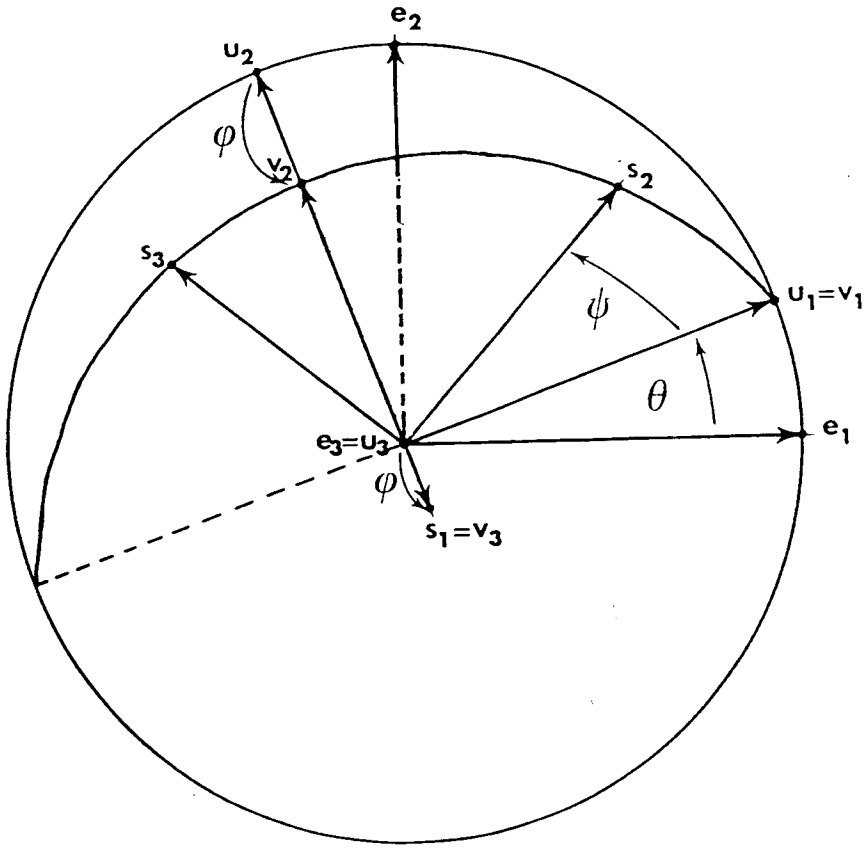
e_2
u_2
φ
v_2
s_2
s_3
$u_1=v_1$
ψ
θ
e_1
$e_3=u_3$
φ
$s_1=v_3$

Fig 2.2

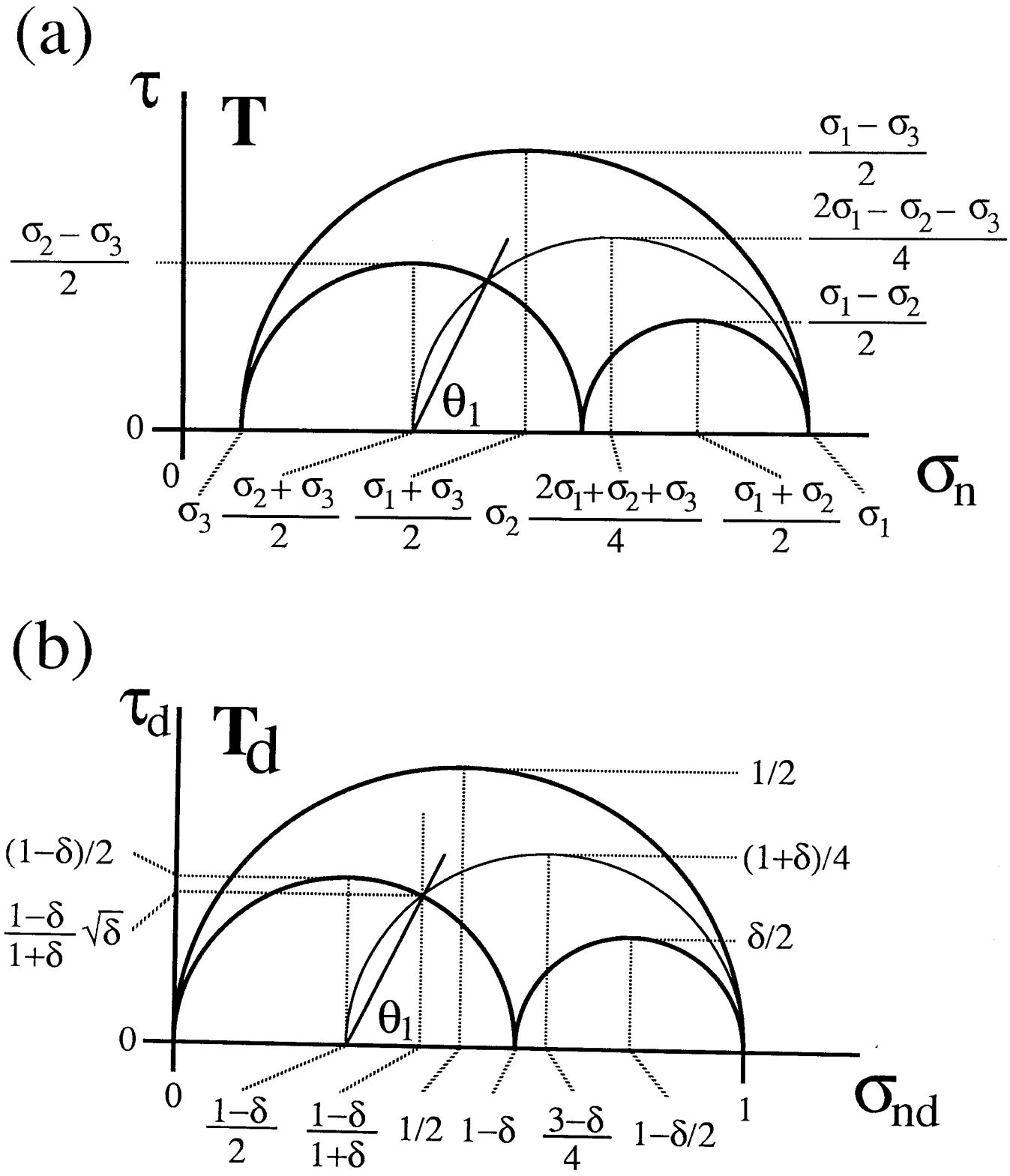
(a)
τ
T
$\frac{\sigma_1-\sigma_3}{2}$
$\frac{2\sigma_1-\sigma_2-\sigma_3}{4}$
$\frac{\sigma_2-\sigma_3}{2}$
$\frac{\sigma_1-\sigma_2}{2}$
θ1
0
0
σ3
$\frac{\sigma_2+\sigma_3}{2}$
$\frac{\sigma_1+\sigma_3}{2}$
σ2
$\frac{2\sigma_1+\sigma_2+\sigma_3}{4}$
$\frac{\sigma_1+\sigma_2}{2}$
σ1
σn
(b)
τd
Td
1/2
(1−δ)/2
(1+δ)/4
$\frac{1-\delta}{1+\delta}\sqrt{\delta}$
δ/2
θ1
0
0
$\frac{1-\delta}{2}$
$\frac{1-\delta}{1+\delta}$
1/2
1−δ
$\frac{3-\delta}{4}$
1−δ/2
1
σnd

Fig. 2.3

Fig. 3.1(a)

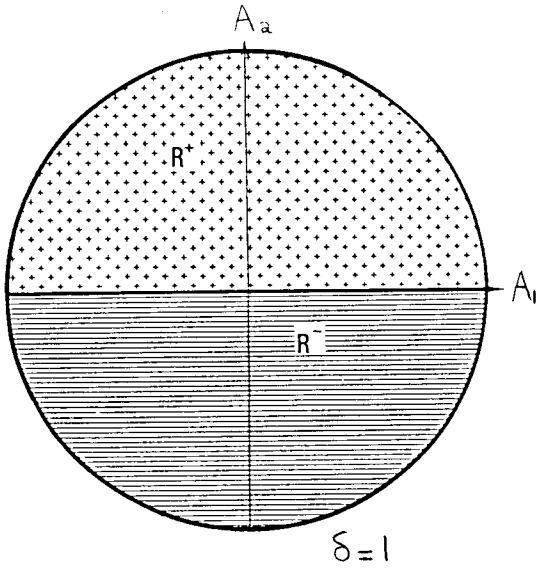

δ = 1

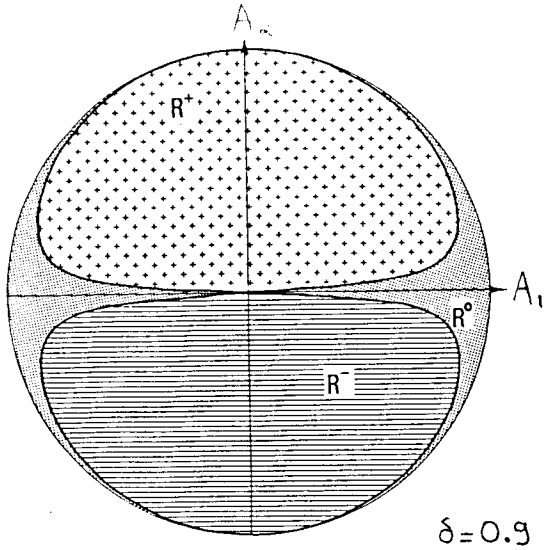

δ = 0.9

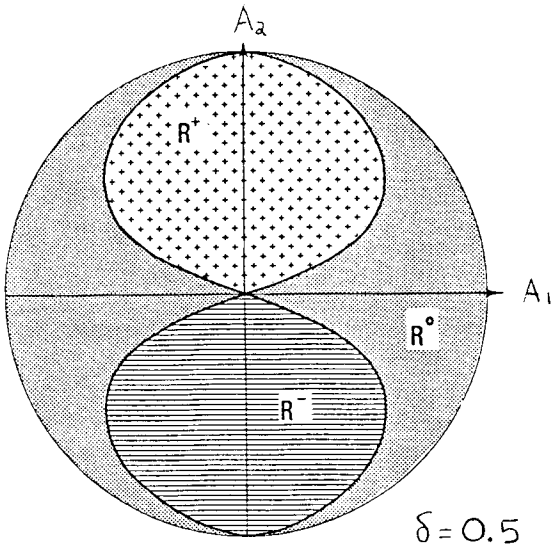

δ = 0.5

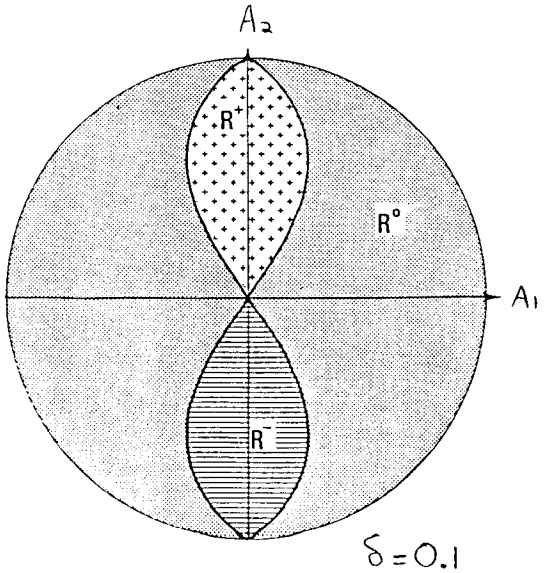

δ = 0.1

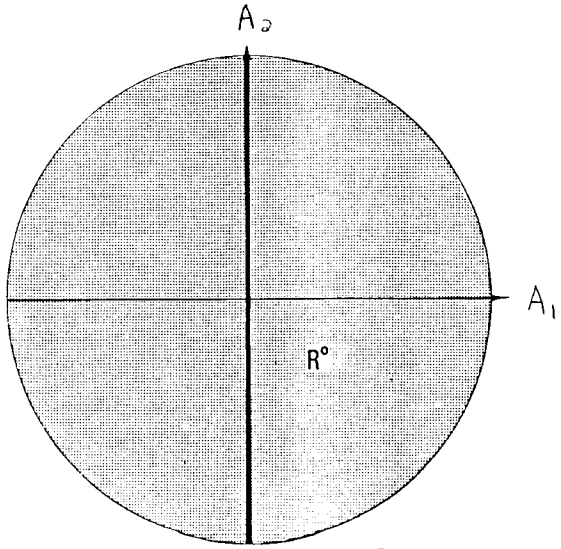

δ = 0.0

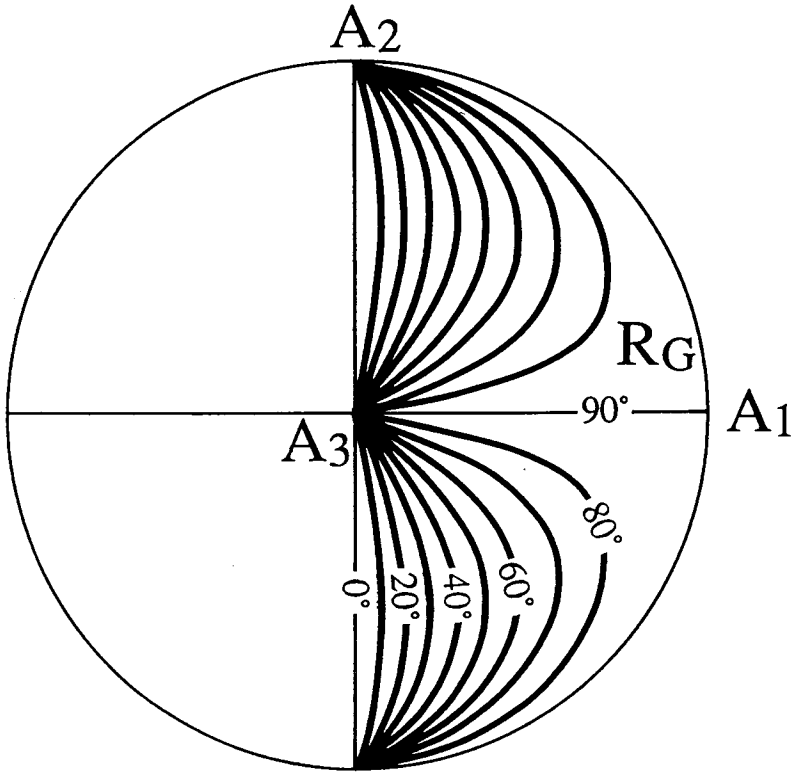

Fig. 3.1 (b)

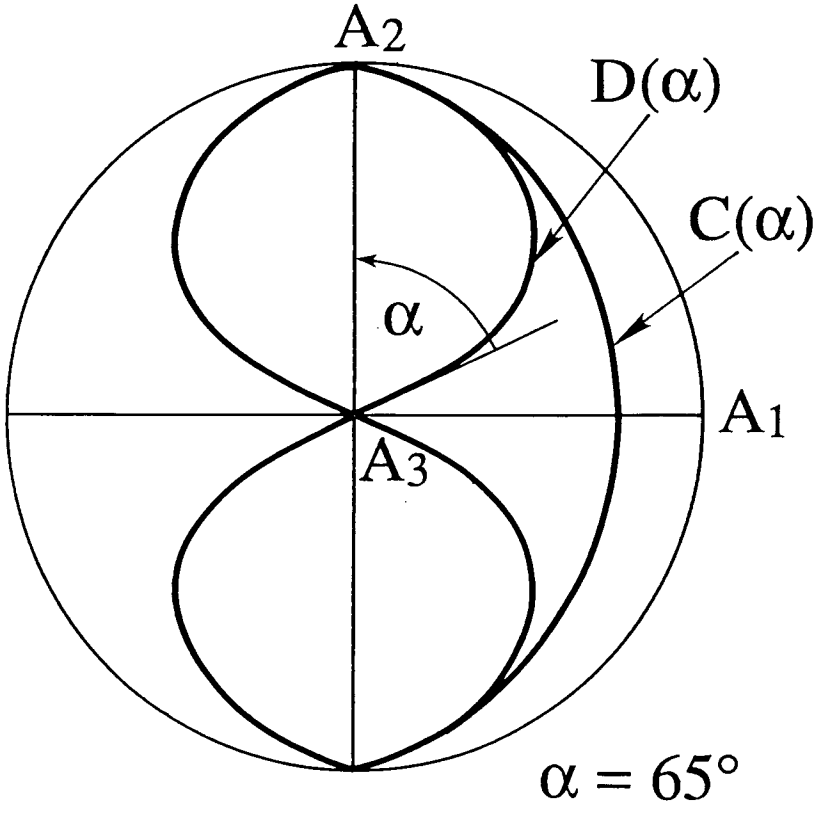

Fig. 3.2

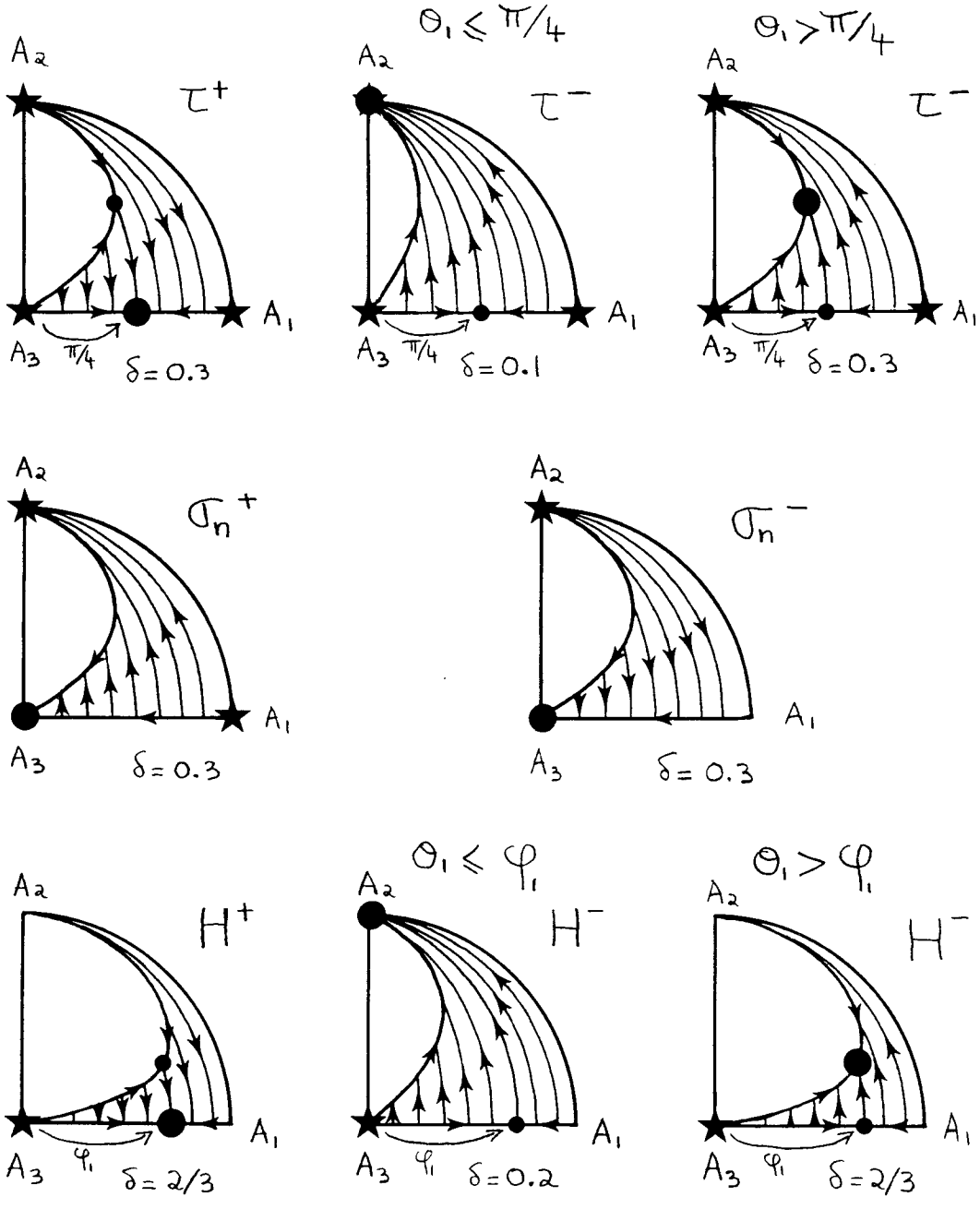

- Relative maximum
- Absolute maximum
- $\varphi_1 = \varphi_0/2 + \pi/4$
- ★ Absolute minimum

FIG 3.3

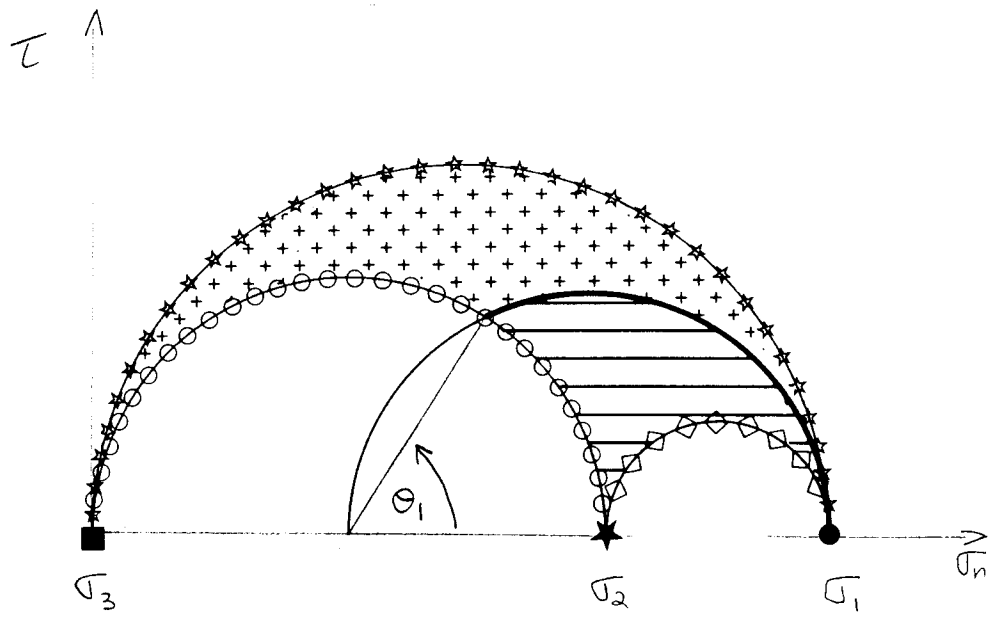

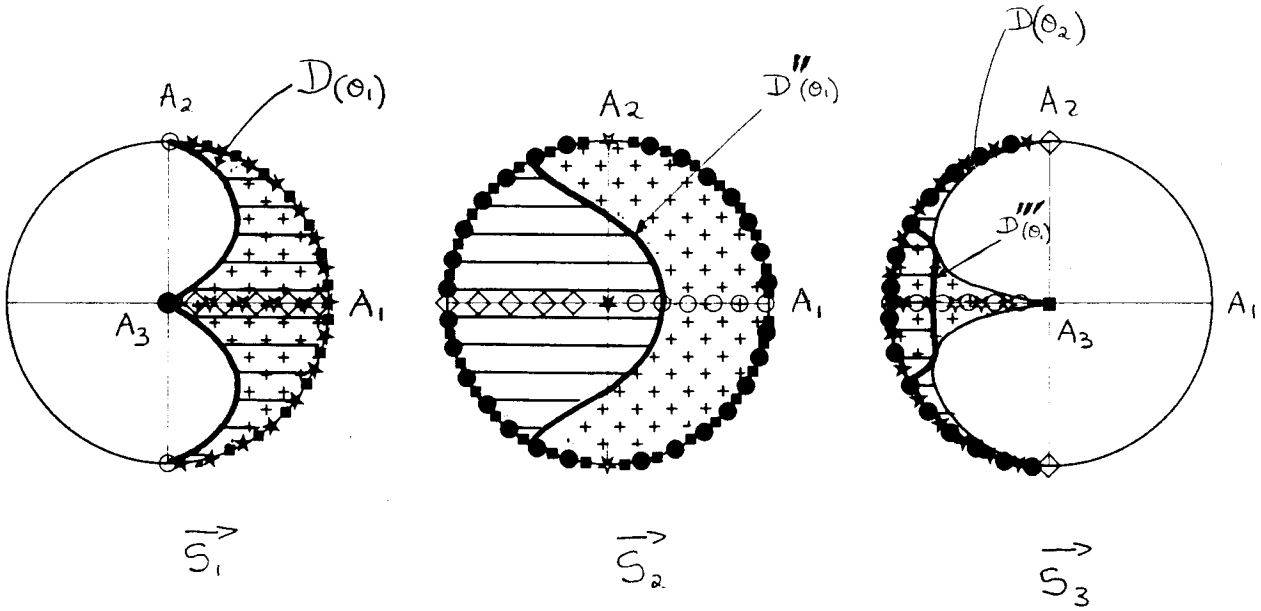

FIG 3.4

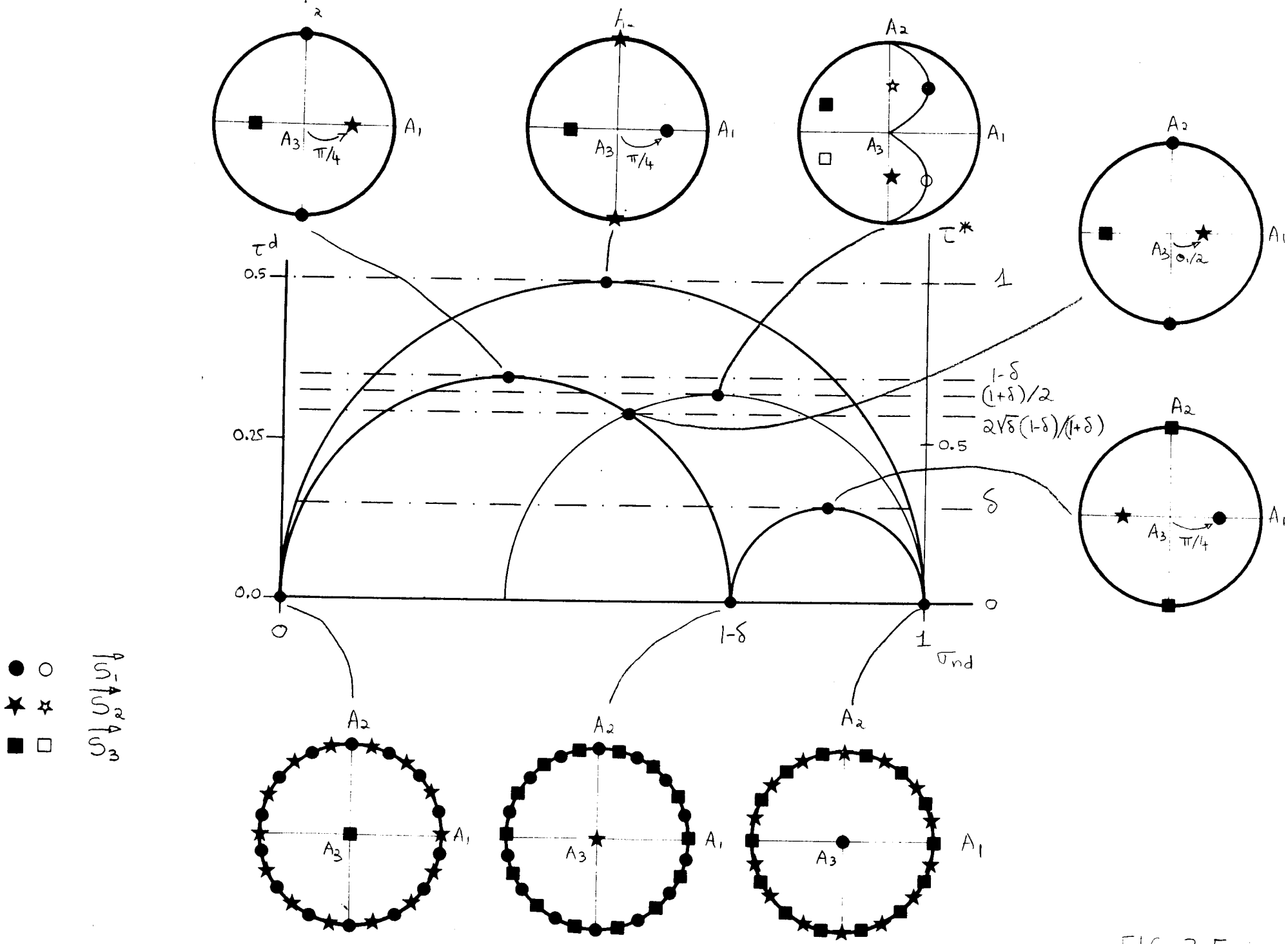

FIG 3.5

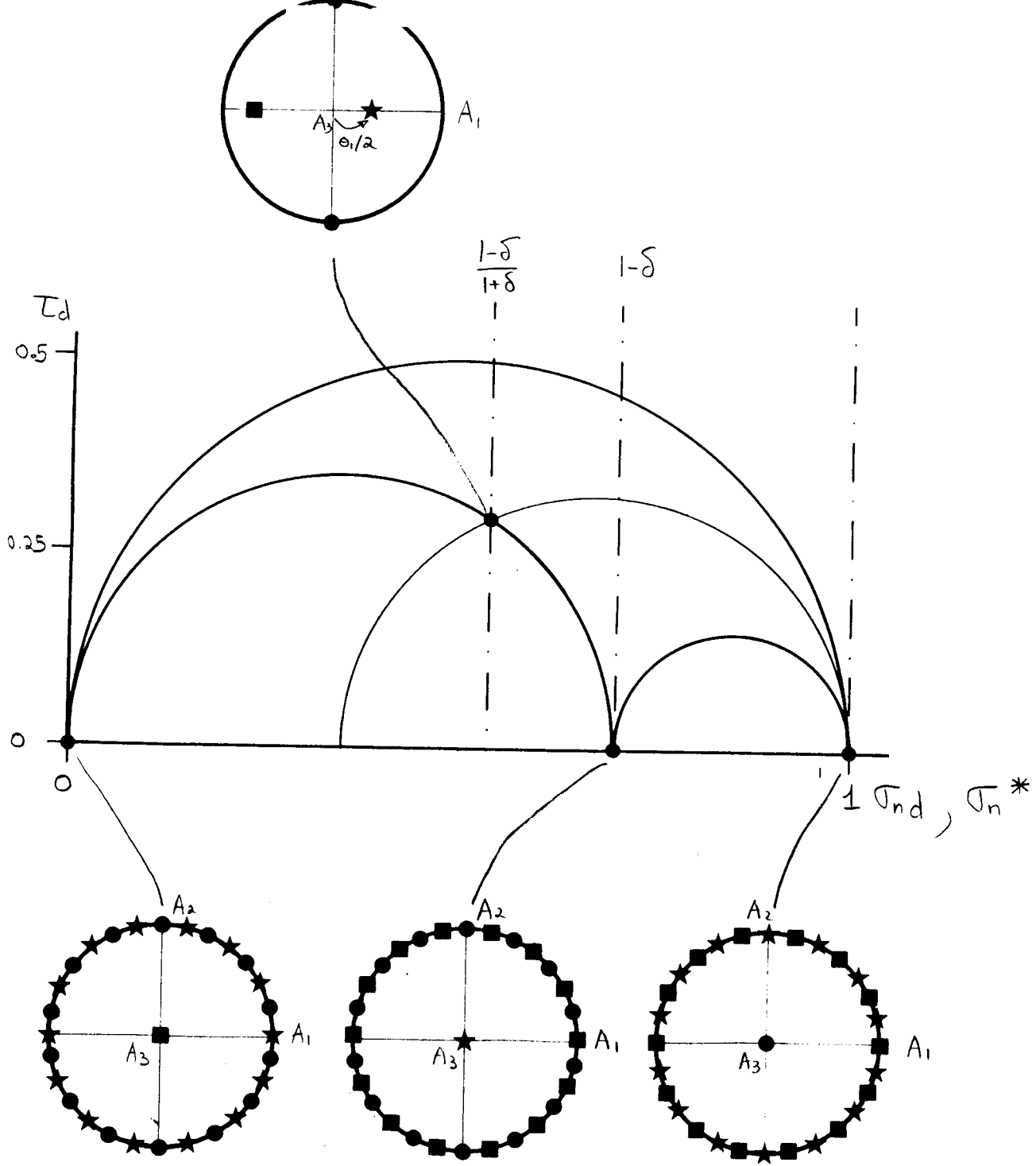
A1
A3
θ1/2
1-δ/1+δ
1-δ
τd
0.5
0.25
0
0
1 σnd , σn*
A2
A3
A1
A2
A3
A1
A2
A3
A1
σ1 σ2 σ3

FIG 3.6

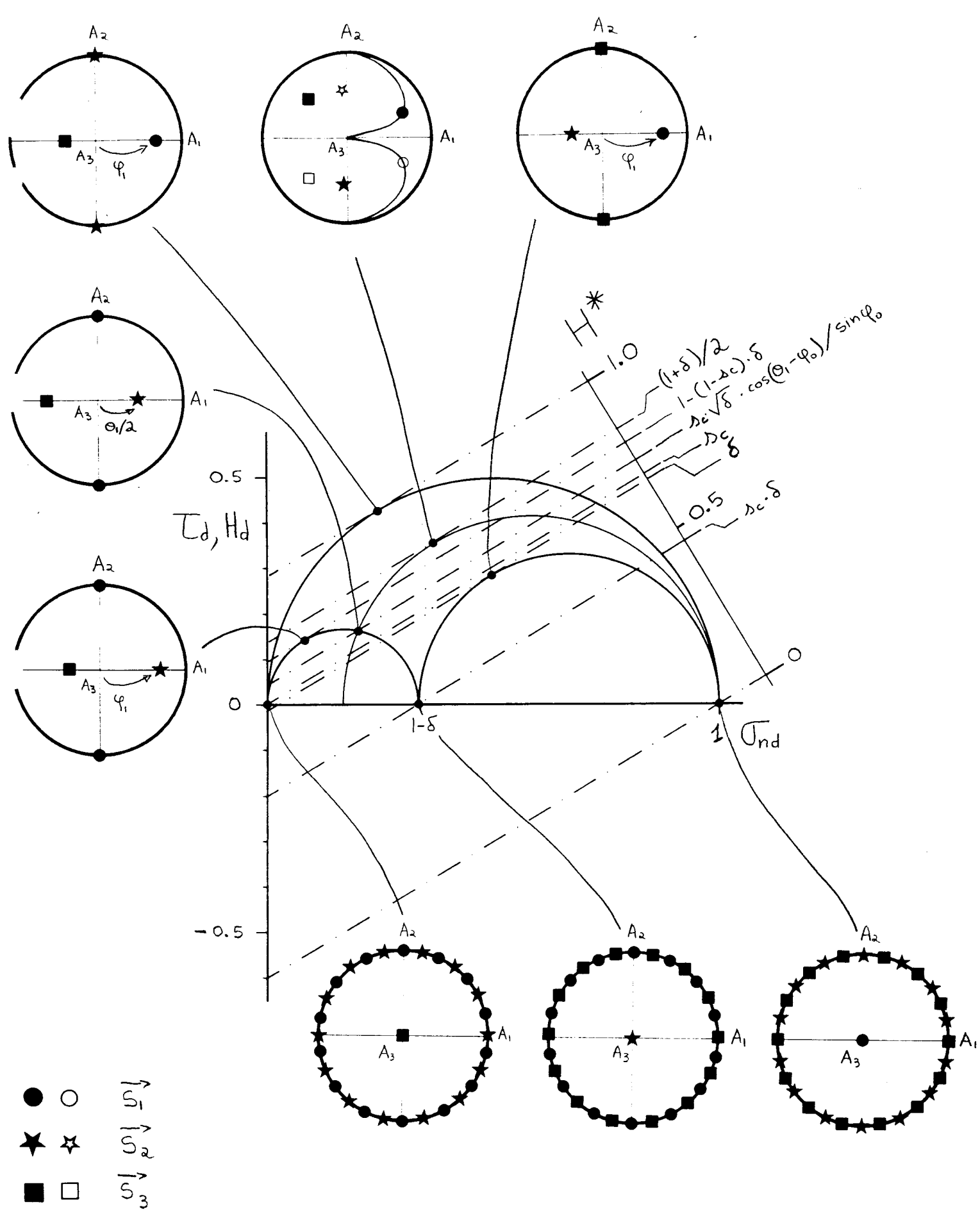
A2
A1
A3
φ1
θ1/2
H*
1.0
(1+δ)/2
1-(1-sc).δ
sc√δ · cos(θ1-φ0)/sinφ0
sc δ
0.5
sc.δ
Td, Hd
0.5
0
-0.5
1-δ
1
σnd
S1
S2
S3

FIG 3.7

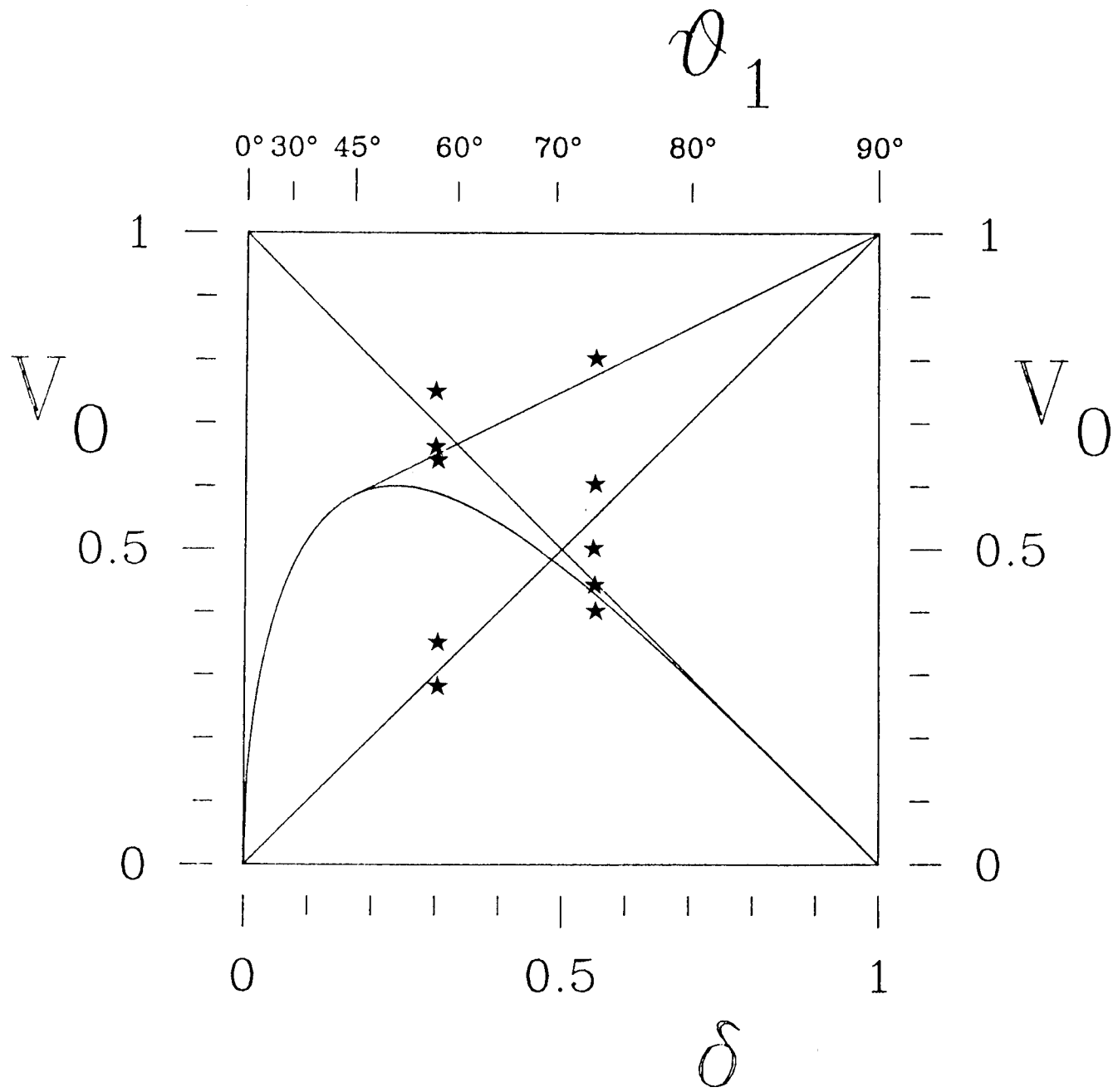

FIG 3.8

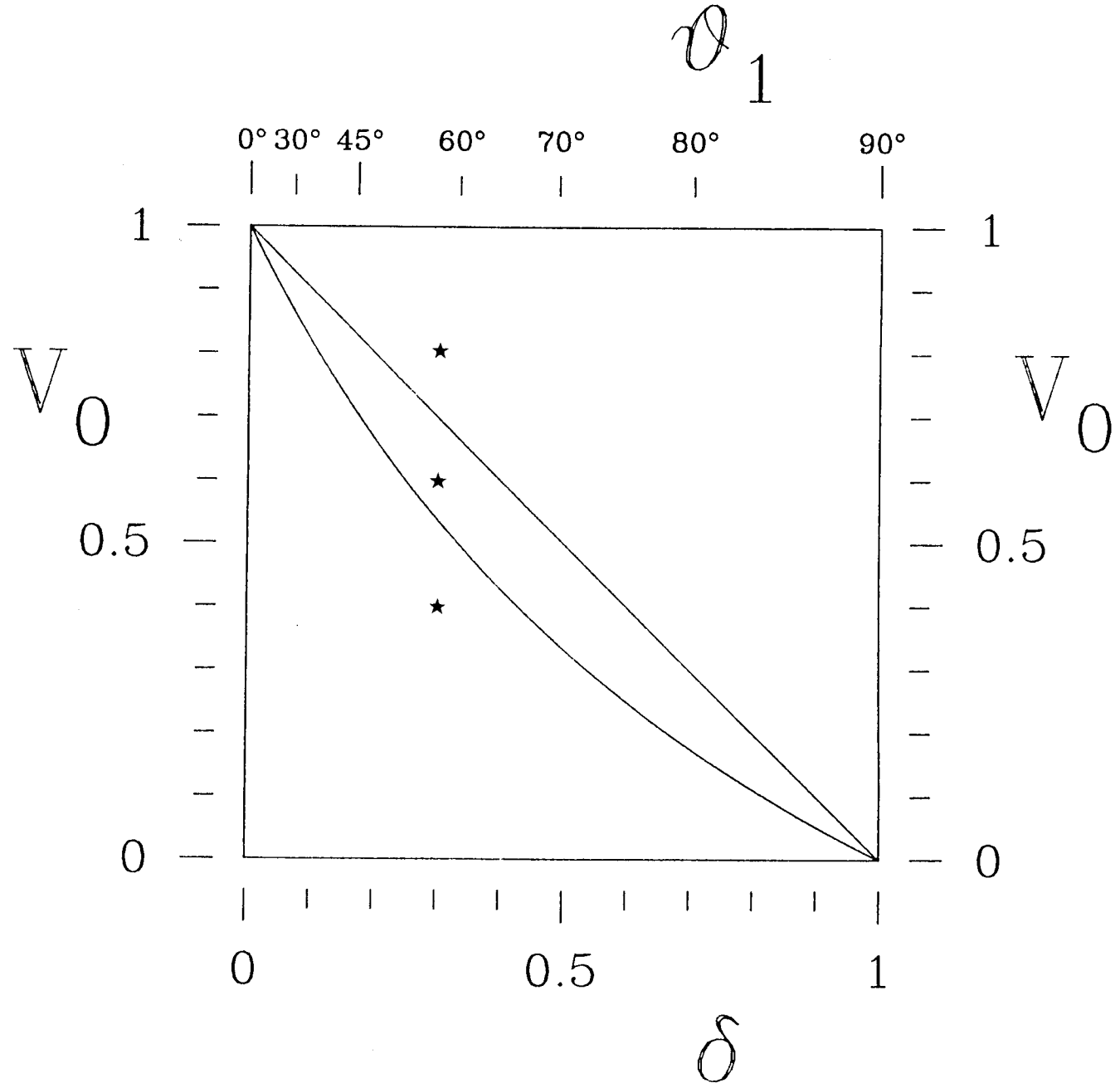

FIG 3.9

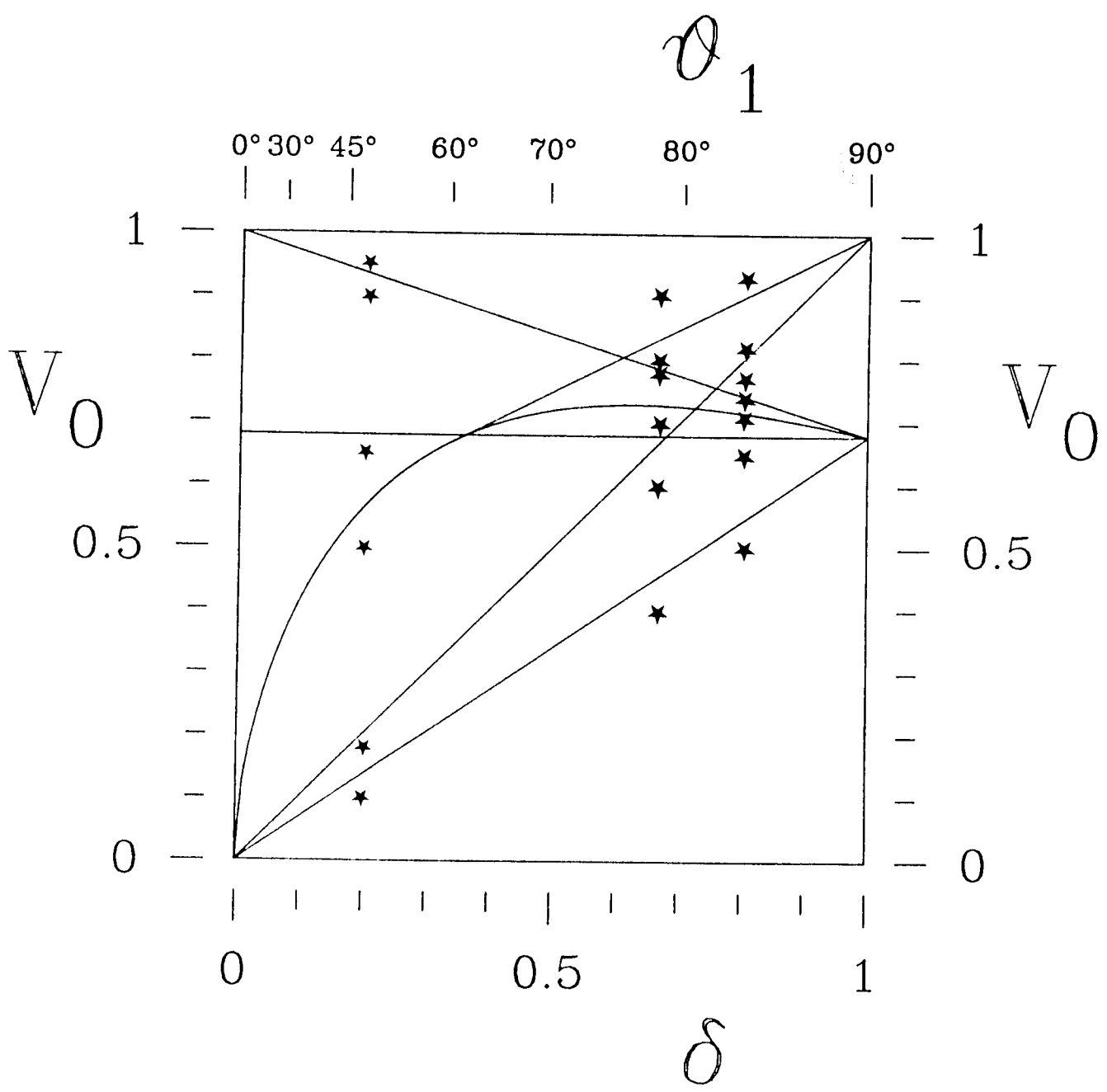

FIG 3.10

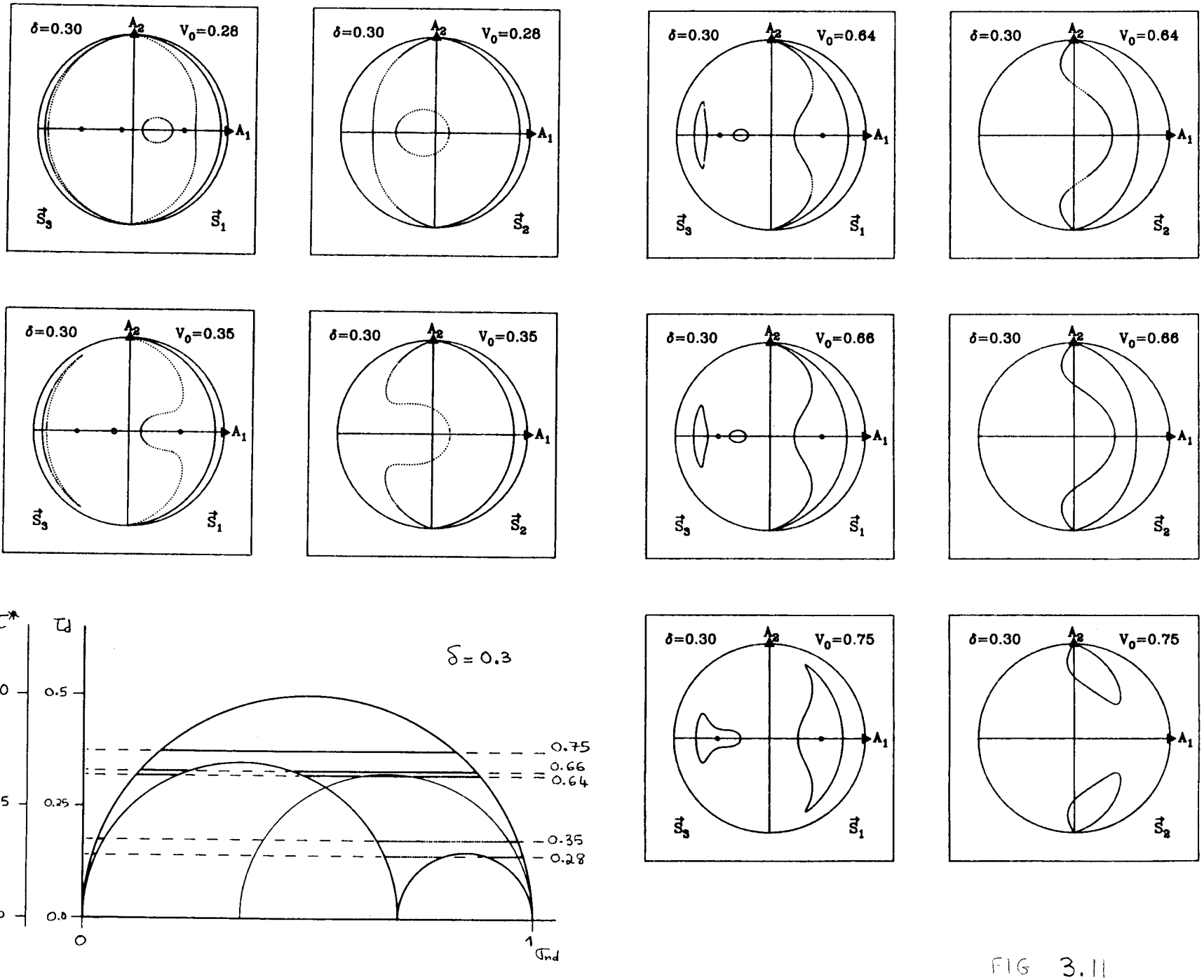
δ=0.30
V0=0.28
δ=0.30
V0=0.28
δ=0.30
V0=0.64
δ=0.30
V0=0.64
δ=0.30
V0=0.35
δ=0.30
V0=0.35
δ=0.30
V0=0.66
δ=0.30
V0=0.66
δ=0.30
V0=0.75
δ=0.30
V0=0.75
A2
A1
S3
S1
S2
τ*
τd
δ = 0.3
1.0
0.5
0.5
0.25
0.0
0.0
0
1
τnd
0.75
0.66
0.64
0.35
0.28

FIG 3.11

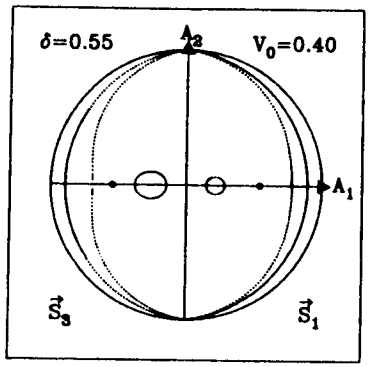
δ=0.55
V0=0.40
A2
A1
S3
S1

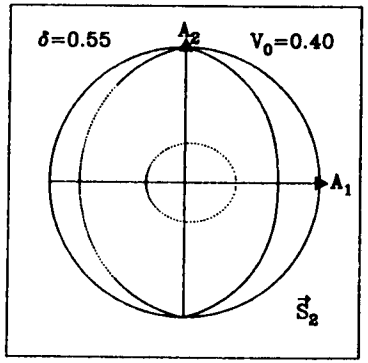
δ=0.55
V0=0.40
A2
A1
S2

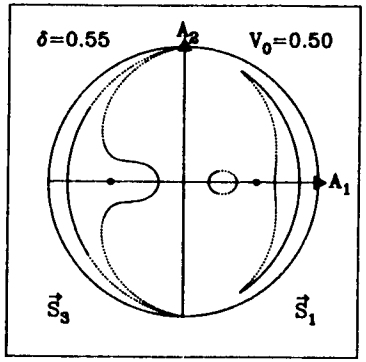
δ=0.55
V0=0.50
A2
A1
S3
S1

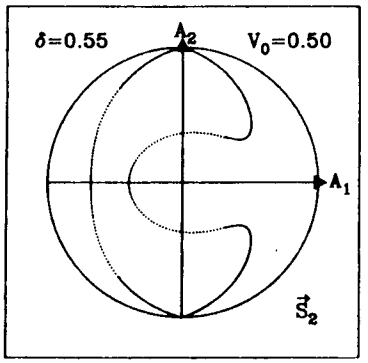
δ=0.55
V0=0.50
A2
A1
S2

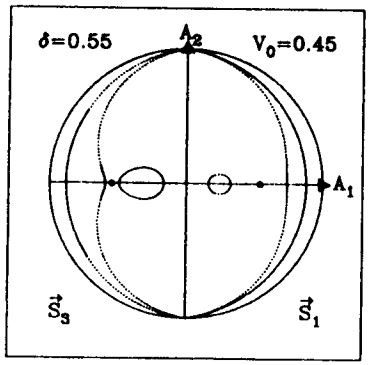
δ=0.55
V0=0.45
A2
A1
S3
S1

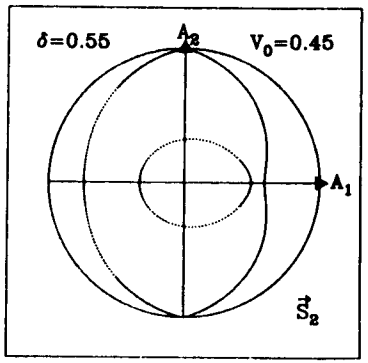
δ=0.55
V0=0.45
A2
A1
S2

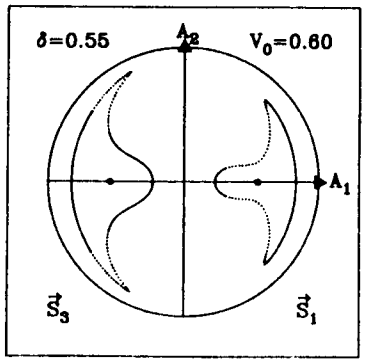
δ=0.55
V0=0.60
A2
A1
S3
S1

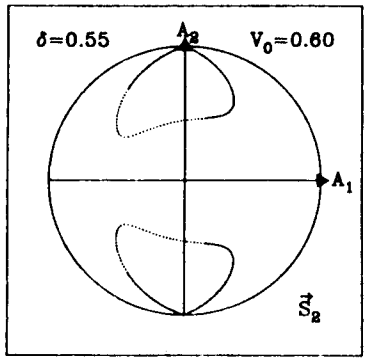
δ=0.55
V0=0.60
A2
A1
S2

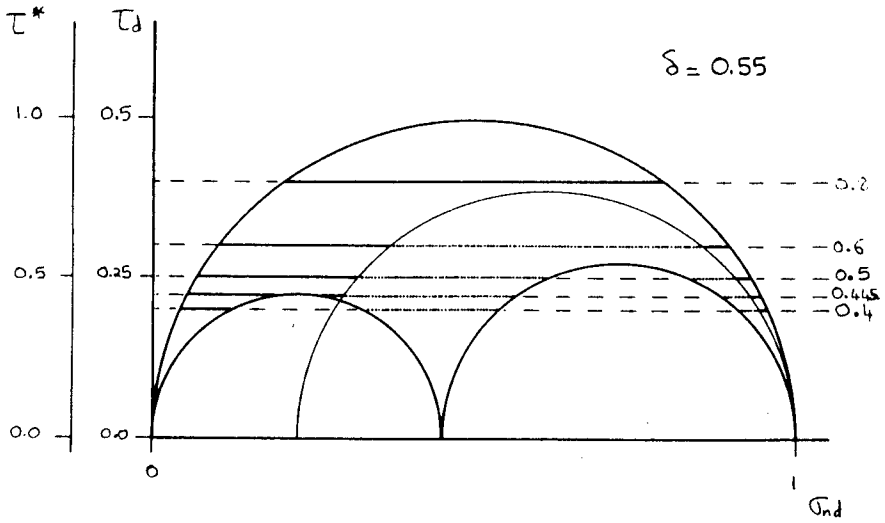
τ*
τd
δ = 0.55
1.0
0.5
0.5
0.25
0.0
0.0
0
1
τnd
0.6
0.5
0.45
0.4

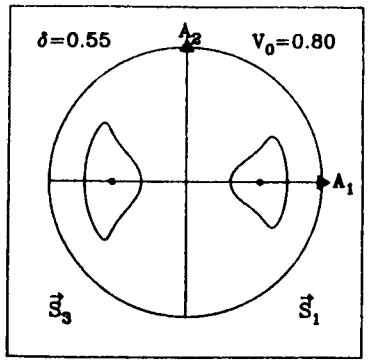
δ=0.55
V0=0.80
A2
A1
S3
S1

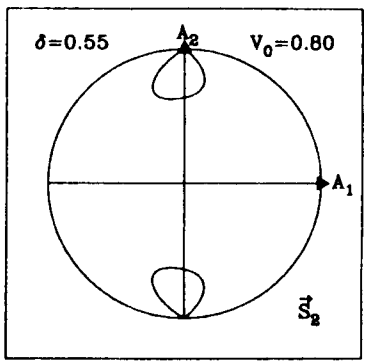
δ=0.55
V0=0.80
A2
A1
S2

FIG 3.12

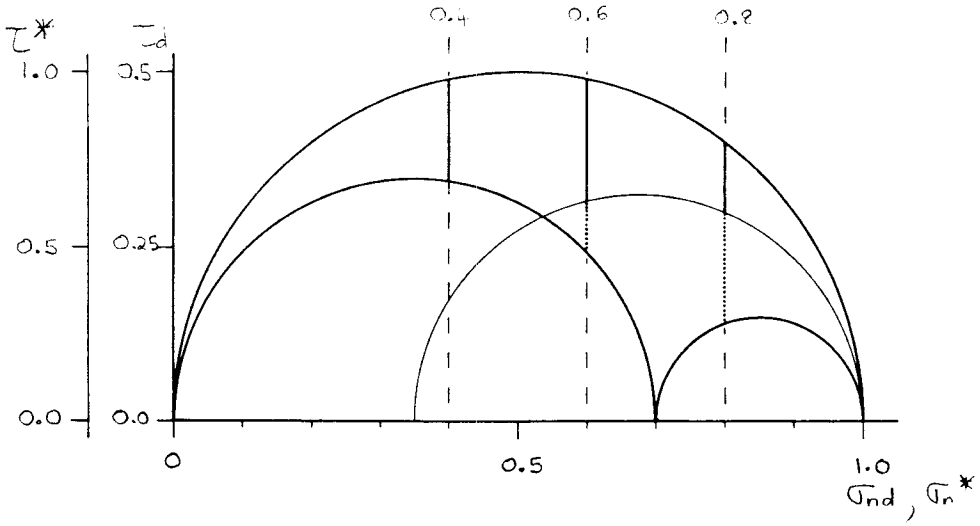
τ*
τd
1.0
0.5
0.0
0.5
0.25
0.0
0.4
0.6
0.8
0
0.5
1.0
σnd , σn*

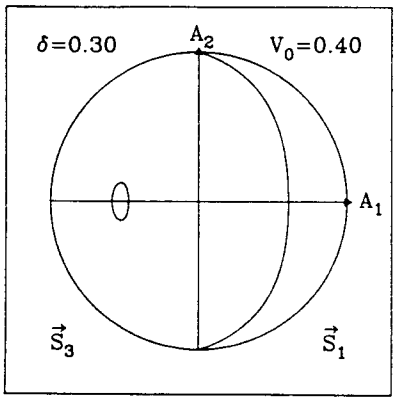
δ=0.30
A2
V0=0.40
A1
S3
S1

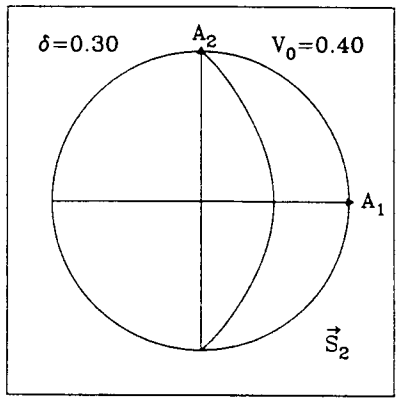
δ=0.30
A2
V0=0.40
A1
S2

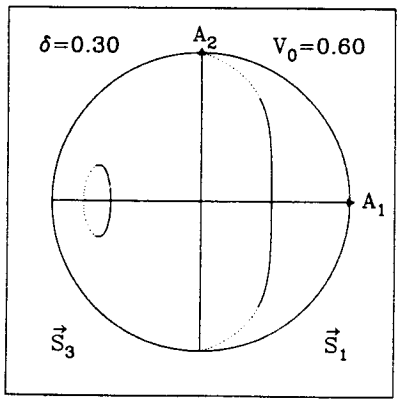
δ=0.30
A2
V0=0.60
A1
S3
S1

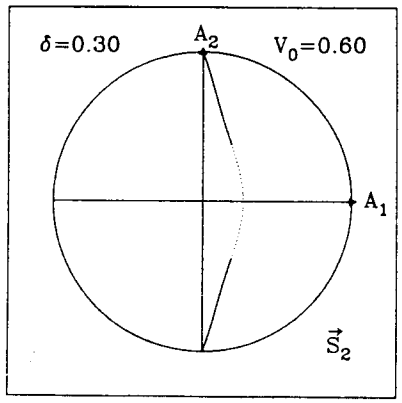
δ=0.30
A2
V0=0.60
A1
S2

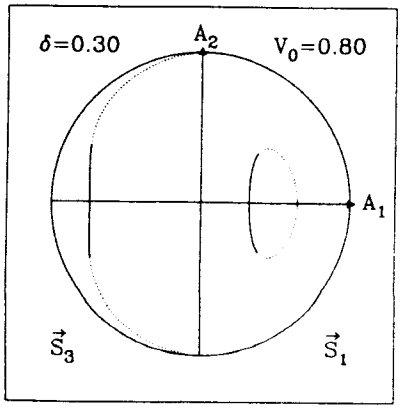
δ=0.30
A2
V0=0.80
A1
S3
S1

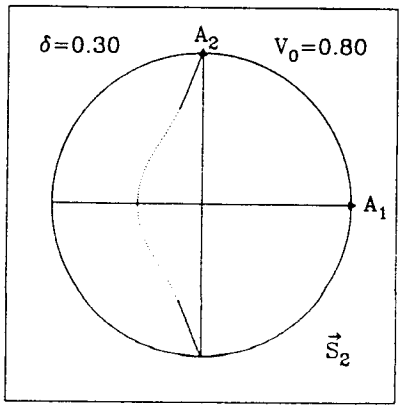
δ=0.30
A2
V0=0.80
A1
S2

FIG 3.13

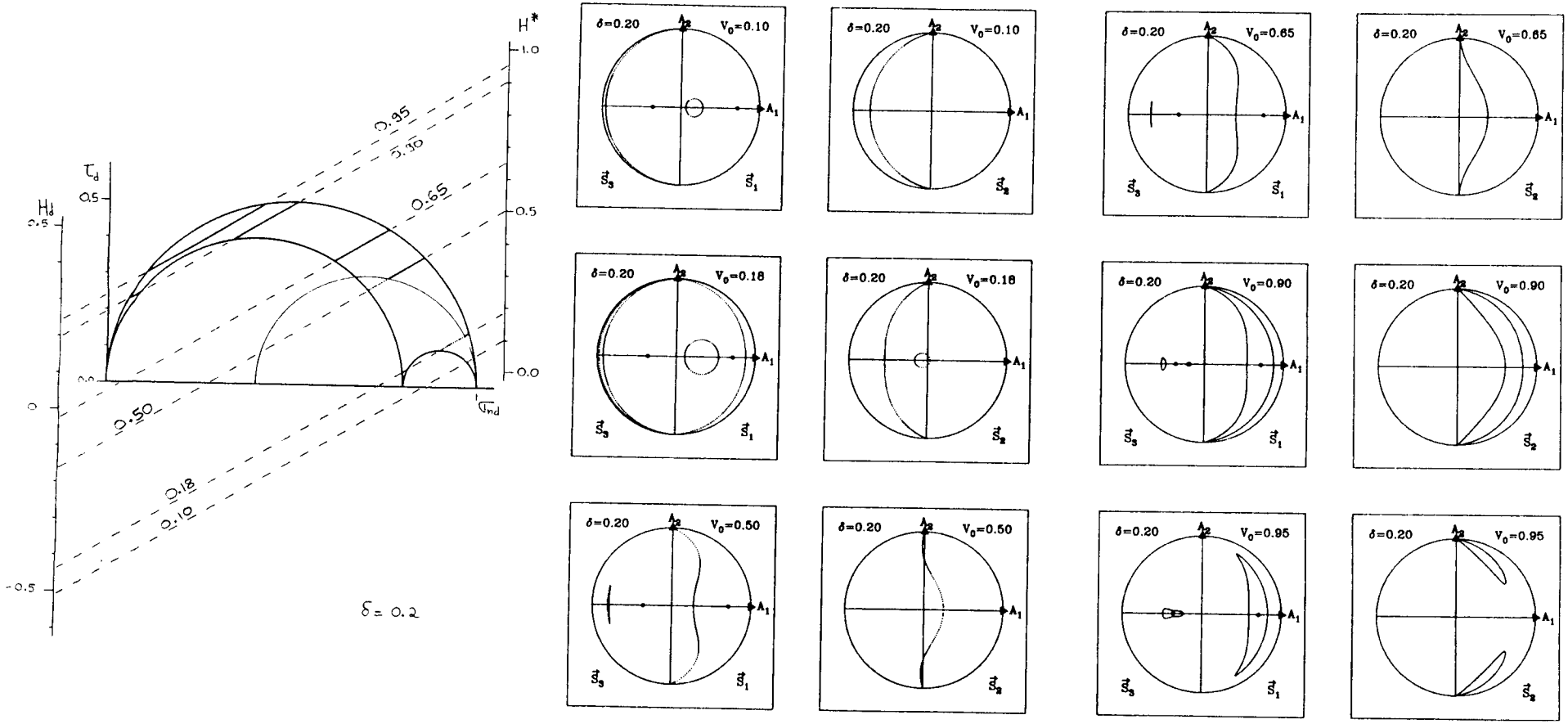
H*
1.0
0.5
0.0
τd
0.5
Hd
0.5
0
-0.5
0.35
0.35
0.65
0.50
0.18
0.10
τnd
δ=0.20
V0=0.10
δ=0.20
V0=0.10
δ=0.20
V0=0.65
δ=0.20
V0=0.65
δ=0.20
V0=0.18
δ=0.20
V0=0.18
δ=0.20
V0=0.90
δ=0.20
V0=0.90
δ=0.20
V0=0.50
δ=0.20
V0=0.50
δ=0.20
V0=0.95
δ=0.20
V0=0.95
A1
A2
S3
S1
S2

δ = 0.2

FIG 3.14

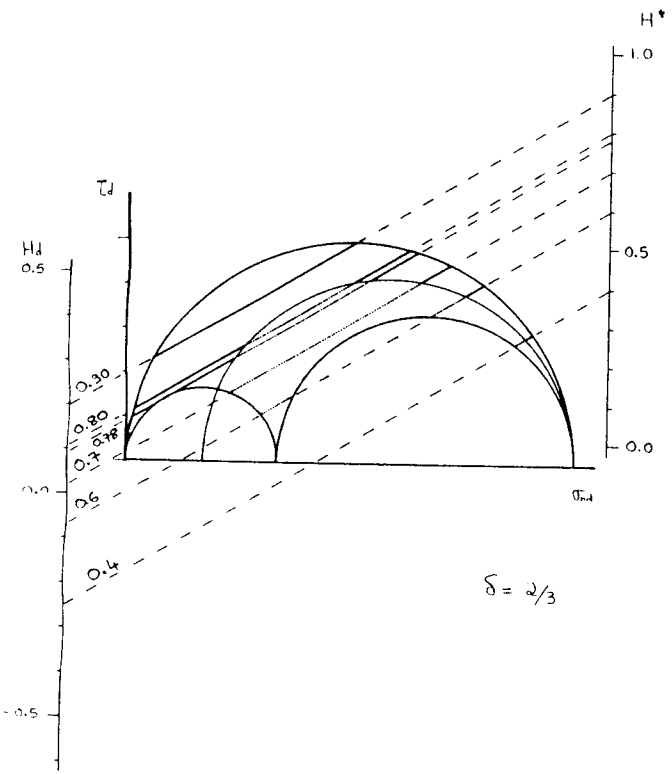
H*
1.0
0.5
0.0
0.5
0.30
0.80
0.78
0.6
0.4
δ = 2/3

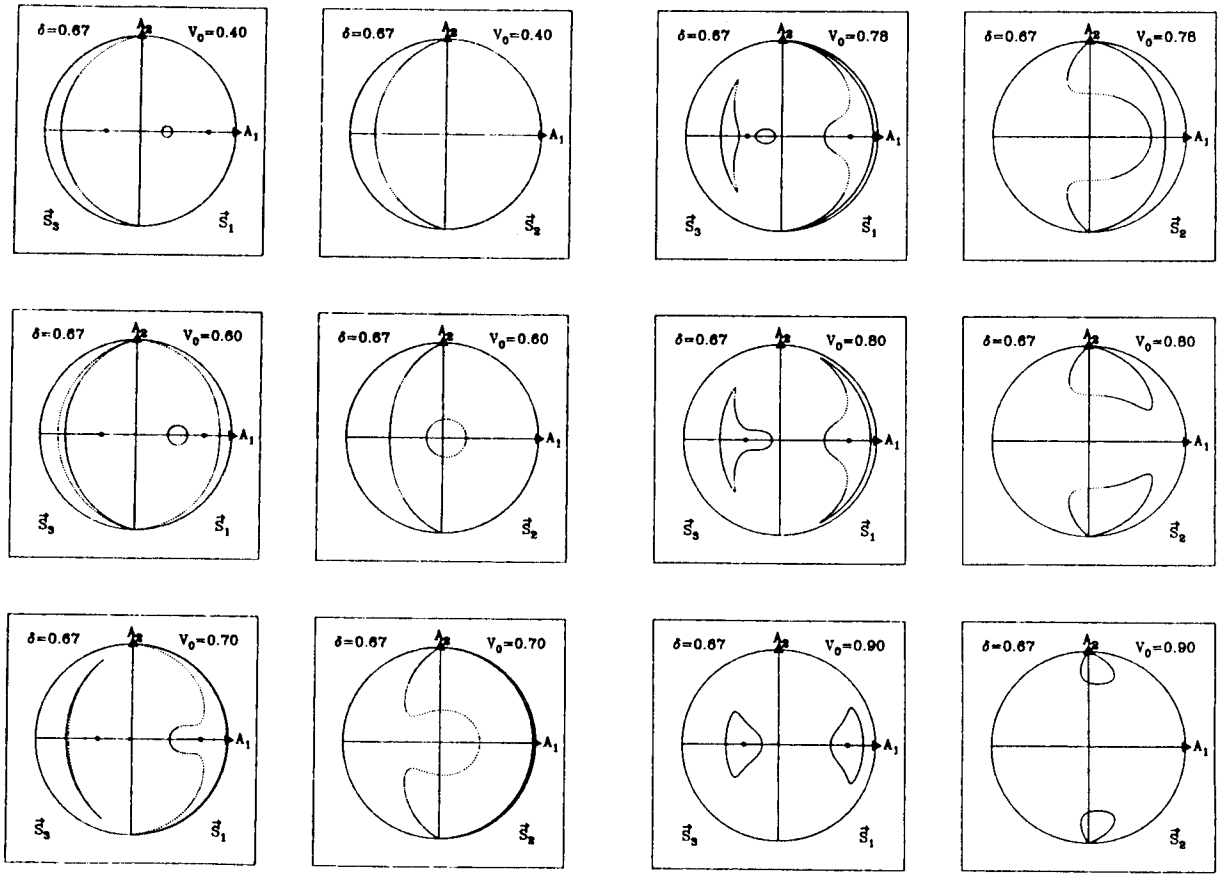
δ=0.67
V0=0.40
δ=0.67
V0=0.40
δ=0.67
V0=0.78
δ=0.67
V0=0.78
δ=0.67
V0=0.60
δ=0.67
V0=0.60
δ=0.67
V0=0.80
δ=0.67
V0=0.80
δ=0.67
V0=0.70
δ=0.67
V0=0.70
δ=0.67
V0=0.90
δ=0.67
V0=0.90

FIG 3.15

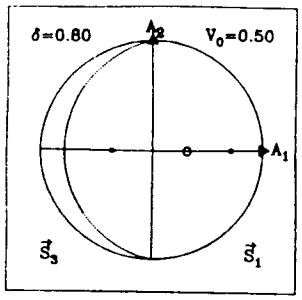
δ=0.80
V0=0.50
A2
A1
S3
S1

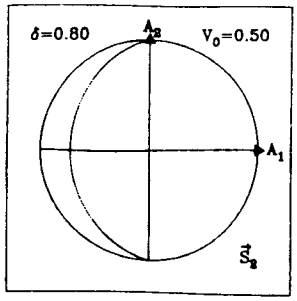
δ=0.80
V0=0.50
A1
S2

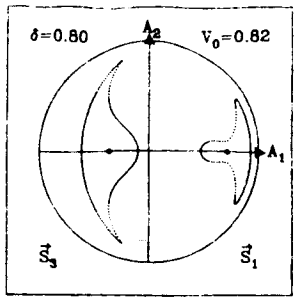
δ=0.80
V0=0.82
A2
A1
S3
S1

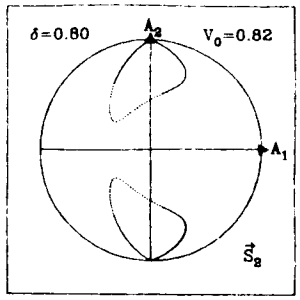
δ=0.80
V0=0.82
A2
A1
S2

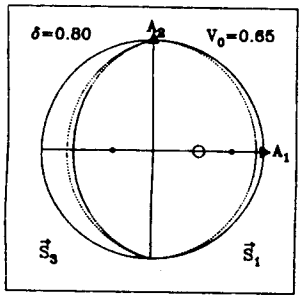
δ=0.80
V0=0.65
A2
A1
S3
S1

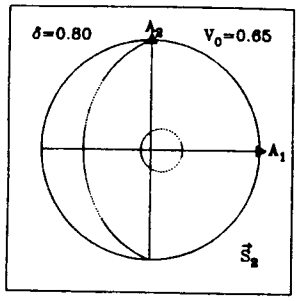
δ=0.80
V0=0.65
A1
S2

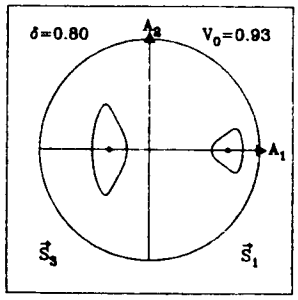
δ=0.80
V0=0.93
A2
A1
S3
S1

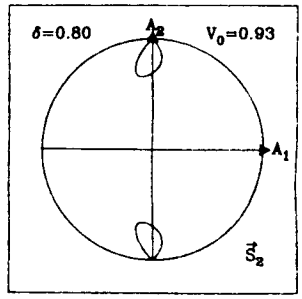
δ=0.80
V0=0.93
A2
A1
S2

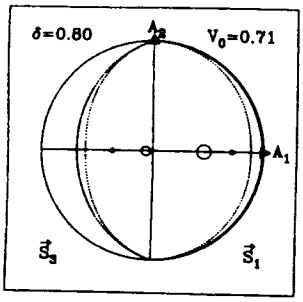
δ=0.80
V0=0.71
A2
A1
S3
S1

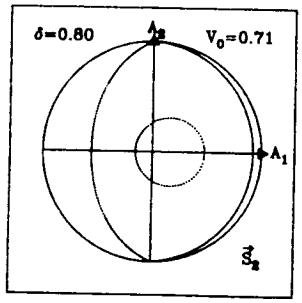
δ=0.80
V0=0.71
A1
S2

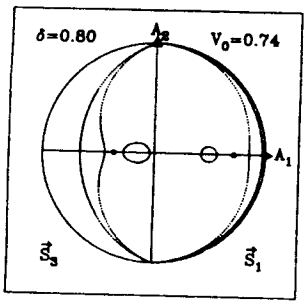
δ=0.80
V0=0.74
A2
A1
S3
S1

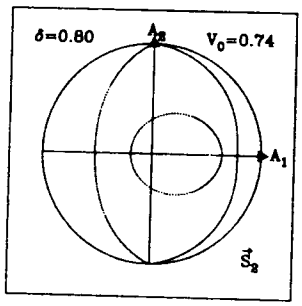
δ=0.80
V0=0.74
A1
S2

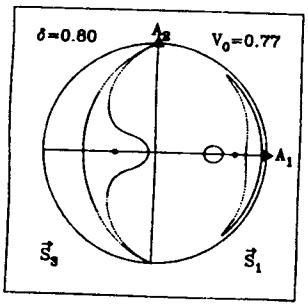
δ=0.80
V0=0.77
A2
A1
S3
S1

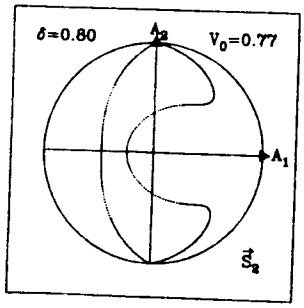
δ=0.80
V0=0.77
A1
S2

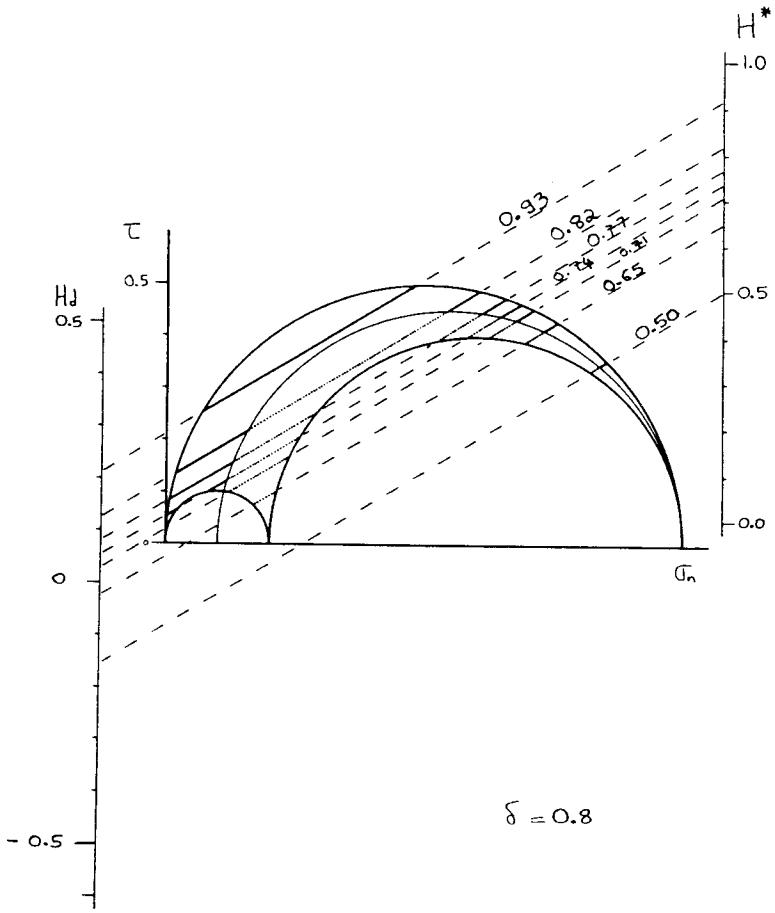
H*
1.0
0.5
0.0
τ
0.5
Hd
0.5
0
- 0.5
0.93
0.82
0.77
0.74
0.71
0.65
0.50
σn
δ = 0.8

Fig 3.16

FIG 3.17

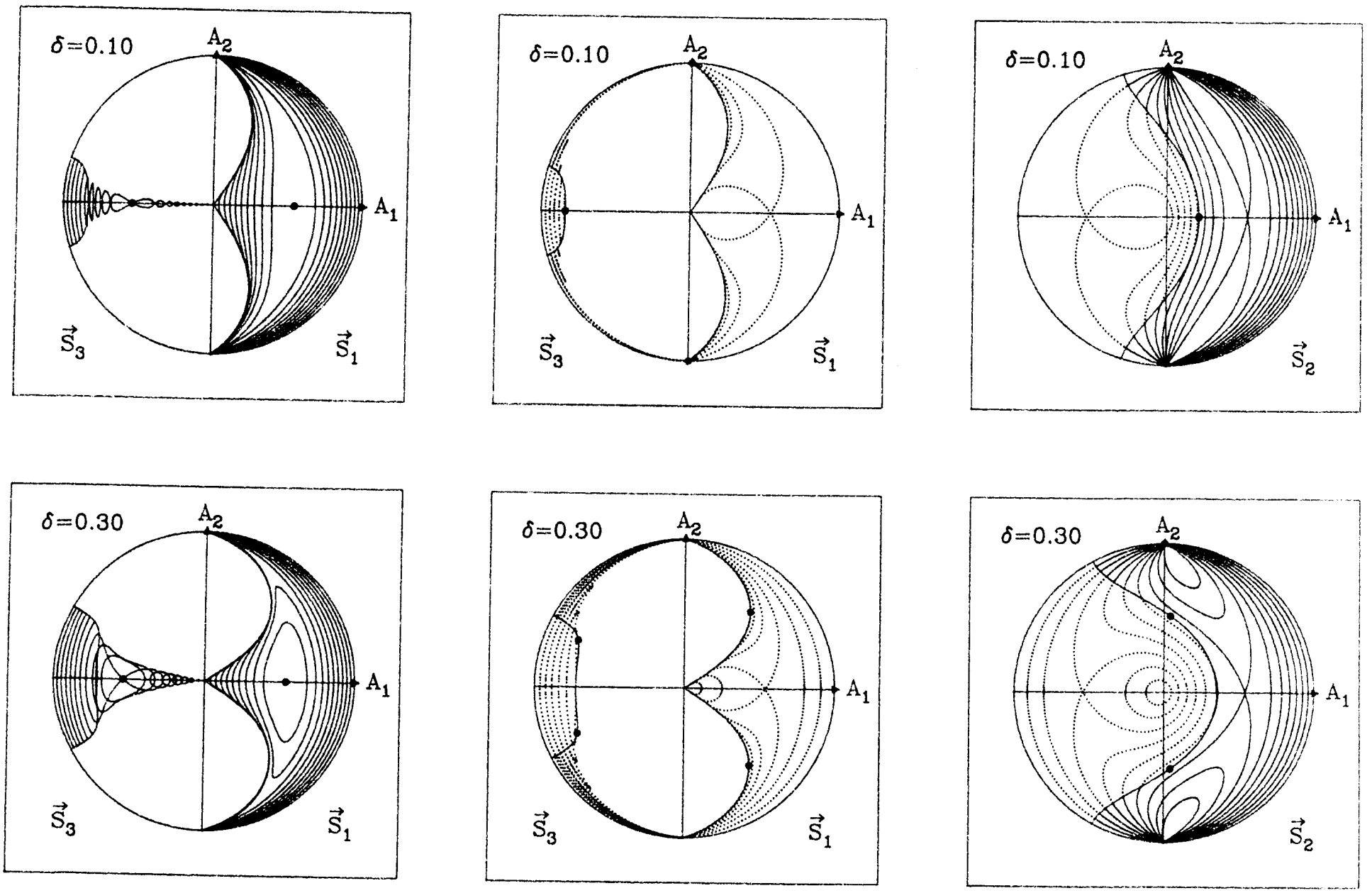
δ=0.10
A2
A1
S3
S1
δ=0.10
A2
A1
S3
S1
δ=0.10
A2
A1
S2
δ=0.30
A2
A1
S3
S1
δ=0.30
A2
A1
S3
S1
δ=0.30
A2
A1
S2

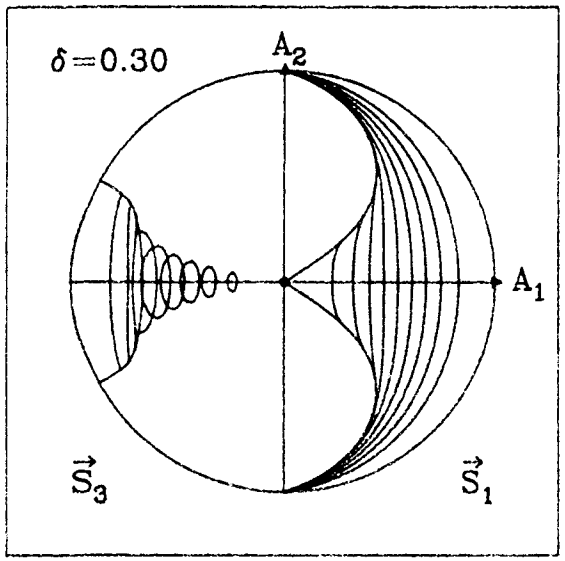
δ=0.30
A2
A1
S3
S1

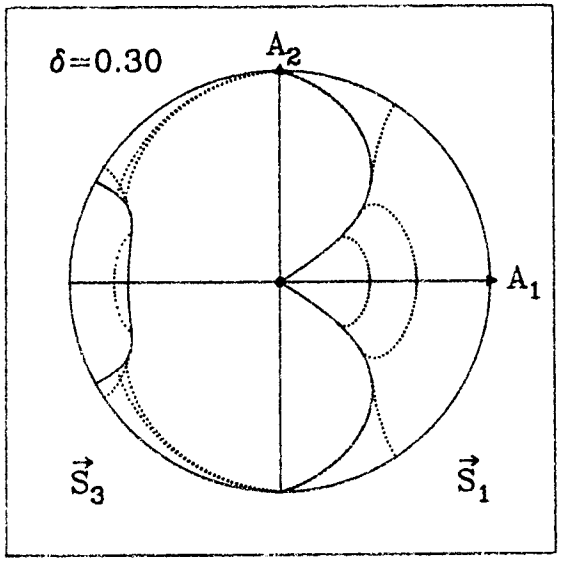
δ=0.30
A2
A1
S3
S1

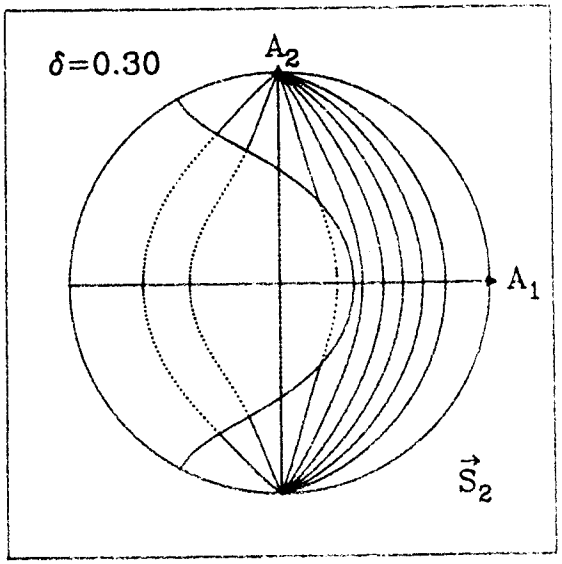
δ=0.30
A2
A1
S2

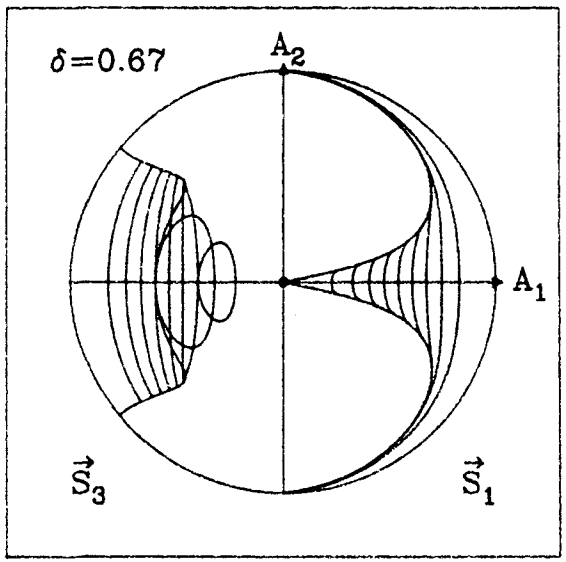
δ=0.67
A2
A1
S3
S1

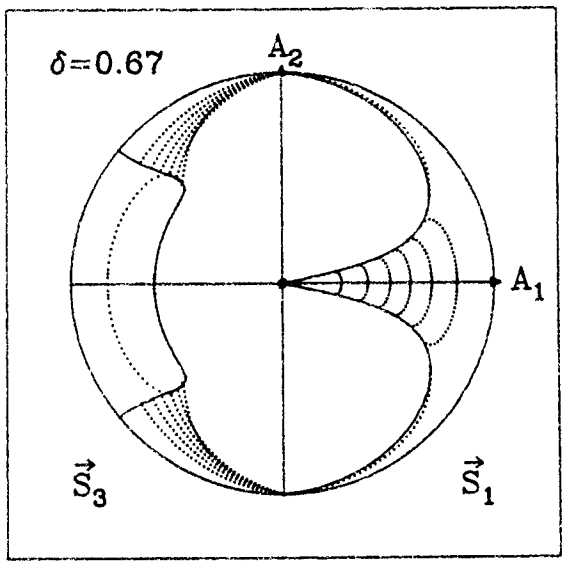
δ=0.67
A2
A1
S3
S1

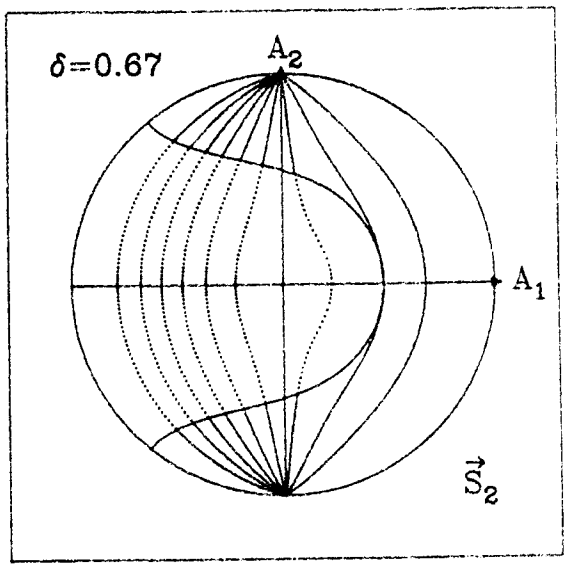
δ=0.67
A2
A1
S2

FIG 5.19

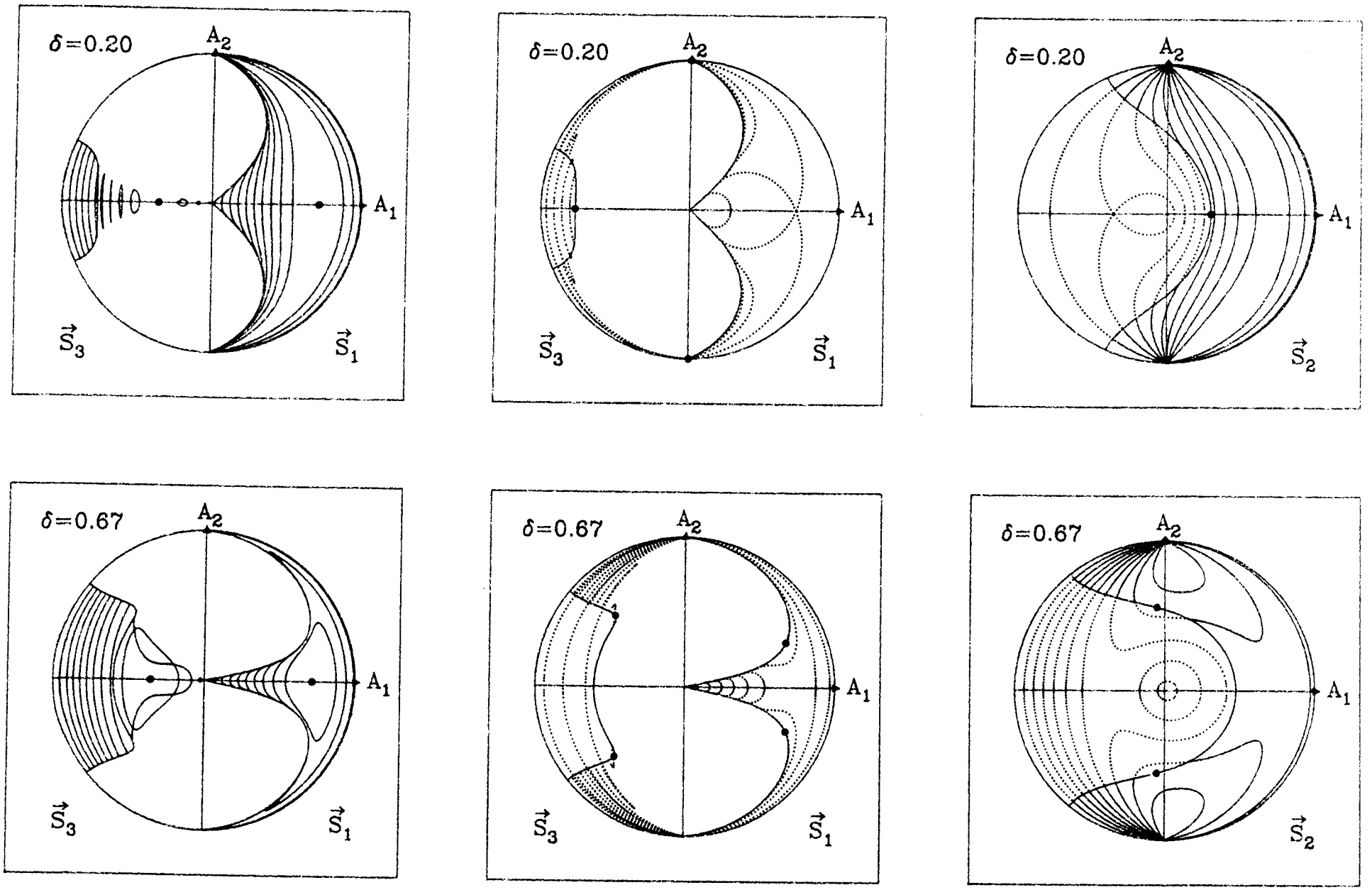
δ=0.20
A2
A1
S3
S1
δ=0.20
A2
A1
S3
S1
δ=0.20
A2
A1
S2
δ=0.67
A2
A1
S3
S1
δ=0.67
A2
A1
S3
S1
δ=0.67
A2
A1
S2

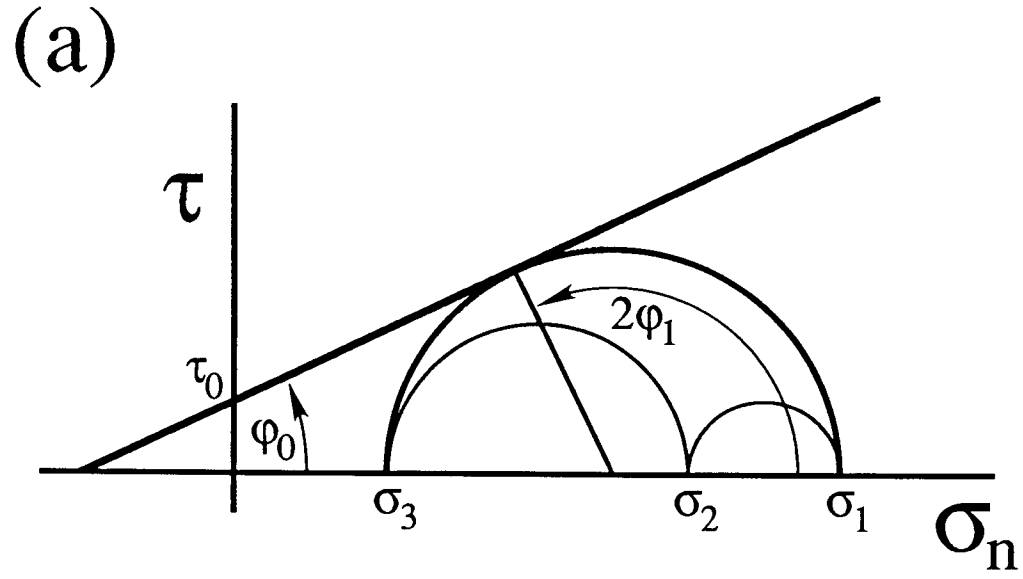

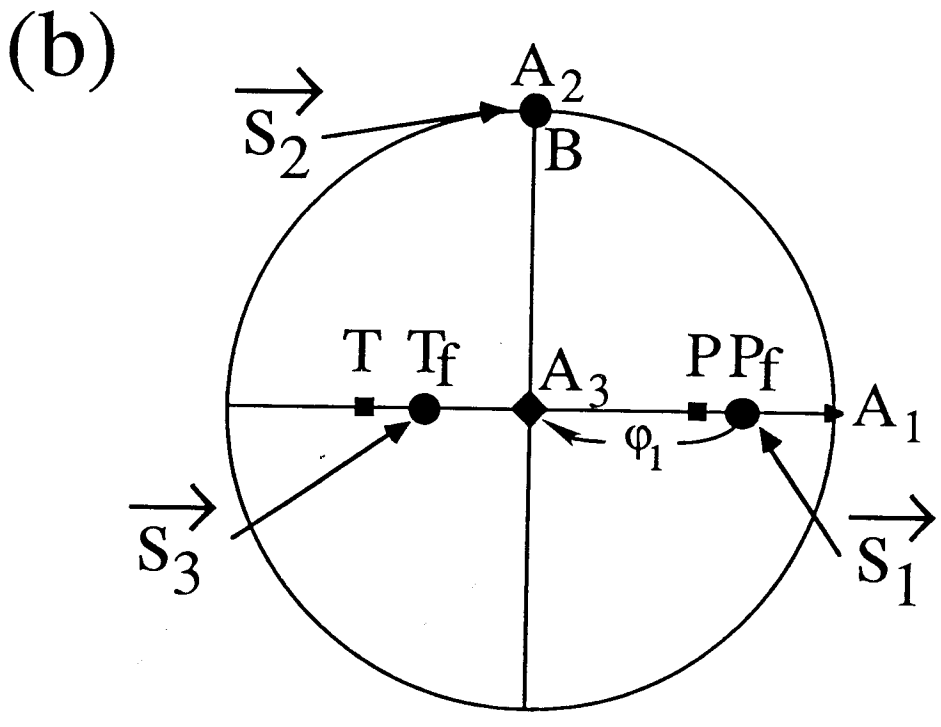

Fig. 4.1

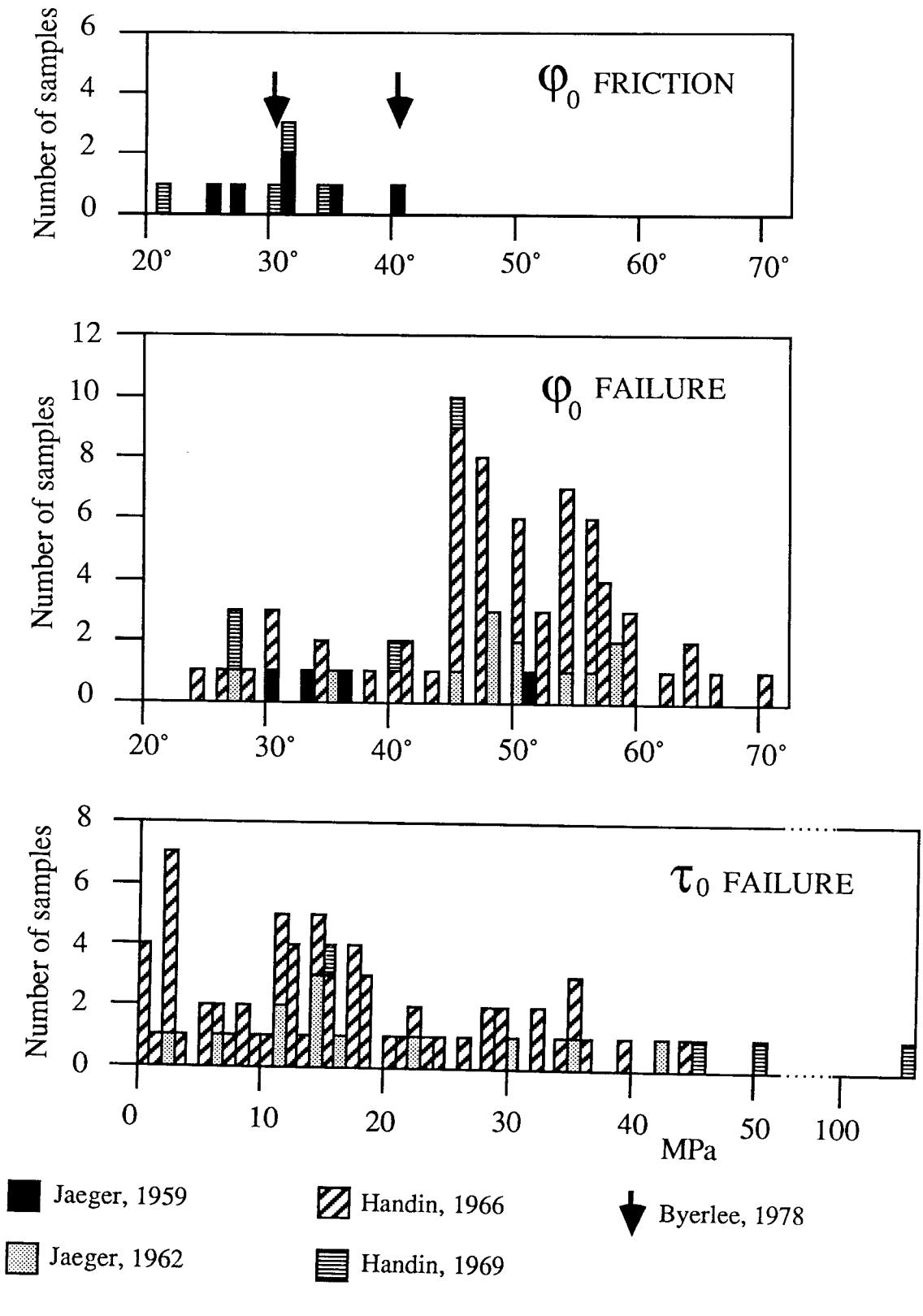
Number of samples
6
4
2
0
20°
30°
40°
50°
60°
70°
φ0 FRICTION
12
10
8
6
4
2
0
φ0 FAILURE
8
6
4
2
0
τ0 FAILURE
0
10
20
30
40
50
100
MPa
Jaeger, 1959
Jaeger, 1962
Handin, 1966
Handin, 1969
Byerlee, 1978

Fig. 4.2

(a)

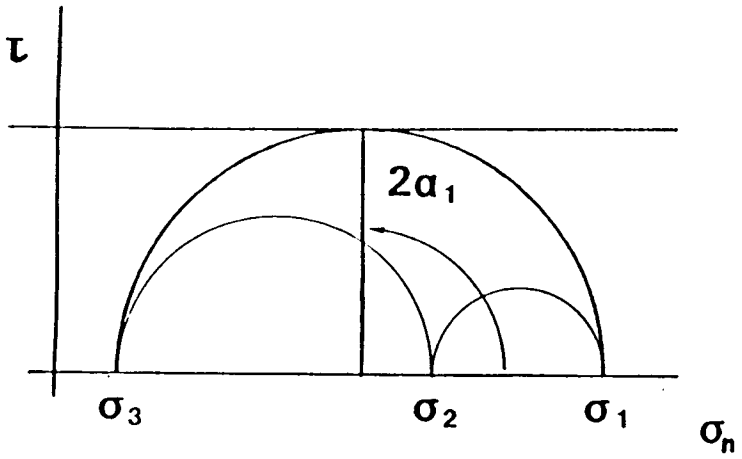

(b)

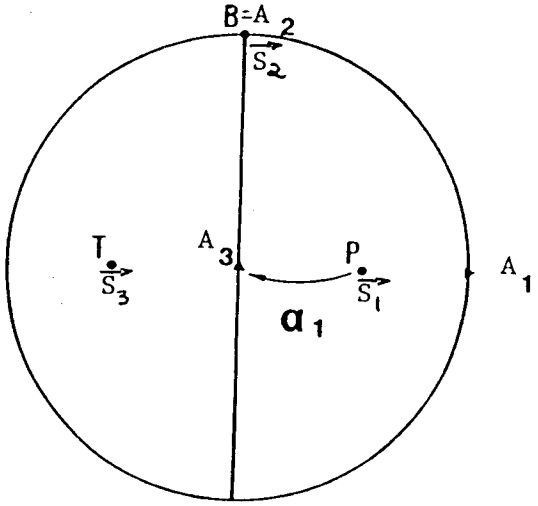

Fig 4.3

(a)

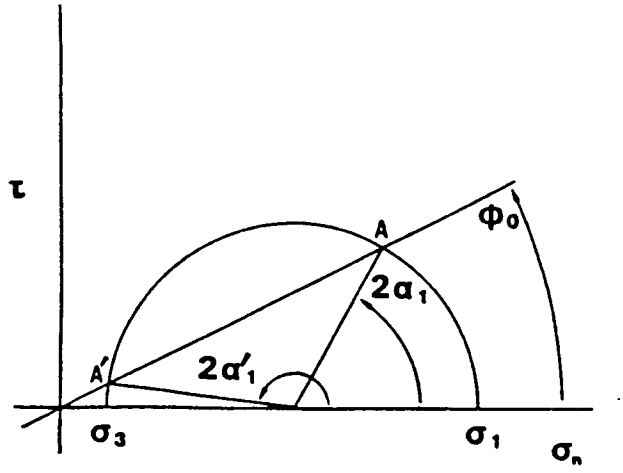

(b)

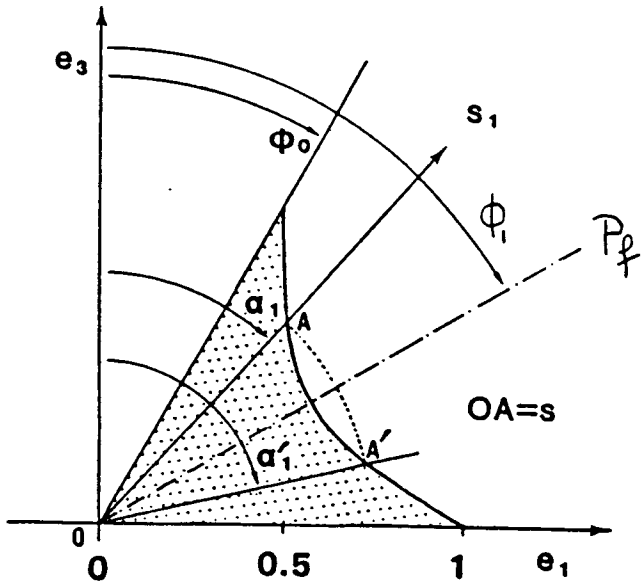

Fig 4.4

(a)

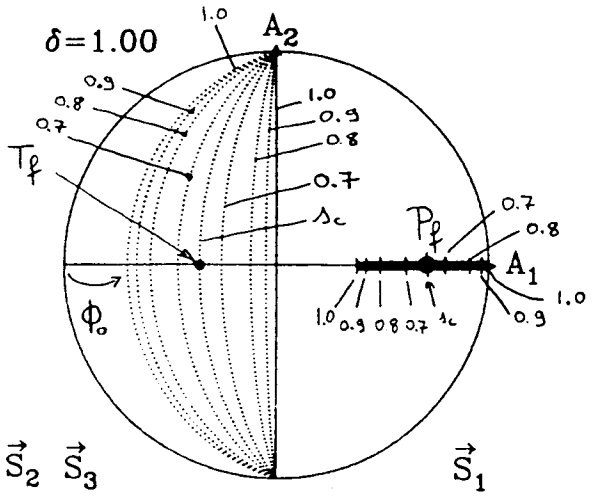
δ=1.00
A2
A1
Tf
Pf
Sc
Φo
1.0
0.9
0.8
0.7
S2 S3
S1

(b)

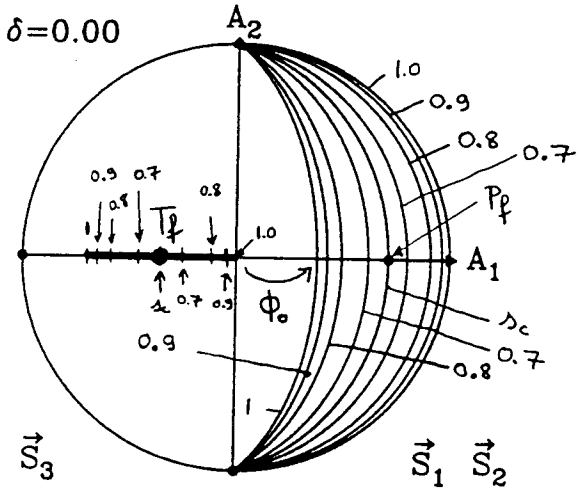
δ=0.00
A2
A1
Tf
Pf
Sc
Φo
1.0
0.9
0.8
0.7
S3
S1 S2

Fig 4.5

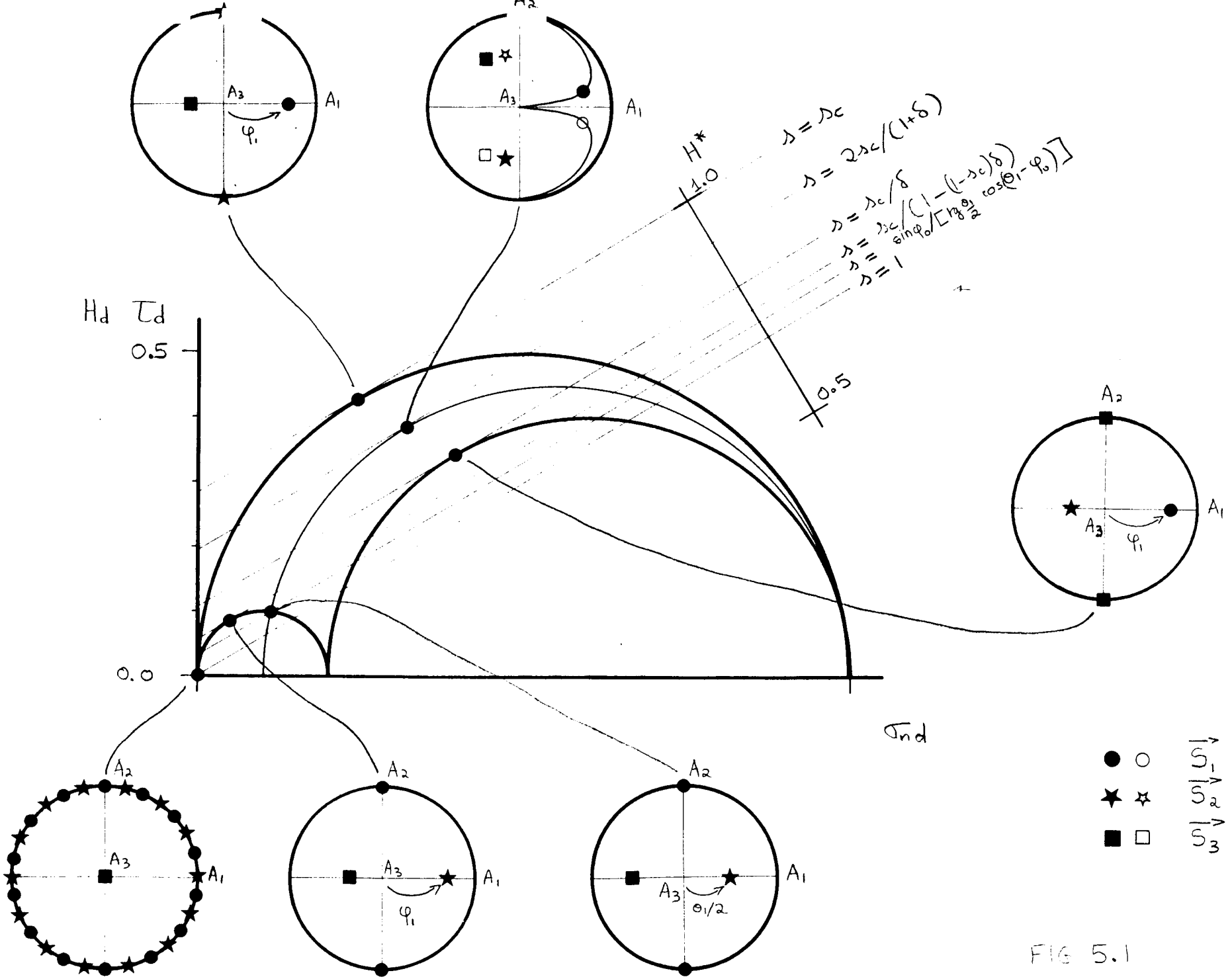
A3
A1
φ1
A2
H*
1.0
0.5
λ = λc
λ = 2λc/(1+δ)
λ = λc/δ
λ = λc/(1−(1−λc)δ)
λ = λc/[sinφ0/[ηg sinθ1/2 cos(θ1−φ0)]]
λ = 1
Hd τd
0.5
0.0
σnd
θ1/2
S1
S2
S3

FIG 5.1

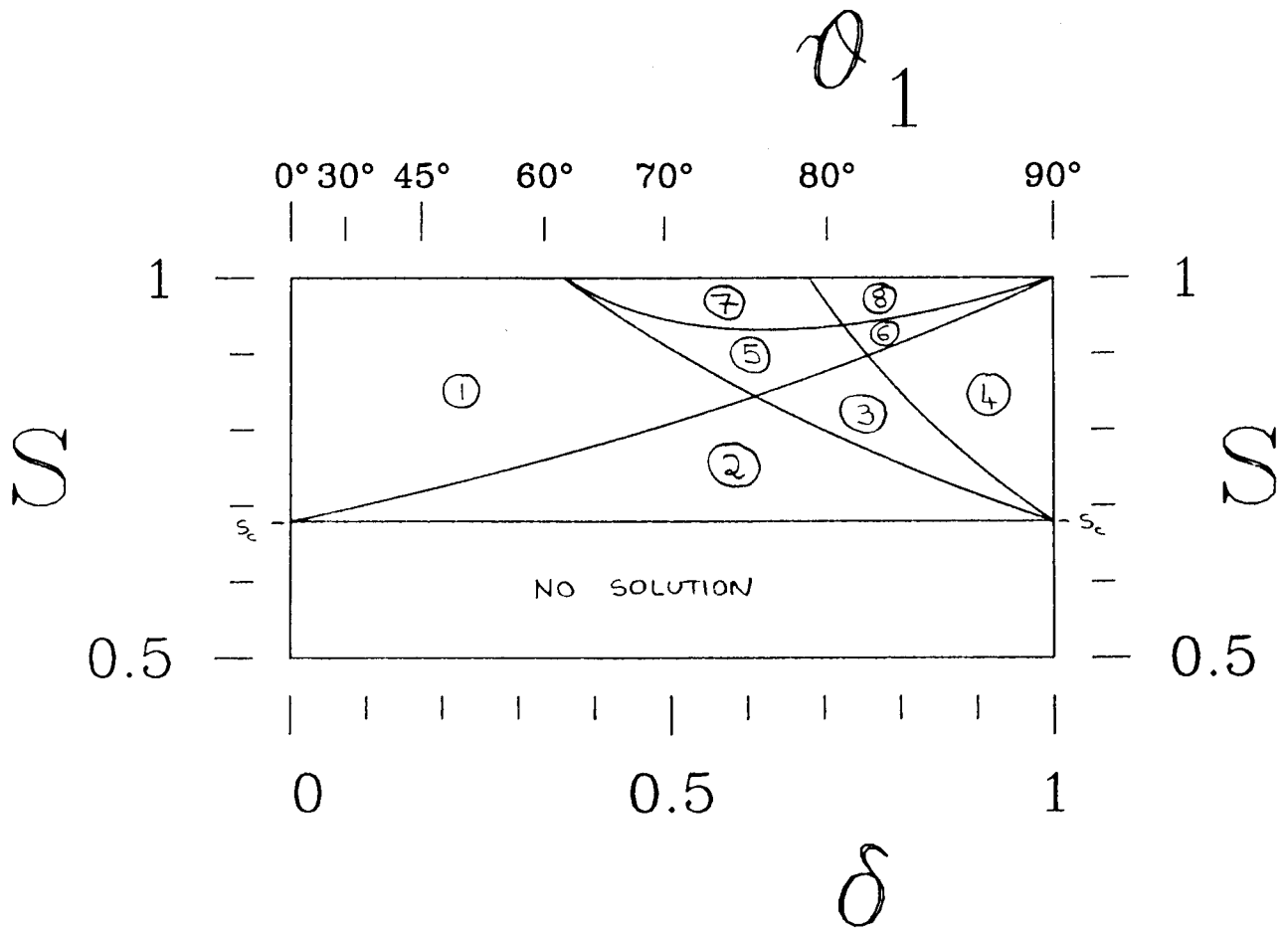
θ_1
0° 30° 45° 60° 70° 80° 90°
1
0.5
S
S_c
NO SOLUTION
1
2
3
4
5
6
7
8
0
0.5
1
δ

FIG 5.2

FIG 5.3

$\delta = 0.795$

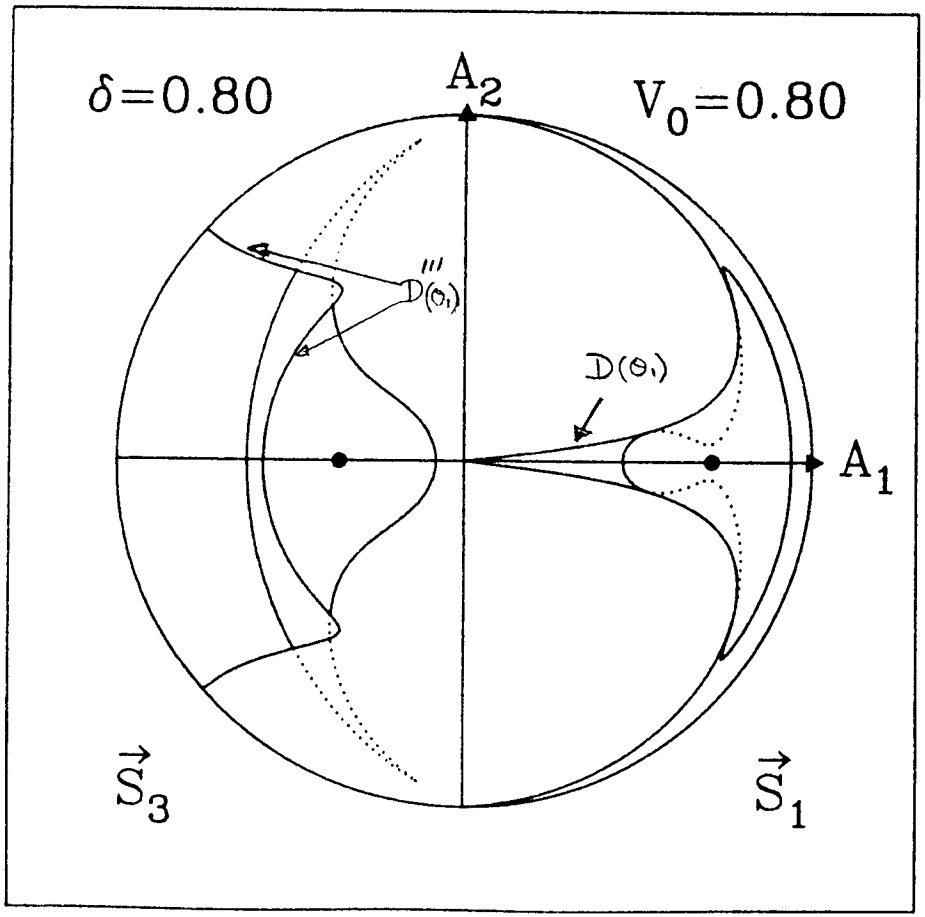

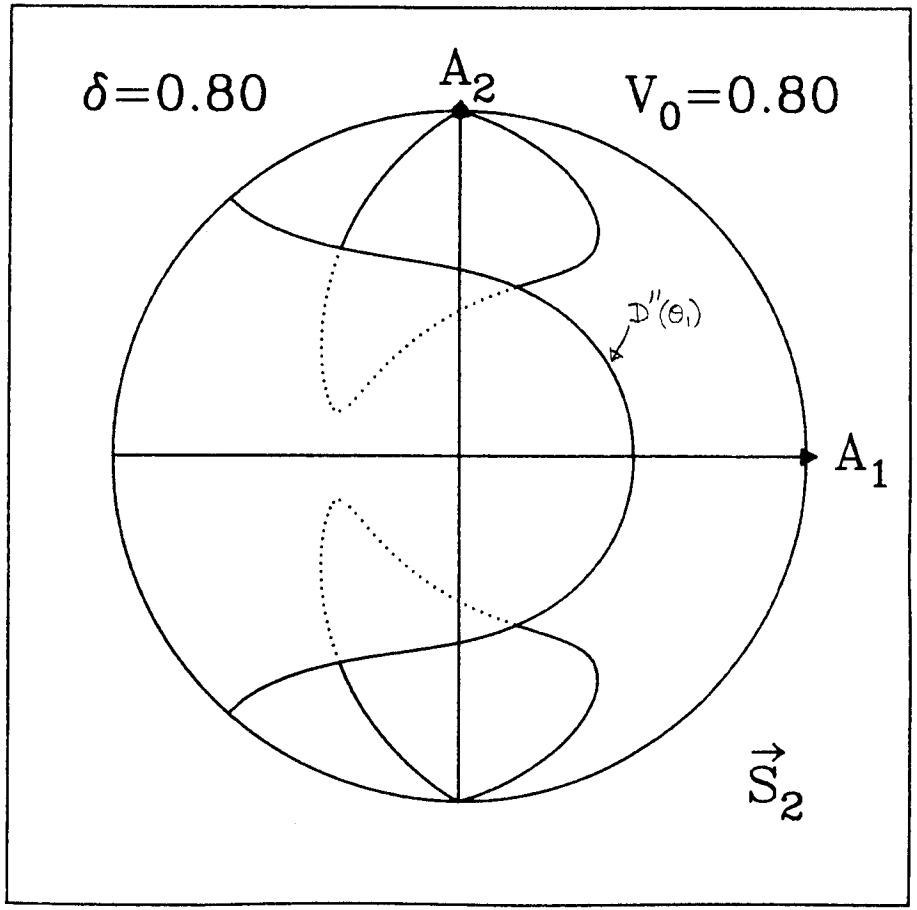

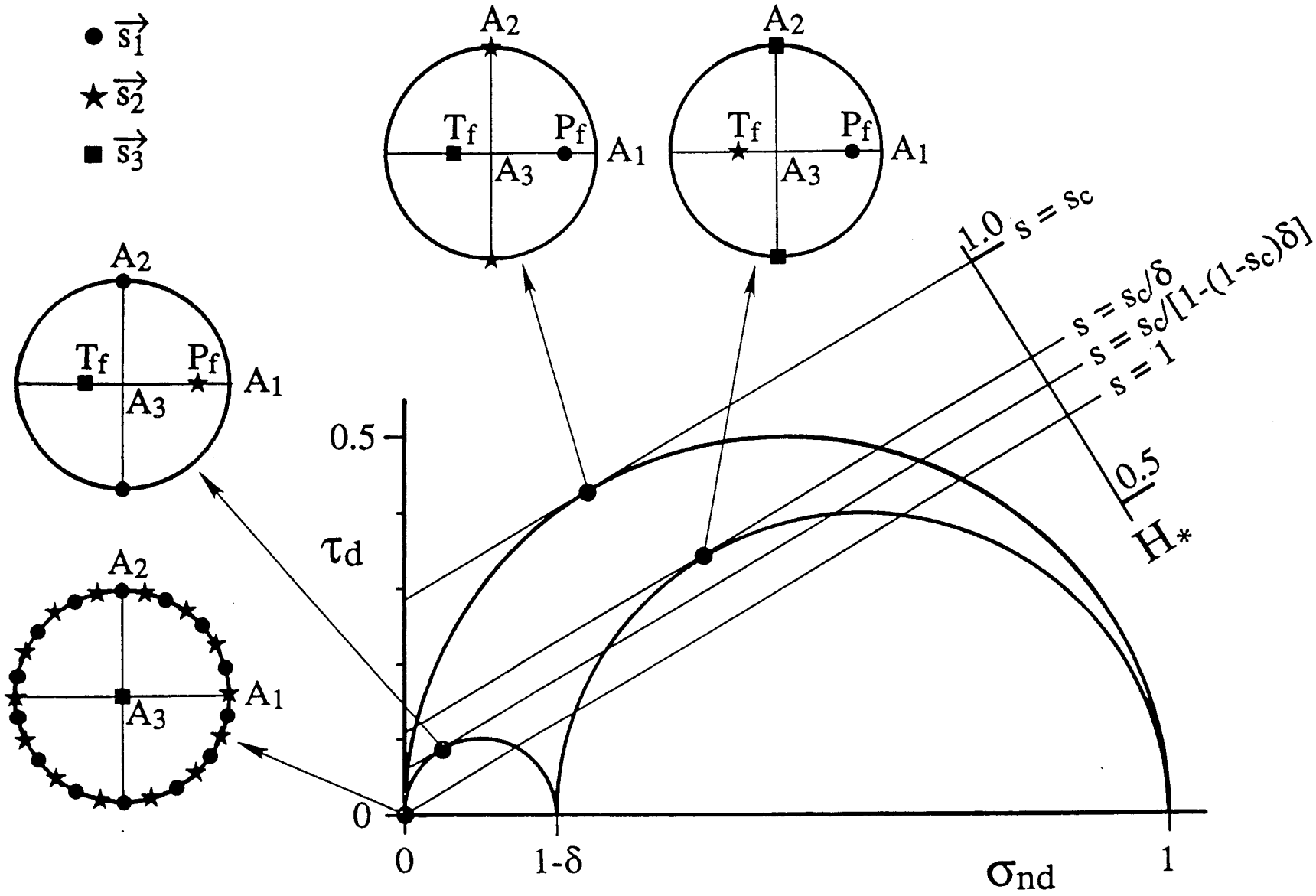
$\vec{s_1}$
$\vec{s_2}$
$\vec{s_3}$
A2
Tf
Pf
A1
A3
1.0 s = sc
s = sc/δ
s = sc/[1-(1-sc)δ]
s = 1
0.5
H*
τd
σnd
0.5
0
0
1-δ
1

Fig. 5.4

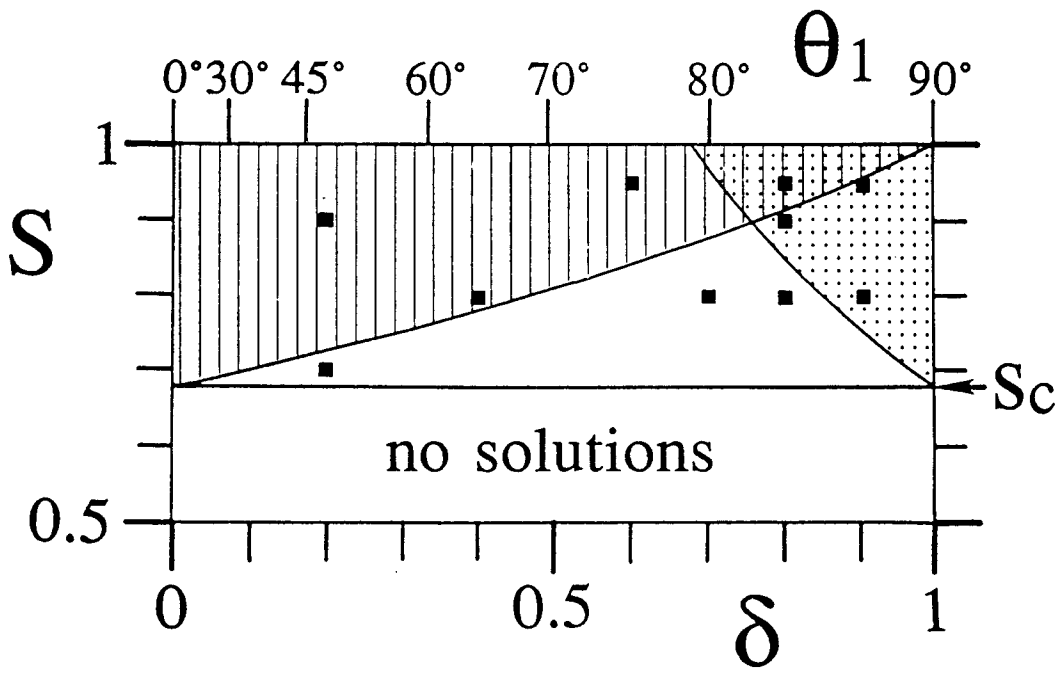

Fig. 5.5

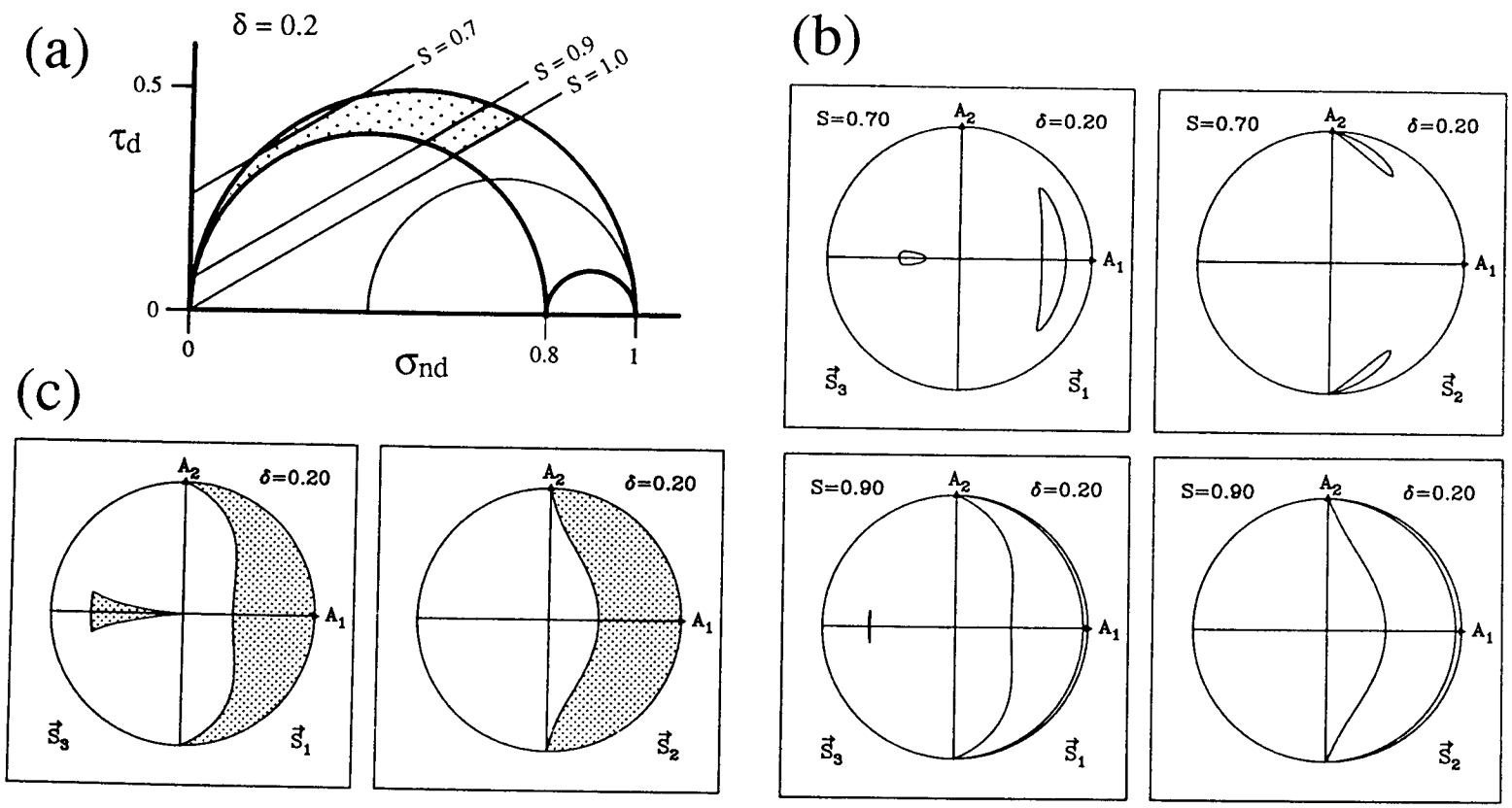
(a)
δ = 0.2
S = 0.7
S = 0.9
S = 1.0
0.5
τd
0
0
0.8
1
σnd
(b)
S=0.70
A2
δ=0.20
A1
S=0.70
A2
δ=0.20
A1
S=0.90
A2
δ=0.20
A1
S=0.90
A2
δ=0.20
A1
(c)
A2
δ=0.20
A1
A2
δ=0.20
A1

Fig. 5.6

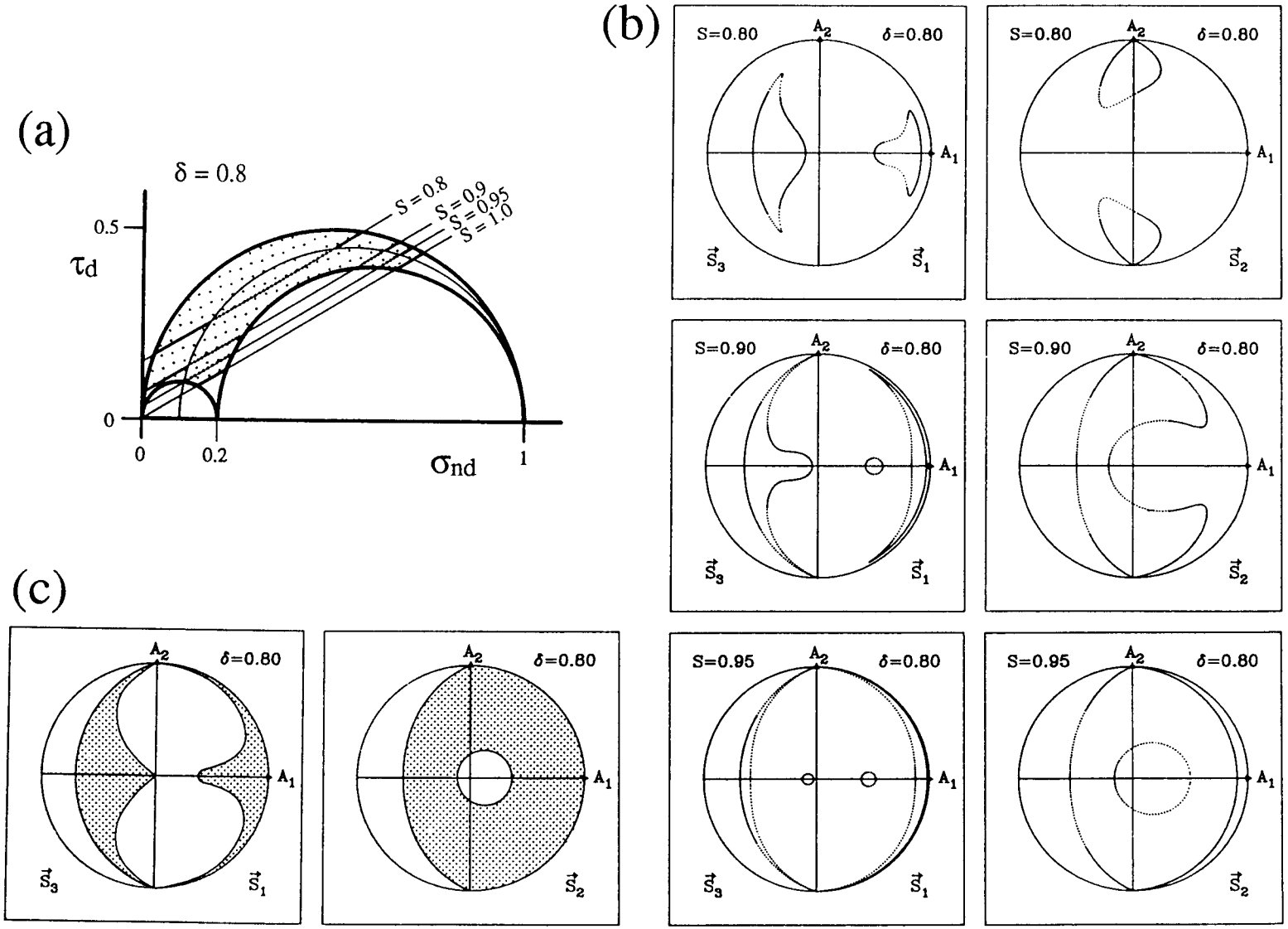
(a)
δ = 0.8
S = 0.8
S = 0.9
S = 0.95
S = 1.0
0.5
τd
0
0
0.2
σnd
1
(b)
S=0.80
δ=0.80
S=0.90
δ=0.80
S=0.95
δ=0.80
(c)
δ=0.80
A2
A1
S3
S1
S2

Fig. 5.7

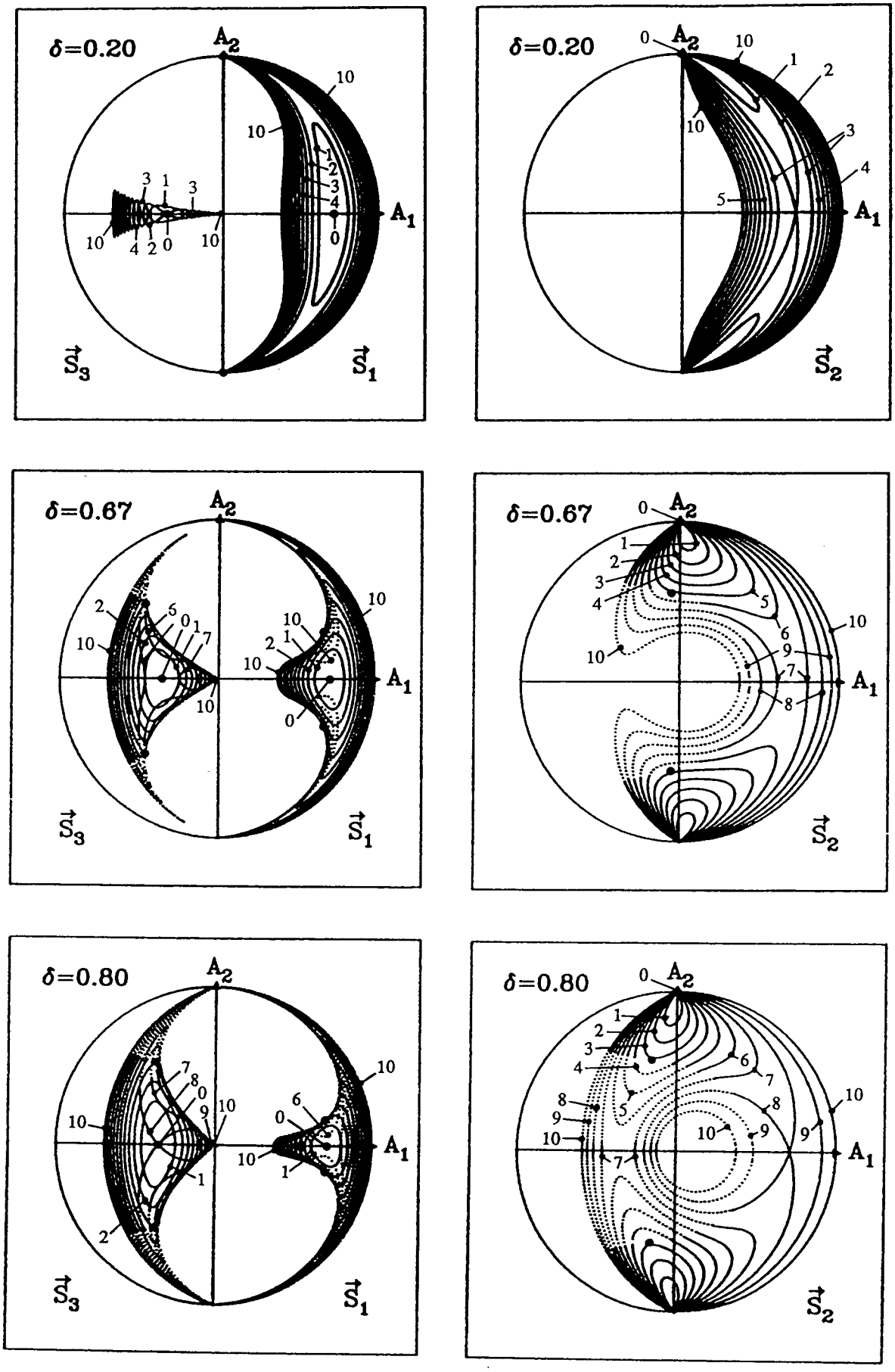
δ=0.20
A2
A1
S3
S1
δ=0.20
A2
A1
S2
δ=0.67
A2
A1
S3
S1
δ=0.67
A2
A1
S2
δ=0.80
A2
A1
S3
S1
δ=0.80
A2
A1
S2

Fig. 5.8

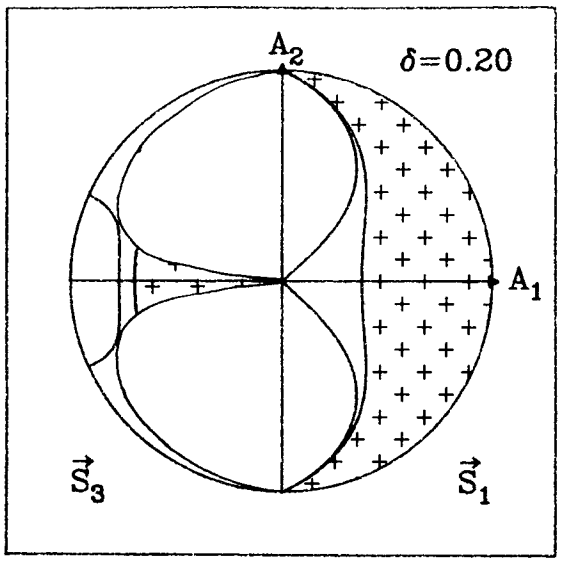
A2
δ=0.20
A1
S3
S1

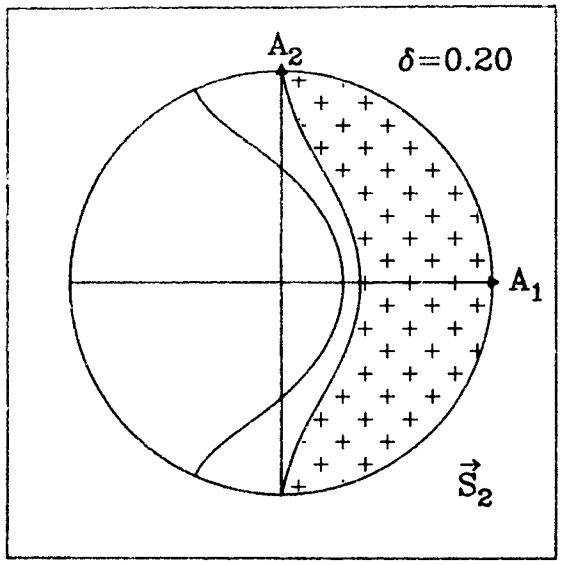
A2
δ=0.20
A1
S2

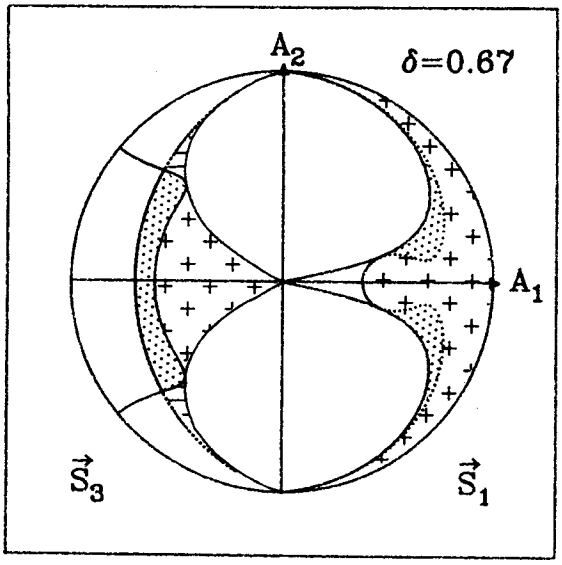
A2
δ=0.67
A1
S3
S1

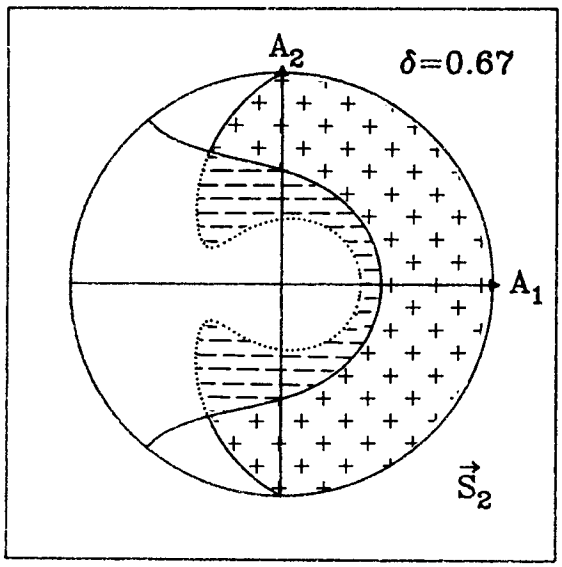
A2
δ=0.67
A1
S2

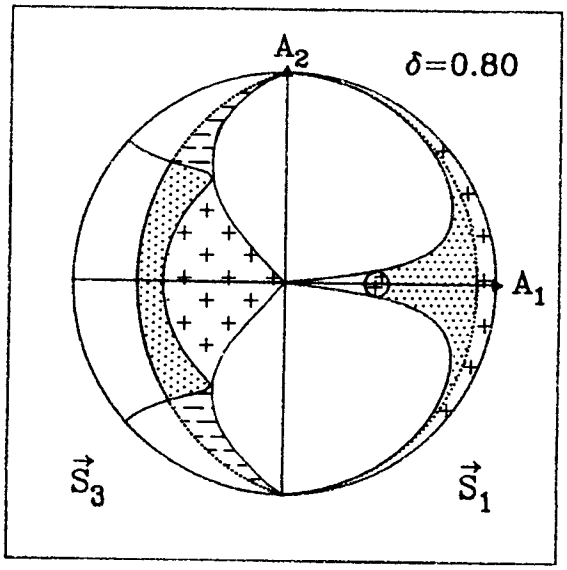
A2
δ=0.80
A1
S3
S1

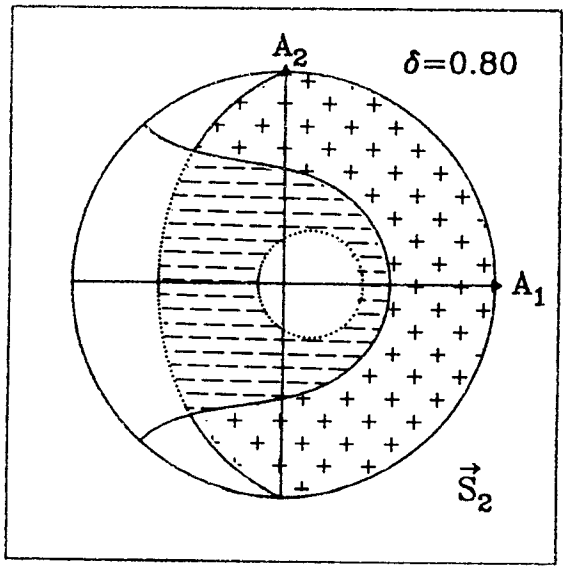
A2
δ=0.80
A1
S2

Fig. 5.9

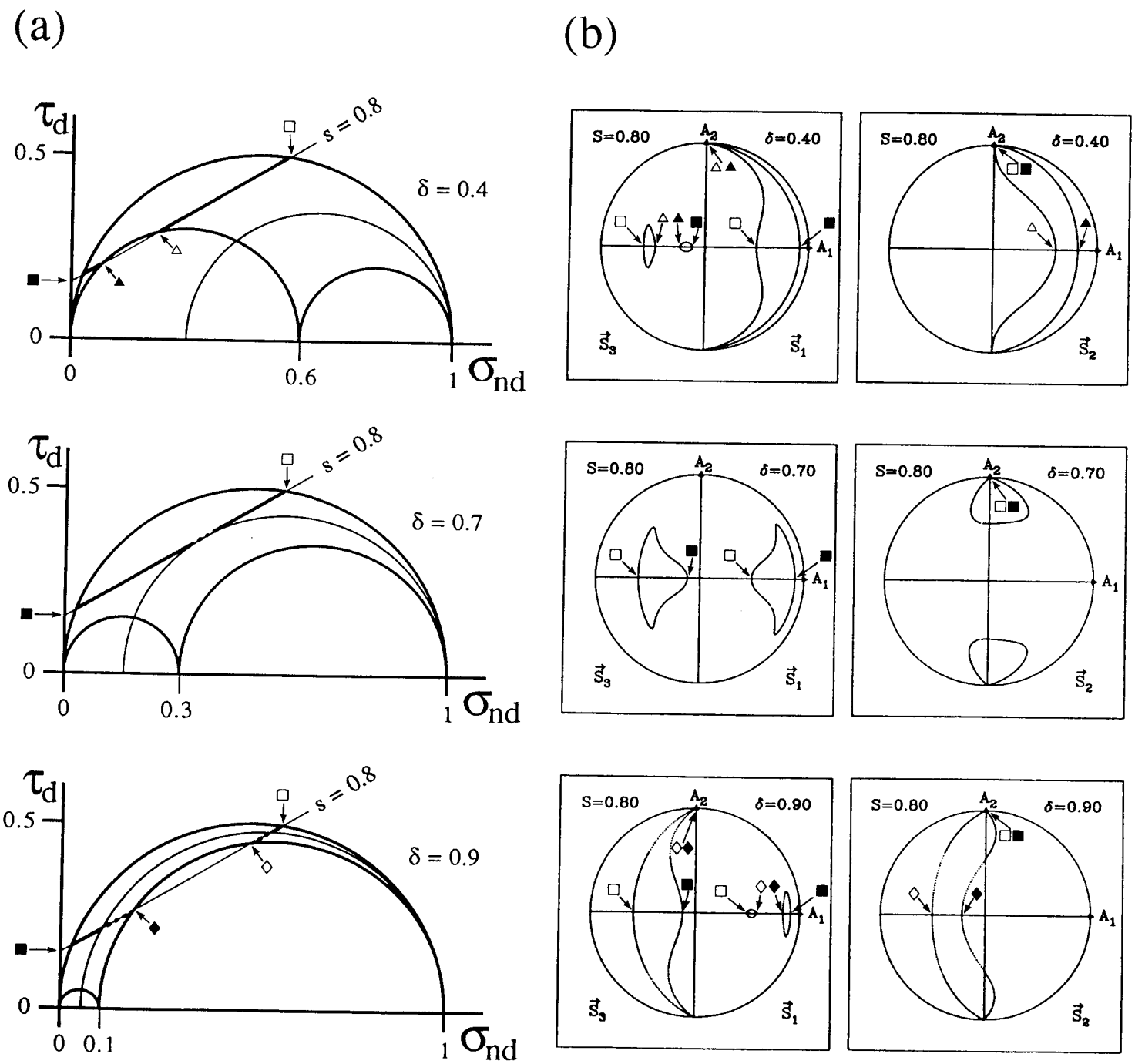
(a)
(b)
τ_d
0.5
0
0
0.6
1
σ_{nd}
s = 0.8
δ = 0.4
τ_d
0.5
0
0
0.3
1
σ_{nd}
s = 0.8
δ = 0.7
τ_d
0.5
0
0
0.1
1
σ_{nd}
s = 0.8
δ = 0.9
S=0.80
δ=0.40
S=0.80
δ=0.40
S=0.80
δ=0.70
S=0.80
δ=0.70
S=0.80
δ=0.90
S=0.80
δ=0.90
A_2
A_1
$\vec{s}_3$
$\vec{s}_1$
$\vec{s}_2$

Fig. 5.10

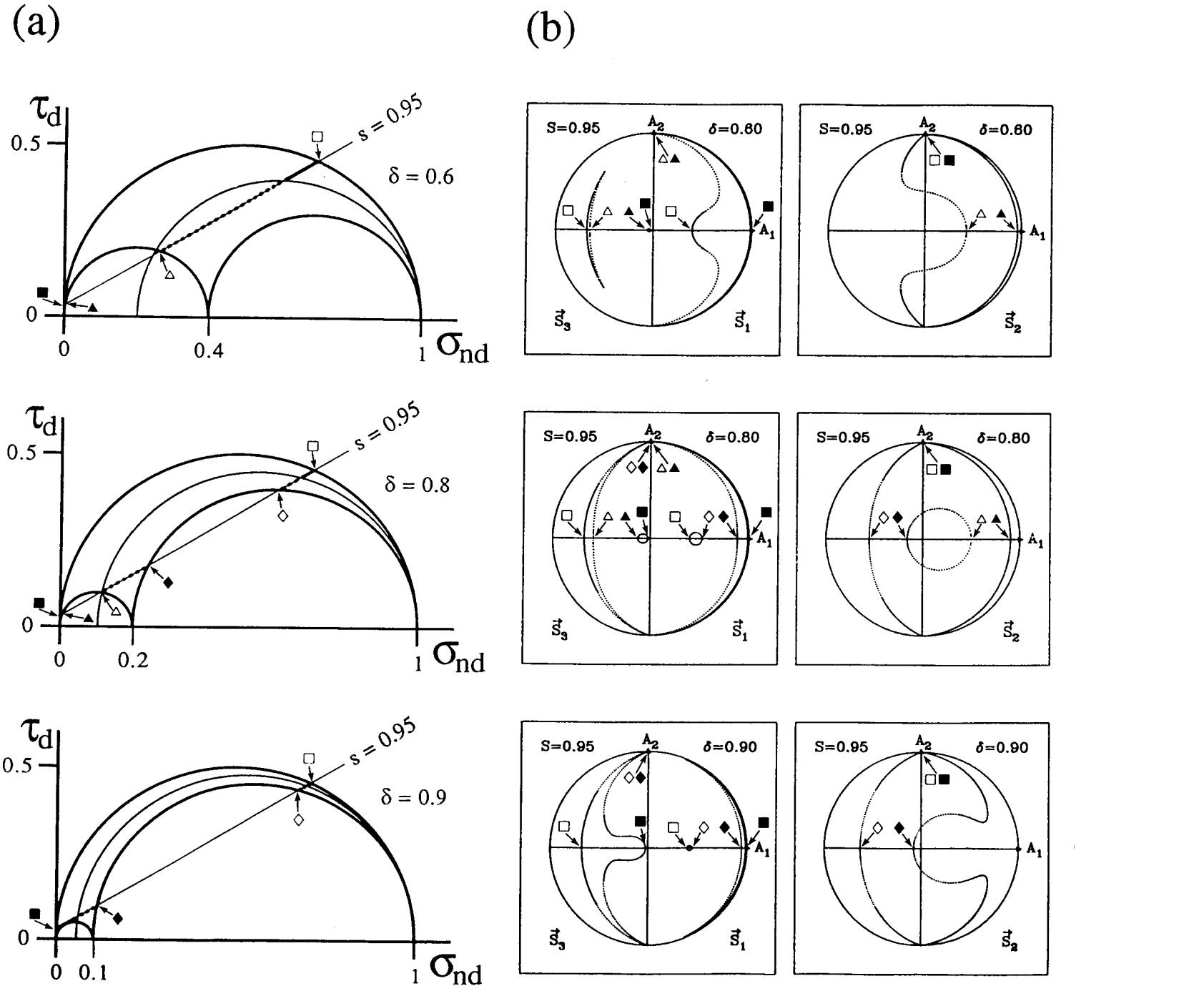
(a)
(b)
τ_d
0.5
0
0
0.4
1
σ_{nd}
s = 0.95
δ = 0.6
δ = 0.8
δ = 0.9
0.2
0.1
S=0.95
δ=0.60
δ=0.90
A_2
A_1
$\vec{S}_3$
$\vec{S}_1$
$\vec{S}_2$

Fig. 5.11

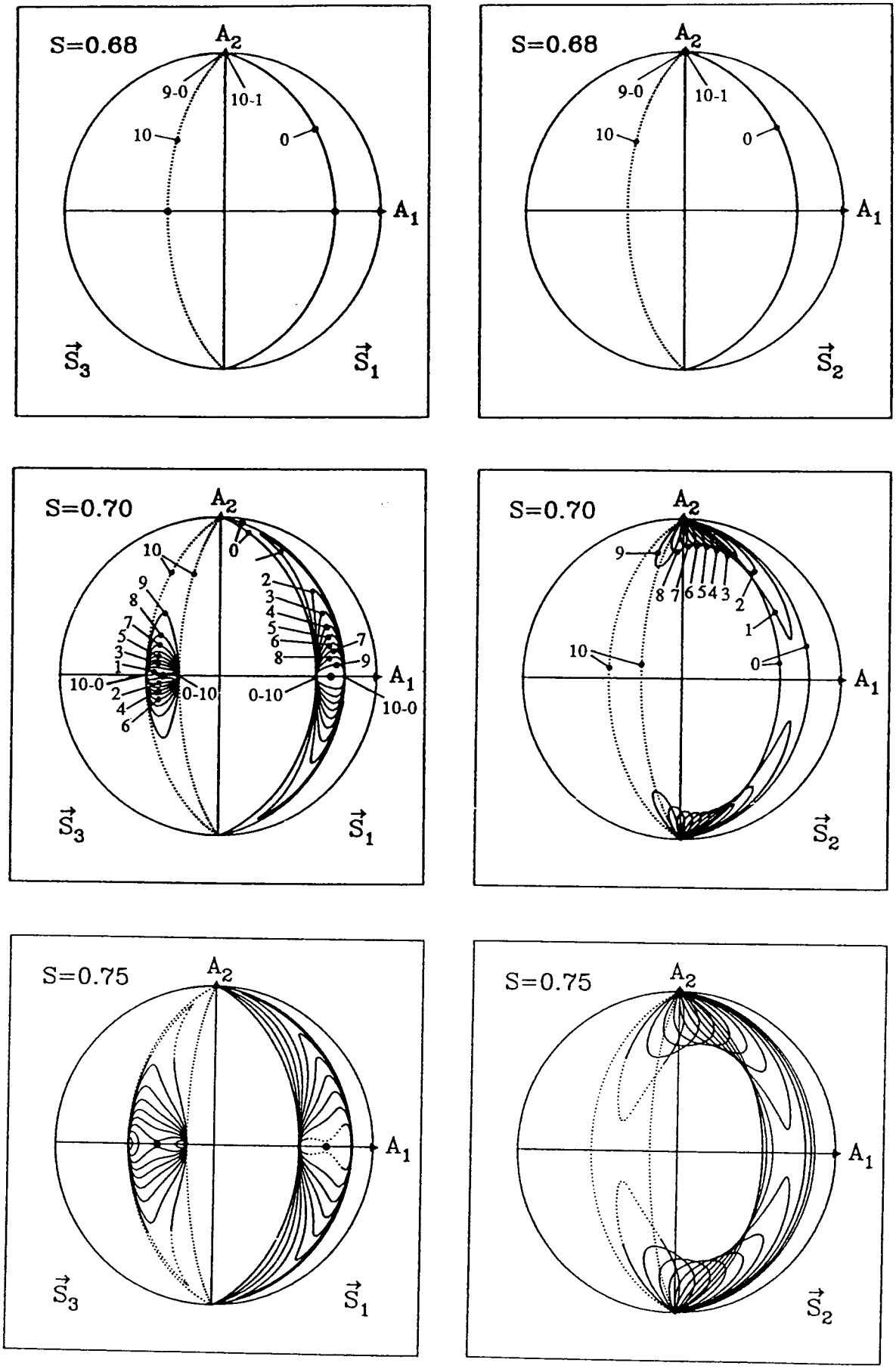
S=0.68
A2
9-0
10-1
10
0
A1
S3
S1
S=0.68
A2
9-0
10-1
10
0
A1
S2
S=0.70
A2
10
0
9
8
7
5
3
1
2
4
6
10-0
0-10
0-10
10-0
A1
S3
S1
S=0.70
A2
9
8 7 6 5 4 3
2
1
10
0
A1
S2
S=0.75
A2
A1
S3
S1
S=0.75
A2
A1
S2

Fig. 5.12

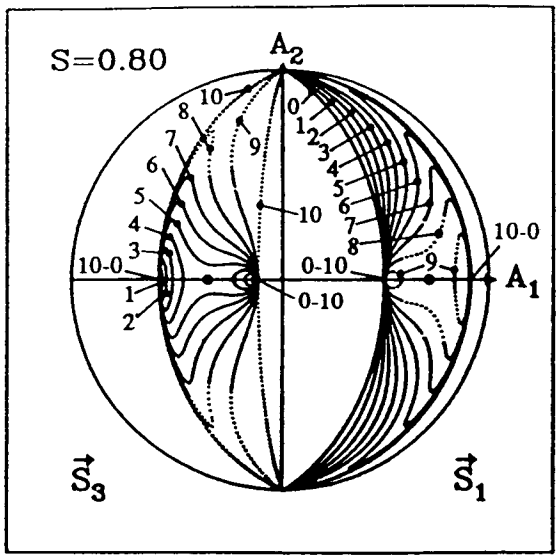

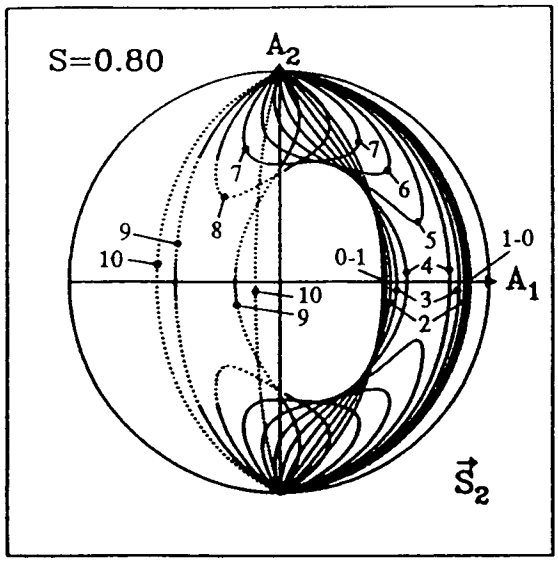

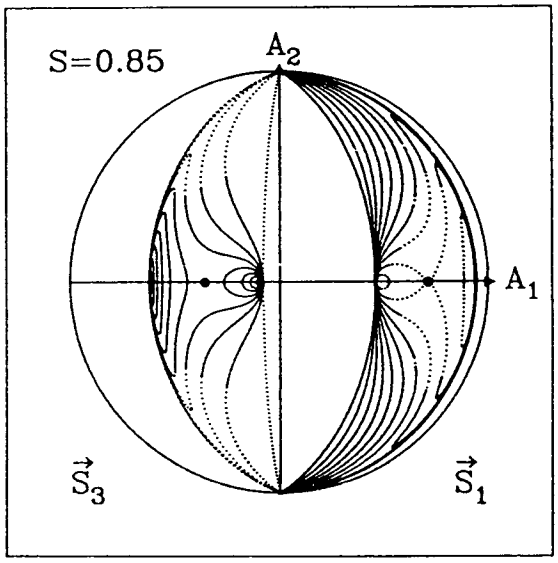

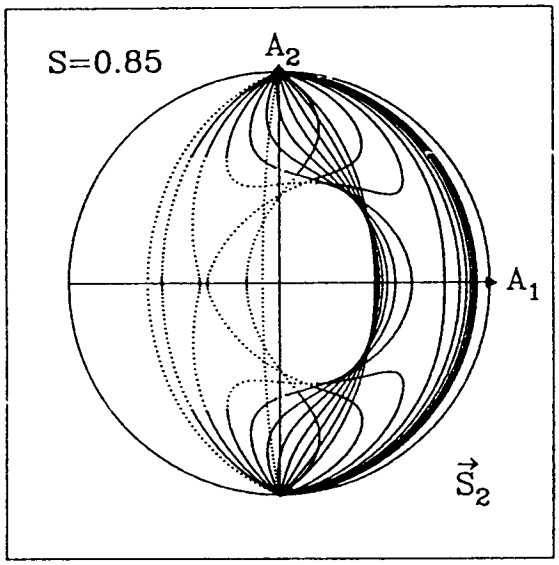

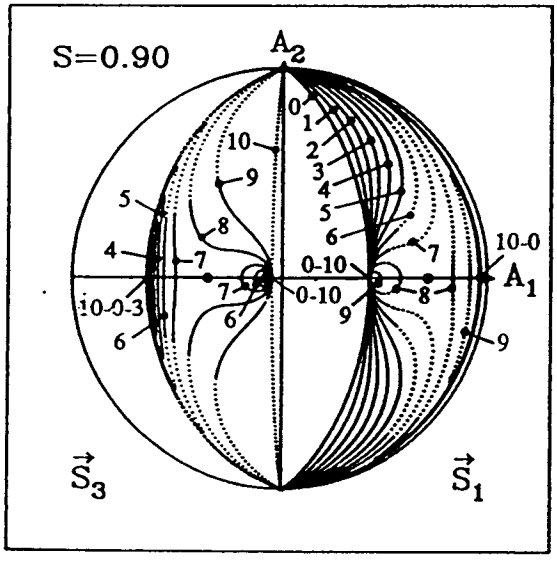

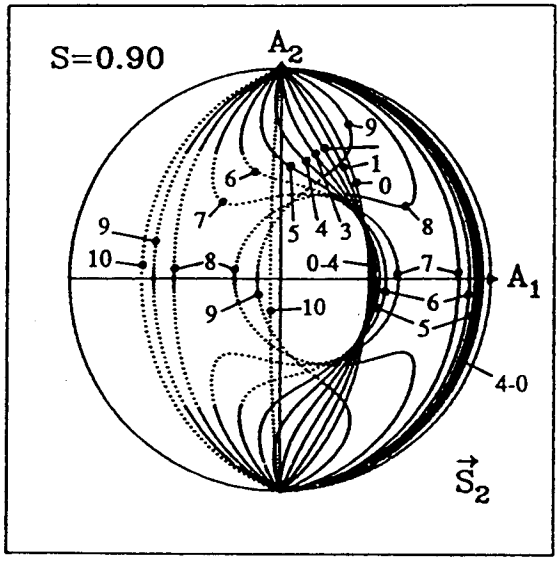

Fig 5.12
(continued)

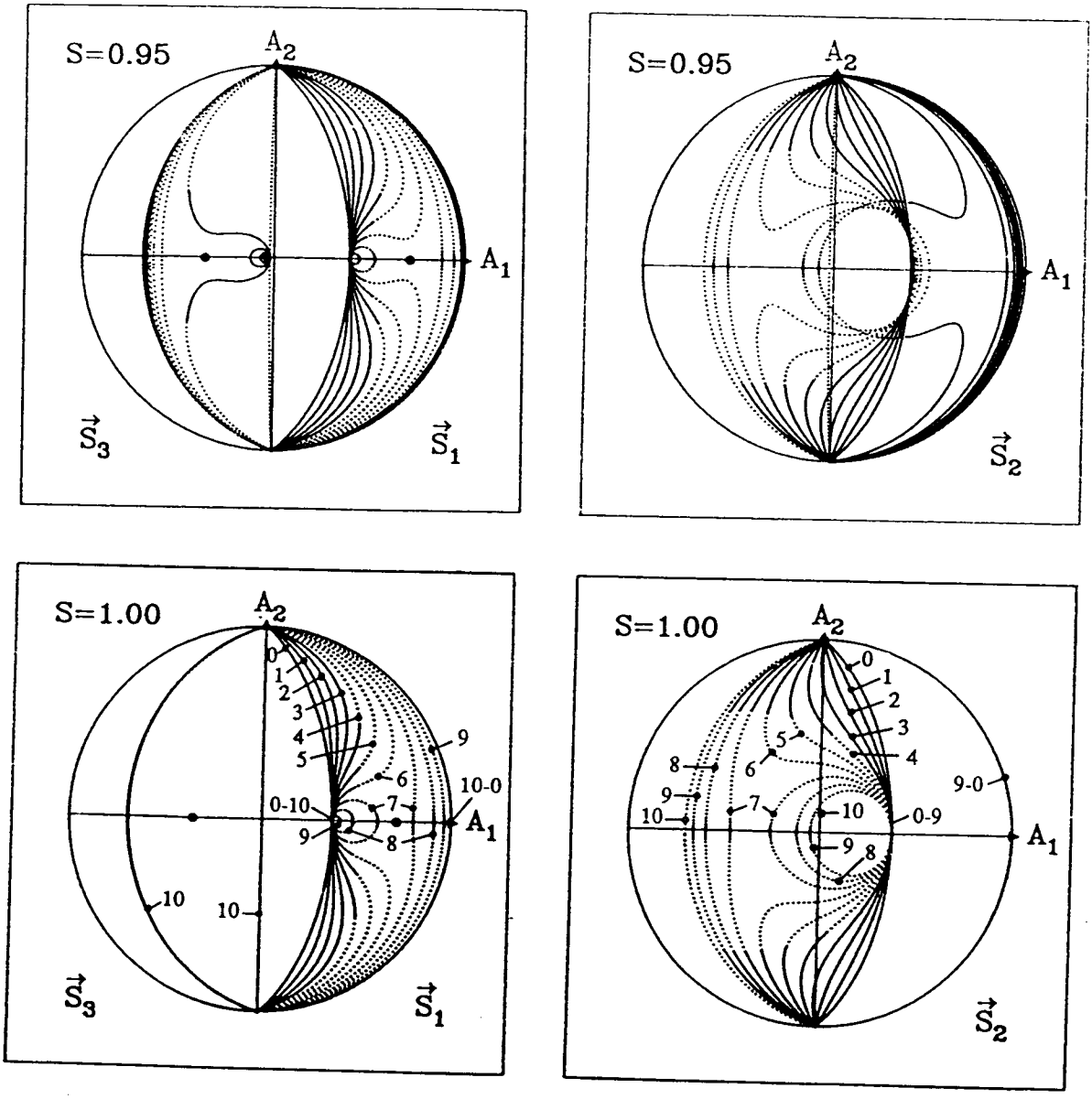
S=0.95
A2
A1
S3
S1
S=0.95
A2
A1
S2
S=1.00
A2
0
1
2
3
4
5
6
7
8
9
10-0
0-10
A1
10
10
S3
S1
S=1.00
A2
0
1
2
3
4
5
6
7
8
9
10
9-0
0-9
A1
S2

Fig. 5.12
(end)

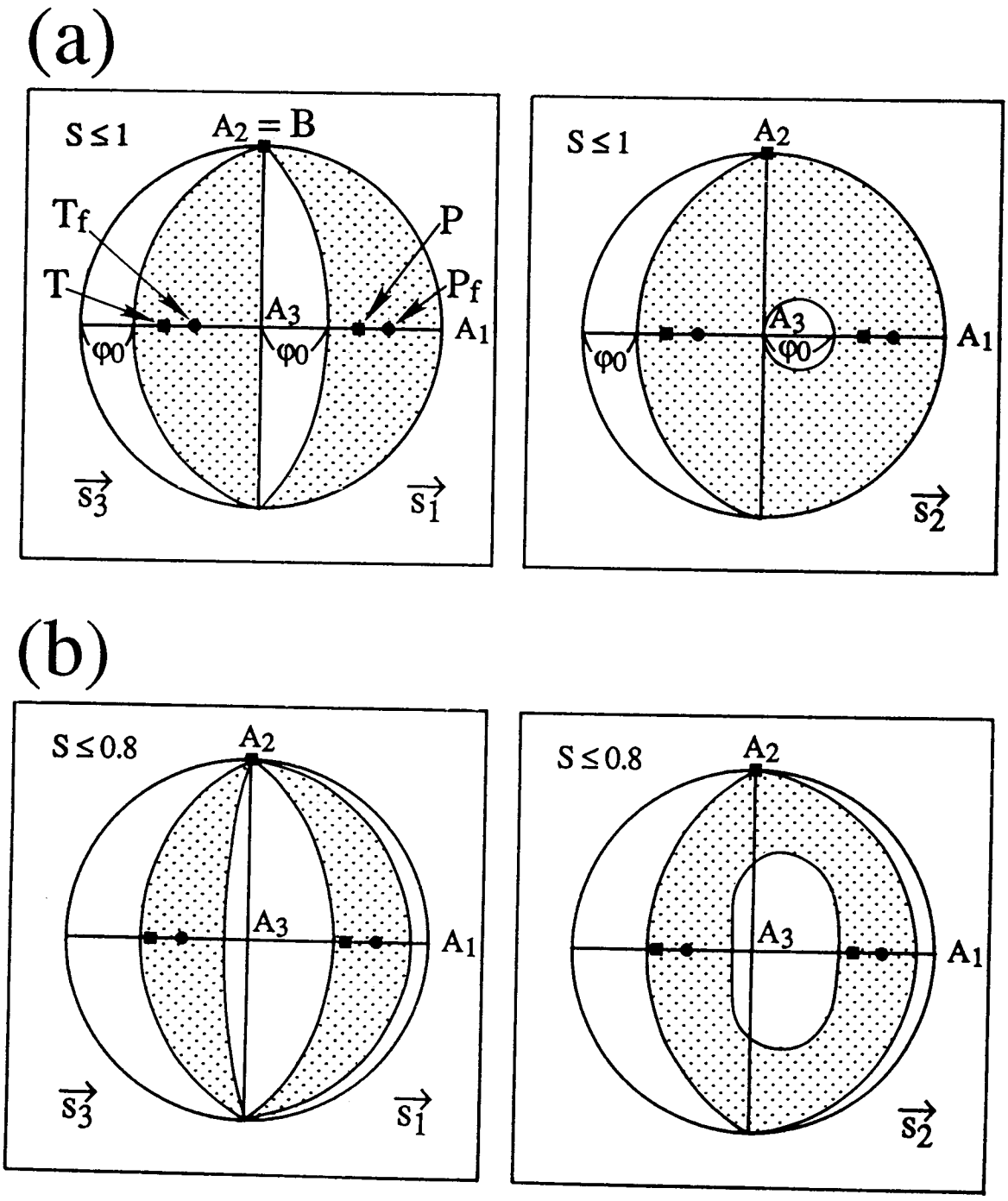
(a)
S ≤ 1
A2 = B
Tf
T
P
Pf
A3
A1
φ0
φ0
s3
s1
S ≤ 1
A2
A3
A1
φ0
φ0
s2
(b)
S ≤ 0.8
A2
A3
A1
s3
s1
S ≤ 0.8
A2
A3
A1
s2

Fig. 6.1